Diffusion in highly confined channels: A transition state theory for hopping

A Thesis Submitted to the
College of Graduate and Postdoctoral Studies
in Partial Fulfillment of the Requirements
for the degree of Doctor of Philosophy
in the Department of Department of Chemistry
University of Saskatchewan
Saskatoon

By
Sheida Ahmadi

©Sheida Ahmadi, Sep/2019. All rights reserved.

Permission to Use

In presenting this thesis in partial fulfilment of the requirements for a Postgraduate degree from the University of Saskatchewan, I agree that the Libraries of this University may make it freely available for inspection. I further agree that permission for copying of this thesis in any manner, in whole or in part, for scholarly purposes may be granted by the professor or professors who supervised my thesis work or, in their absence, by the Head of the Department or the Dean of the College in which my thesis work was done. It is understood that any copying or publication or use of this thesis or parts thereof for financial gain shall not be allowed without my written permission. It is also understood that due recognition shall be given to me and to the University of Saskatchewan in any scholarly use which may be made of any material in my thesis.

Requests for permission to copy or to make other use of material in this thesis in whole or part should be addressed to:

Head of the Department of Chemistry
165 Thorvaldson Building
110 Science Place
University of Saskatchewan
Saskatoon, Saskatchewan
Canada
S7N 5C9

Abstract

Brownian particles restricted to narrow, quasi-one dimensional channels exhibit a dynamic transition from single file diffusion (SFD) to normal diffusion for tracer particle diffusion as the channels' confinement becomes less severe and the pore diameter is wide enough for the particles to hop past each other. The dynamics of a tracer particle in the crossover regime can be described in terms of a hopping time, τ_{hop}, that measures the average time for a tagged particle to escape the cage formed by its immediate left and right neighbors. The hopping time contains all the details of the systems such as the density, particle–particle and particle–wall interactions and has a potential to lead to a better understanding of diffusion and the control of transport in confined single file fluids.

The main goal of this thesis is to develop a Transition State Theory (TST) approach to the calculation of the hopping time in Single file fluids. The method rigorously transforms the process of a particle escaping its cage, in a many particle single-file system, into a problem involving two particles attempting to pass each other in a small system isobaric–isothermal ensemble. The validity of this approach is examined theoretically and computationally for a system of two–dimensional ideal gas particles and a two–dimensional hard disc system. The proposed method correctly predicts the hopping times for the full range of pore radii studied for the ideal gas system. For the case of hard discs, inclusion of the prefactor calculations is necessary, because of its dependency on the channels' diameter, and leads to a quantitative prediction of hopping time.

To demonstrate the effect particle-particle interactions have on diffusion in single file fluids, the hopping time and TST barriers are calculated for a system of soft repulsive discs with $U_{ij} = \frac{1}{r_{ij}^{\alpha}}$, and $\alpha = 5 - 100$. The result shows the method overestimates the hopping time for the narrower channels and underestimates it for the wider channels, which could be related to the assumptions made in deriving the partition function for the system, and also the kinetic prefactor calculations. Nevertheless, the method resulted in a quantitative prediction of hopping times within a factor of two.

It has previously shown that various components of a mixture may experience different hopping barriers, leading to differences in tracer particle mobility. This thesis explores the possibility that enantiomers confined to a chiral channel exhibit different hopping times. The free energy barriers for the R- and S- enantiomers of Bromochlorofluoromethane, $CHFClBr$, inside carbon nanotubes are calculated using the TST isothermal isobaric ensemble method, but are found to exhibit no difference. However, when the molecule, channel shapes, and interactions are modified to enhance the chiral interaction, the R- and S- enantiomers exhibit differences in their free energy barriers. In addition, reversing the chirality of the modified nanotube, reverses the relative heights of the barrier obtained for the two pairs of enantiomers, confirming that the chirality plays an important role in controlling the hopping barrier heights.

Acknowledgements

I would like to express my deep gratitude to my research supervisor, Prof. Richard Bolwles, for his patient guidance, enthusiastic encouragement, and his valuable and constructive ideas throughout my time as his student. Without his guidance and persistent help this dissertation would not have been possible.

I would also like to thank my committee members, Dr. Ian Burgess, Dr. Matthew Paige, and Dr. Raymond Spiteri, for their suggestions and thoughtful feedback. Special thanks to Dr. Raymond Spiteri for his mentoring and extensive professional guidance anytime that I needed his help.

I thank my fellow labmates, Mahdi Zaeifi–Yamchi, Wikai Qi, Cletus C. Asuquo, Ebenezer Gwirah, Zhongquan Chen, Josh Gramlich, and Xin Wang for all their support and encouragement in keeping my progress going.

To my husband, Anthony, who his love, support, and encouragement have enriched my soul and inspired me to pursue and complete this research.

Contents

List of Tables

List of Figures

List of Abbreviations

TST	Transition State Theory
TS	Transition State
MSD	Mean Square Displacement
SFD	Single File Diffusion
MC	Monte Carlo
MD	Molecular Dynamics
MFPT	Mean First Passage Time
FJ	Fick–Jacobs
LJ	Lennard Jones
NMR	Nuclear Magnetic Resonance
GCPSO	Gauranteed Convergence Particle Swarm Optimization
CNT	Carbon Nanotube
SWCNT	Single Walled Carbon Nanotubes
MWCNT	Multi–Walled Carbon Nanotubes
PTA	Paratartaric Acid
TA	Tartaric Acid
MBAR	Multistate Bennett Acceptance Ratio

List of Symbols

J_i	Flux of particle i
D	Normal diffusion coefficient
D_x	Normal diffusion coefficient in x direction
c	Concentration
P	Probability
t	Time
P_0	Probability density
P^*	Probability of being at the transition state
l	Averaged longitudinal free volume
ρ	Density
R_p	Radius of pore
σ	Diameter of particles or atoms
ε	Lennard Jones potential's well–depth defined for the molecules
$\varepsilon_C^{\text{wall}}$	Lennard Jones potential's well–depth defined for carbon atoms on the nanotubes wall
σ_C^{wall}	Diameter of carbon atom on carbon nanotubes wall
$\digamma$	Diameter of carbon nanotube
$h_s(\nu, t/\nu')$	Velocity Distribution Function
$h_0(\nu)$	Equilibrium Velocity Distribution Function
$\psi(t)$	Velocity Auto–correlation Function
$I_S(z)$	Modified Bessel function
$L_s(z)$	Modified Stuve function
Θ	Heaviside function
$M(t)$	Time correlation function
n	Number of particles inside small Isobaric–isothermal system
N	Number of particles
$\Delta(N, P, T)$	Isobaric–isothermal ensemble partition function
$Q(N, V, T)$	Canonical ensemble partition function
Q_{ig}	Ideal gas partition function, canonical ensemble
V_o	Volume scale
L	Length
f	Mobility factor
T	Temperature
p	Pressure
p_l	Longitudinal pressure
F	Helmholtz free energy
G	Gibbs free energy
ΔG^*	Free energy barrier at the transition state
$\hat{G}$	Thermodynamic potential
r_ij	The distance between particle i and j
x_c	Longitudinal distance between the shell molecule and the cages molecule
E	Internal energy
S	Entropy
U	Interaction Potential
α	Power–law exponent for a repulsive potential
η	Power–law exponent for hopping time scaling
p_l	Longitudinal pressure

μ	Chemical potential
ν	Velocity
ω	Viscosity
k_B	Boltzmann constant
$1d$	One dimensional
$2d$	Two dimensional
$3d$	Three dimensional
Δ	Displacement
Λ	The de Broglie Wavelength
k_{AB}	Rate constant
k	Rate Coefficient
k_{TST}	Crossing rate
ϑ	kinetics prefactor
τ_{hop}	Hopping Time
A	Hopping prefactor
x_c	longitudinal distance between the shell particle and the caged particle
ϕ	Occupied volume
nm	Nano meter
eV	Electron volt
$\overrightarrow{C}$	Chiral vector
$\overrightarrow{a_2}$	Unit cell vector
$\overrightarrow{a_2}$	Unit cell vector
γ	Chiral angle
k	Spring constant

Chapter 1

Background

1.1 Introduction

Diffusion is the bridge between the microscopic and macroscopic world and is originated from the random thermal motion of molecules in all states of matter with rates that vary over many orders of magnitude. The rate of the diffusion varies from $0.00001 cm/min$ in solids to 5 cm/min in gases. In liquids, its rate is about 0.05 cm/min at room temperature. Diffusion successively happens along with other phenomena and when it has the slowest rate in the sequence, it can be used to control the overall rate of the process. For example, diffusion is the limiting factor in efficiency of commercial distillations, in liquid–liquid extractions, in acid–base reactions, and also in reactions which involve using porous catalysts [9].

Diffusion of liquids in structured geometries is observed from the nano– to the microscale in a large variety of natural and artificial confined geometries such as living biological cells [10], nanoporous materials and zeolites [11, 12, 13], carbon nanotubes [14, 15, 16], ion channels [17], micro–fluidic channels [18, 19, 20, 21], confined colloids [22, 23], and metal organic framework [24, 25]. Understanding particle motion within such systems that have widths of a few molecular diameters is a fundamental problem in statistical mechanics [26]. The geometrical confinement of the system imposed on the motion of the particles is what all these systems have in common. A good model system for such confined geometries is one, two, or three dimensional channels or pores. In narrow channels, with restricted geometries, the dynamics of tracer particle diffusion is largely influenced by the confinement of the system which may significantly differ from the normal diffusion behavior. In a system of Brownian particles, when the channel becomes so narrow that two particles cannot pass each other, the diffusion switches from normal to Single File Diffusion (SFD). In normal diffusion, the mean square displacement of a tagged particle increases linearly with time but in SFD the mean square displacement of a tagged particle increases linearly with the square root of time because the particles are permanently caged.

The transport dynamic of liquids in confined narrow channels become more interesting when the channel diameter is just above the particles passing thresholds, where particle passing is rare but still possible. In such systems, at short times, the particles are caged by their left and right neighbors, and exhibit single

file diffusion behavior. However, after some time the particles will finally hop their neighbors, and in a long time limit their diffusion become Fickian [27, 28]. The dynamics of the particles in the transition region, from single file to normal diffusion can be characterised in terms of a hopping time, τ_{hop}, that measures the average time a particle takes to escape its cage. The interesting feature of this phenomenological theory is that the hopping time captures all the important factors that contribute to the diffusive properties of the fluid. The hopping time is also directly related to the tracer particle diffusion via $D_x \sim (\tau_{hop})^{1/2}$ and can be measured numerically, if not analytically [28, 29, 30, 31, 32].

Based on a simple Transition State Theory (TST) approach [30, 31], the average time that it takes for two particles to pass each other, τ_{hop}, is related to the normalized probability of finding two particles on top of each other. The goal of the present research is to develop a TST model for calculating τ_{hop} as a predictive tool for understanding the fundamental properties of diffusion in a variety of confined systems. Small differences in the free energy barrier associated for particle passing can lead to a significant difference in their diffusion coefficient. Beside the scientific interest in understanding the new physics resulting from small system effects, a better understanding of the confinement effects on diffusion is necessary for many agricultural, pharmaceutical and geophysical industries. For example, diffusion can be used for time–controlled drug delivery by controlling the diffusion of protein drugs through nano–channels [21], for the separation of mixtures [29, 33, 34, 35], or the extraction of oil in porous rocks in the oil industry [36].

This Chapter is organized as follows: Section 1.2 provides an introduction and review of diffusion in confined geometries, highlighting the difference between single and normal tracer particle diffusion. Section 1.3 reviews the development of the phenomenological hopping time theory for the diffusion coefficient (D_x) in quasi–one–dimensional systems. Section 1.4 describes the development and the applications of Transition State Theory (TST) in activated processes in liquids. Section 1.5 focuses on the application of the isobaric-isothermal (N, P, T) ensemble for small systems in the nanoscale regime, as this forms the appropriate ensemble for a particle caged between two neighbors. Section 1.6 describes the scope of the thesis.

1.2 Diffusion in Liquids

1.2.1 Normal Diffusion

In a one dimensional (1d) steady state system, where the concentration does not change with time, Fick's first law is written as

$$J_i = -D_x(\frac{dc_i}{dx}), \tag{1.1}$$

where J_i represents the flow of particles i across a reference plane (z) which is defined to be perpendicular to the direction of the flow, D_x is the diffusion coefficient along the x direction, and c_i is the concentration of a labeled particle i. It should be mentioned that Fick's first law is a simplified version of his second law

of diffusion, where $(\frac{dc_i}{dx}) \neq 0$. For systems that are not in a steady state, the concentration change in units of time at any position is proportional to the flux change at that position,

$$\frac{\partial c_i}{\partial t} = -\frac{\partial J_i}{\partial x} = \frac{\partial [D_x(\partial c_i/\partial x)]}{\partial x}. \tag{1.2}$$

Assuming that the diffusion coefficient, D_x, is independent of the concentration then,

$$\frac{\partial c_i(x,t)}{\partial t} = D_x \frac{\partial^2 c_i}{\partial x^2}. \tag{1.3}$$

This is the Fick's fundamental law of diffusion, known as the second Fick law of diffusion. Fick faced difficulties verifying the validity of his equation due to complications in regards to measuring the second derivative of a concentration versus distance. However, he was successful in completing a series of experiments for a unique system of salt in water which was performed only in stationary states, where $\frac{\partial c}{\partial t} = 0$ [37, 38]. He studied the diffusion of salt in water through different length cyliderical tubes that were connected to salt and pure water reservoirs. And he measured the amount of salt diffusing out of the terminal section of the tubes as a function of time [38].

After Fick's phenomenological approach on the basics of diffusion, Albert Einstein provided atomistic insight into diffusion by considering the "random walk" of the diffusing particles. The random walk of particles was discovered for the first time by Robert Brown (1773-1858) when he studied the motion of small particles in a sample of fluid containing living pollen grains [39]. While examining the motion of the immersed particles in water, he observed that they are consistently and randomly moving, with their motion causing changes in the particles position, and changes in their direction. He concluded that "These motions were such as to satisfy me that, after frequently repeated observation, they arose neither from currents in the fluid, nor from its gradual evaporation, but belonged to the particle itself". In 1905 Einstein discovered the mathematical form of Brownian motion, when he was studying the suspension of particles in a fluid as his doctorate thesis on osmotic pressure. He showed that for the steady state, and where the solute molecules are much larger than the solvent molecules, the diffusion coefficient of a suspended Brownian particle is given by [38],

$$D = \frac{k_B T}{6\pi\omega R}, \tag{1.4}$$

where k_B is the Boltzmann constant, and T is the temperature, ω is the solvent viscosity, and R is the particles' radius. Einstein made two assumptions, (1) he described the successive position of a tagged particle within a sufficiently small time intervals, t, by assuming the tagged particle's move is independent of the movement of all the other particles, and (2) he assumed that in a long time limit, the displacement, Δx, of the particles in a given time interval along a given direction, x, can be described by a symmetrical Gaussian distribution function, $f(\Delta x)$, (the theory of Brownian motion). Based on these assumptions, he obtained an equation for the diffusivity of the particles, at the microscopic level,

$$D_x = \frac{1}{2\tau}\int_{-\infty}^{+\infty} \Delta x^2 f(\Delta x) \mathrm{d}\Delta x = \frac{1}{2t}\langle \Delta x_t^2 \rangle. \tag{1.5}$$

This equation is called the Einstein relation and connects a macroscopic quantity, the diffusion coefficient, to a microscopic one which is the mean square displacement of the particles. Eq. 1.5 in 3d is [38]

$$\langle \Delta x_t^2 \rangle = 6Dt. \tag{1.6}$$

In 1965-1967, Jepsen [40], Lebowitz and Percus [41] calculated the exact solution for a self distribution function, $f_s(x - x_0, \nu, t/\nu')$, for a tagged particle in an infinite many–body system of one–dimensional hard rods with diameter of σ which results in Einstein relation. In this system, the hard spherical particles undergo deterministic dynamics involving elastic collisions, that allows the particles to simply exchange velocities at each collision. The self distribution function gives the probability density of finding a particle at position x with velocity ν' at time t when it was initially located at x_0 with velocity ν at $t = 0$. Integrating $f_s(x - x_0, \nu, t/\nu')$ over x and averaging it over the particles' initial positions, x_0, yields the conditional velocity distribution function,

$$h_s(\nu, t/\nu') = \int f_s(x - x_0, \nu, t/\nu') \mathrm{d}x. \tag{1.7}$$

Considering the velocity distribution function being Gaussian, the equilibrium velocity distribution function, $h_0(\nu')$, is defined as

$$h_0(\nu) = (2\pi/\beta m)^{-1/2} \exp[-\beta m \nu^2/2], \tag{1.8}$$

where $\beta = 1/k_B T$ and m is the particle mass. Multiplying $h_s(\nu, t/\nu')$ by the equilibrium velocity distribution function, $h_0(\nu')$, yields the self–velocity distribution function. The velocity auto–correlation function can be obtained from the self–velocity distribution as

$$\psi(t) = \int \nu h_s(\nu, t/\nu') \nu' h_0(\nu) \mathrm{d}\nu \mathrm{d}\nu'. \tag{1.9}$$

The self diffusion coefficient, D_x, can be obtained from the velocities by integrating the defined velocity auto–correlation function,

$$D_x = \int_0^\infty \psi(t) \mathrm{d}t. \tag{1.10}$$

In the long time limit, D_x for the system of hard rods reduces to,

$$D_x = \frac{1 - \rho\sigma}{\rho} \int_0^\infty \nu g(\nu) \mathrm{d}\nu, \tag{1.11}$$

where $g(\nu)$ is the normalized function of the initial velocities. The probability density function for the system, $P(x, t)$, calculates the probability of finding the tagged particle at position x which was initially located at the origin. At higher concentrations, the probability of finding a particle at location x at time t, $P(x, t)$, will be higher, and the opposite is true at lower concentrations. Therefore, the concentration term in Eq. 1.3 can be replaced by the probability density function to give $P(x, t)$

$$\frac{\partial P(x,t)}{\partial t} = D_x \frac{\partial^2 P(x,t)}{\partial x^2}. \tag{1.12}$$

By assuming that at $t = 0$, the particles are initially located at the origin, $P(x, 0) = \delta(x)$, where $\delta(x)$ is Dirac delta function, the probability distribution function reduces to a Gaussian,

$$P(x,t) = \frac{N}{\sqrt{4\pi D_x t}} \exp\left(-x^2/4D_x t\right), \tag{1.13}$$

where N is the total number of particles in the system. Taking the variance of Eq. 1.13 yields,

$$\langle \Delta x_t^2 \rangle = 2\mathrm{D}_x t. \tag{1.14}$$

where $\langle \Delta x_t^2 \rangle = \langle (x(t) - x(0))^2 \rangle$ is the mean square displacement, MSD, of a tagged particle at time t. The translational Brownian motion of particles or molecules which is originated from random fluctuations of particles in space can be related to the diffusion coefficient. Particles' motion in a system of interacting particles is described by Eq. 1.14 and diffusion behavior of systems obeying this equation is called normal diffusion where the MSD of particles increases linearly with time [42].

1.2.2 Single File Diffusion

Harris [43] and Levitt [44] discovered that a tagged particle in a one–dimensional (1d) system of hard rods with a Brownian background exhibits anomalous diffusion behavior, where the MSD increases linearly as the square root of time, instead of normal diffusion behavior. In systems with single file diffusion behavior the sequence of particles either remains the same over time or stays the same for long enough that the diffusive motion of the particles is controlled by the strong constraint of single–file systems [45]. To satisfy this condition in the quasi–one–dimensional system of hard rods, the radius of the channel is required to be smaller than the particle passing threshold. In this system, $P(x, t)$ is given by

$$P(x,t) = \frac{\sqrt{\rho/(1-\rho\sigma)}}{2\ (\pi \mathrm{D}_x t)^{1/4}} \exp\left(-(\rho/(1-\rho\sigma))|x - x_0|^2[\pi/\sqrt{16 D_x t}]\right) \tag{1.15}$$

where ρ is the density of the rods and σ is the particle diameter. The variance is then,

$$\langle \Delta x_t^2 \rangle = 2 f_x t^{1/2}, \tag{1.16}$$

where f_x is the 1d single–file mobility factor [44, 45, 46] defined by,

$$f_x = l\sqrt{\frac{D_0}{\pi}} = \frac{1-\rho\sigma}{\rho}\sqrt{\frac{D_0}{\pi}} = D_0\sqrt{\frac{2t_c}{\pi}}, \tag{1.17}$$

where l is the averaged longitudinal free volume between two nearest neighbors in a single–file system, σ is the particles' diameter, ρ is the 1d number density, D_0 the intrinsic diffusion coefficient of a single particle, and $t_c = l^2/2D_0$ is the average time that it takes for the particles to collide. Eq. 1.16 shows that, unlike the normal diffusion, in single file systems the MSD of a tracer particle along the tube axis increases as the square root of time. The movement of individual particles in such quasi–one–dimensional channels,

where their mutual passage is restricted (or not allowed), is described by single file diffusion (SFD). The concept of SFD has been used in both experimental and theoretical studies. Single file diffusion is observed in various physical, chemical, and biological processes such as ions and water passing through narrow pores in biological membranes [10, 17, 22, 47, 48], diffusion in molecular sieves such as zeolites [12, 13, 49, 50], carbon nanotubes [51], or metal organic frameworks [24, 25], and charge-carrier diffusion in one dimensional channels [52]. At the molecular level, SFD has been verified in adsorbate molecules confined in zeolites using pulsed field gradient nuclear magnetic resonance (NMR) [49, 53, 54] and gas mixtures restricted to polycrystalline dipeptide channels [55]. However, observing SFD in NMR studies is subjected to uncertainty in systems where different diffusion mechanism might be responsible [14, 15]. Single file diffusion has also been observed in nano– and micro–fluidic devices [19, 20], and colloidal systems [22, 23]. For example, Wei *et al*. [22] showed the evidence of single file diffusion for a well-defined system of colloidal spheres inside a set of quasi one-dimensional circular channels created by photolithography. They also calculated the probability distribution of the displacement of the individual particles in their experiment and showed that it is in a good agreement with the probability distribution obtained by Harris [43] and Levitt [44] for single file systems, see Eq. 1.15.

It is important to point out that the collective mass transport properties of a single file fluid are not effected by the anomalous dynamics of a tracer particle [56, 57, 58, 59, 60]. In particular, normal diffusion can be mapped onto SFD system by considering the exchange of particle identities when two particles collide during a trajectory. This is possible when particles in the system are identical so that after two particles have collided it is not possible to distinguish between passing and non-passing events. As a result, the total displacement of the particles in a quasi-one-dimensional system is not governed by the anomalous MSD of a tracer particle. The evolving density profile in a single file diffusion is then expected to be the same as normal diffusion and the for the system MSD is expected to follow the behaviour captured in Eq. 1.14.

However, the relationship between tracer diffusion and the collective mass transport properties of multi-component systems remains an open question. In this case, it is no longer possible to exchange the identities of the different particle species when they collide, so a particle can become trapped between its neighbours of a different type. This suggest that some elements of mass transport, such as the diffusion of two species as they mix may be influenced by SFD tracer particle diffusion.

1.2.3 Single File to Normal Diffusion Crossover Regime

Understanding the mechanism and diffusion behavior of fluids inside porous materials plays an important role in the success of technologies that rely on the porous materials for separation purposes [45, 61, 62, 63, 64, 65]. In studying diffusion of fluids in narrow pores and channels, a topic of particular interests is the single file to normal diffusion crossover regime [66, 67]. When fluids are diffusing in quasi–one–dimensional channels,

increasing the channel radius just above passing threshold for particles will create a transition region from single file to normal diffusion, where the particles passing is unlikely but still possible. In the crossover regime, when the passage of particles is not dominating, particles exhibit single file diffusion behavior between the jumps and therefore the mean square displacement will be proportional to the square root of the observation time. However, in the long time limit, particles will be able to jump and pass each other and they will exhibit normal diffusion behavior, where the mean square displacement increases linearly with time. In order to observe single file diffusion in the crossover regime, the time intervals between the mutual interaction of adjacent particles in a single file system must be frequent enough to create a correlated movement of the particles. In addition, in the single file to normal diffusion crossover regime the average time that it takes for a tagged particle to escape its local cage must be long compared to the mean time that it takes for a particle to encounter its neighbors [29, 45].

The transition from single file to normal diffusion has been observed in simulation studies of hard spheres [2, 28] and Lennard–Jones particles in confined systems [2, 45]. Figure 1.1 shows the transition from single file to normal diffusion in a computational study of diffusion in a three–dimensional system of hard spheres confined into a structureless cylindrical hard channel using Monte Carlo (MC) simulation methods [2]. At short times, the MSD increases linearly with time because in this region the intrinsic random motion of a free particle dominates. At intermediate times there is the crossover to SFD as the particles are temporarily caged by their neighbors. In this regime the MSD is proportional to $\sim t^{1/2}$. The crossover to normal diffusion then occurs as the particles are able to hop pass each other, and the MSD increases linearly with time, t. When the channels' radius is narrow, $R_p = 1.015$, it takes longer for the particles to jump out of their local cages, so that the crossover from SFD to normal diffusion occurs at later times. As the channels gets wider, it becomes easier for the particles to pass and the crossover regime becomes shorter. This was also a subject of interest in experimental studies, and despite the difficulties associated with an ideal experimentally accessible single file system, there is evidence that supports the occurence of the single file diffusion through experimetal studies [54, 62, 64, 68].

1.3 Hopping Time

Mon and Percus [28] defined hopping time, t_{hop}, as the average time that it takes for a particle to escape the local cage created by its immediate left and right neighbors in a single–file system. Hopping time can be calculated either through theoretical or numerical studies [3, 28, 29, 30, 31, 32], and can be connected to the long time diffusion coefficient as follows: in the crossover regime, for times less than the hopping time, $t < \tau_{hop}$, the particles will have a MSD that obeys single file diffusion dynamics [28],

$$\langle (x_t - x_0)^2 \rangle_{\mathrm{SFD}} \propto \chi l (D_0 t)^{1/2}, \tag{1.18}$$

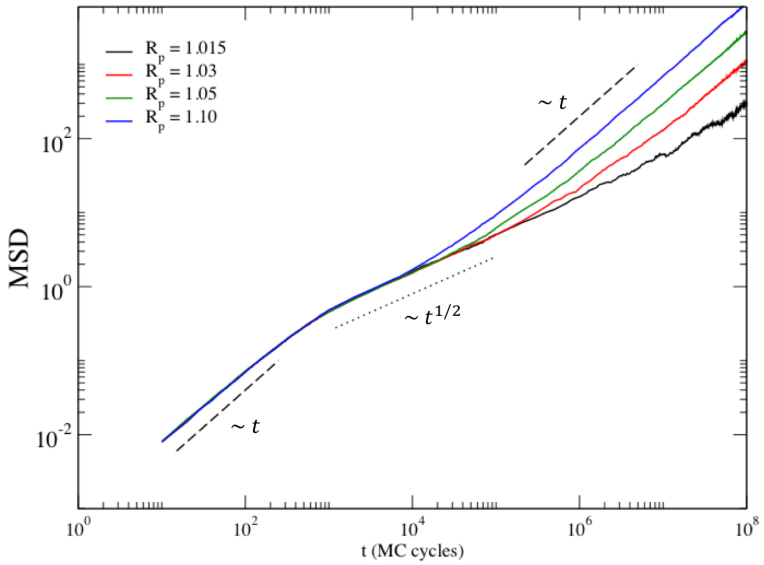

Figure 1.1: The MSD as a function of time, t, for a system of hard spheres confined to a cylindrical channel with hard walls with different pore radii, R_p. The dashed lines represent the proportionality of MSD with $\sim t$ and $\sim t^{1/2}$, respectively, for comparision [2]. Reprinted with permission from ref. [3].

.

where D_0 is the intrinsic diffusion coefficient for the basic particle motion, l is the averaged longitudinal free volume between two nearest neighbors, and χ varies based on the distribution of jumps in the basic particle motion. Mon and Percus stated that at $t > \tau_{hop}$ the tagged particle will make a jump and again will perform SFD for another $t = \tau_{hop}$. The hopping event can occur in either direction and therefore, asymptotically, the particles perform ordinary diffusion in a long time limit, $t \gg \tau_{hop}$. In Eq. 1.18 the time, t, and distance traveled at $t = \tau_{hop}$ can be rescaled in units of τ_{hop}, giving,

$$\langle (x_t - x_0)^2 \rangle / t = \chi l (\tau_{hop})^{1/2} / \tau_{hop} \propto l / (\tau_{hop})^{1/2}, \tag{1.19}$$

where for finite τ_{hop} the linear time dependency of the MSD for Fickian diffusion can be recovered. They concluded that for a system of hard spheres in hard wall cylindrical pores, in the crossover regime, the tracer particle diffusion coefficient, D_x, is proportional to the τ_{hop} as,

$$D_x \propto l / (\tau_{hop})^{1/2}. \tag{1.20}$$

The above derivation was also probed for systems of hard disks in a narrow channel with hard walls [32], hard disk mixtures in a narrow channel with hard walls [29], and hard and soft spheres (with hard and Lennard Jones (LJ) potentials, respectively) confined to narrow pores with hard and LJ walls [3]. The

results showed that Eq. 1.20 was valid for all the studies performed under the condition that the channels diameter is narrow enough for the particles to allow them to experience the SFD diffusion for $t < \tau_{hop}$. This simple phenomenological theory links the long time diffusive dynamics of the fluid to a single local parameter, τ_{hop}. The appealing feature of this theory is that a local parameter captures the effect of all important details of the system such as the particle-particle interactions, the particle-wall interactions, and the density.

As mentioned earlier, the above derivation, Eq. 1.20, is valid when the channels' radius is just above the particles' passing threshold, which for a system of hard particles with diameter of σ, would be near $R_p = \sigma$. However, when the hopping time is short the distance that a particle travels between hops will be proportional to the average distance between the particles, so that the D_x will be proportional to τ_{hop}^{-1} [3, 29, 66].

1.4 Transition State Theory and Fick–Jacobs Analyses for Hopping Time

A number of different approaches have been proposed for the calculation of the hopping time, with the main goal of finding how the hopping time scales with changing pore radius. The escape process can be characterized by using the mean first passage time (MFPT) or transition state theory (TST) descriptions. Based on the MFPT approach, τ_{hop} is the average time that it takes for a diffusing particle to pass another particle for the first time, having started from a random point in configurational space. In a study performed by Bowles, Mon, and Percus [30], the MFPT was calculated for a simple two–dimensional (2d) system of hard disks inside a rectangular hard box. It examined cases where the particles were either diffusing or moving inertially and investigated the τ_{hop} scaling, η, as a function of the height of the box as the particle passing threshold is approached,

$$\tau_{hop} \sim (R_p - \sigma)^{-\eta}. \tag{1.21}$$

Here, $2R_p$ denotes the box height and σ is the disk diameter, so that the passing threshold occurs when $R_p = \sigma$. Two approximate methods of the Fick–Jacobs (FJ) analysis [69, 70] and TST approach [30] were used to drive the scaling behavior of hopping time.

1.4.1 Fick–Jacobs Analyses

Fick–Jacobs analysis can be used to reduce two or three dimensional problems to one dimensional problems by projecting the transverse degrees of freedom onto the longitudinal degrees of freedom using a Zwangzig operator technique [71, 72]. As a result, the FJ approach provides an approximate one-dimensional description of diffusion for the systems with a space-dependent diffusion coefficient [73]. The FJ approach gives a more accurate approximation of diffusion in systems under which the particle distributions equilibrate

faster in transverse directions compared to the longitudinal directions. Later on, the applicability of the FJ approach was intensively investigated for strongly corrugated channels and channels with growing width [74], and different techniques were proposed in order to improve its accuracy [75, 76]. The authors showed that many properties of entropic particles' transport can be successfully predicted by the FJ approach. However, it is not applicable for wide channels and systems with rapidly growing corrugation.

1.4.2 Transition State Theory

A diverse range of fields such as the study of reaction kinetics, diffusion, nucleation theory, and molecule transportation all address the problem of escape from meta-stable states [77]. It was quickly recognized that since rate processes are phenomena that take place on a long-time scale in comparison to the dynamic time scales which characterizes the states of local stability, they are characterized by rare events. Through an extensive discussion given by Svante Arrhenius [78] about various reaction rate data, which vary on a logarithmic scale, the discipline of rate theory was created as a function of the inverse temperature $\beta = (k_B T)^{-1}$. The rate coefficient k, or simply the rate of escape, follows the Van't Hoff-Arrhenius law as [78, 79],

$$k = \vartheta \exp(-\beta U), \tag{1.22}$$

where U represents the activation threshold potential and ϑ is a prefactor. However, a comprehensive and more detailed consideration needs to be given to the significance of activation energy, U, and the pre-factor, ϑ, before further development can occur. The magnitude of the pre-exponential factor ϑ in the Van't Hoff-Arrhenius equation, is one of the important problems to be addressed. Transition State Theory which was developed almost simultaneously in 1935 by Eyring [80], and Evans and Polanyi [81] addressed this issue successfully. Transition State Theory is an activated rate theory which uses an equilibrium based approach where the barrier recrossing effect is not considered. In classical theory, transition state theory is recognized with a "dividing surface" which separates reactant and product regions of configuration space (more generally, of phase space). Therefore, the transition state theory's rate constant is proportional to the total flux of classical trajectories across the dividing surface from the reactant to the product side. This can be calculated by either using the microcanonical TST approach, which uses a delta-function weighting and counts only trajectories of a given total energy, or the canonical TST approach, which uses a Maxwell-Boltzmann weighting at a given temperature. The microcanonical TST assures no trajectory of the given energy crosses the transition state dividing surface more than once, whereas the canonical TST is exact if no trajectory of any energy whatsoever crosses the transition dividing surface more than once. Consequently, the exact (equilibrium) rate constant will be over estimated should re-crossing occur, meaning that the clasical TST provides an upper bound to the true classical rate constant [82].

When barrier re-crossing events are rare, usually attributed to the high barrier height at the dividing surface, the estimates provided by TST are effective. Particles passing each other in a single file system can

be characterized as a rare event, where the relatively high energy barrier makes it difficult for the particles to overcome it when passing each other. Once the particles have crossed this threshold, they remain in their new stable state, the product side, rather than re-crossing the barrier and returning to their original state, the reactant side. A general approach to barrier crossing, developed by Bennett [83] and Chandler [84], is applicable to the cases where the barrier is high in comparison to the thermal energy in the system and reduces to TST when the re-crossing can be ignored. All the approaches have a common underlying principle that the barrier crossing rate is proportional to the probability of finding the system at the top of the barrier. Calculating this probability, even when barrier crossing is rare, is made possible by computational techniques now available [85]. The time of escape, τ_{hop}, is then inversely proportional to the crossing rate. Therefore, for a canonical system of particles trying to pass each other within confinement of a channel the time of escape, τ_{hop}, based on Eq. 1.22 can be expressed as

$$\ln \tau_{hop} = \ln A + \beta \Delta F, \tag{1.23}$$

where A is defined as the hopping time prefactor, ΔF is obtained from the reaction coordinate dependent Helmoltz free energies, and τ_{hop} is inversely related to the crossing rate in the Van't Hoff-Arrhenius law, see Eq. 1.22.

1.4.3 Literature Review on Hopping time Scaling

The Fick–Jacobs approximation was used by Bowles, Mon, and Percus to obtain a one–dimensional treatment for the problem of two hard discs in a rectangular hard box [30]. They assumed that the MFPT is equivalent to the hopping time, τ_{hop}, and defined it as the average time that it takes for a particle to swap places with one of its immediate left and right neighbors in the longitudinal direction of the channels. The second assumption is that they use a reduced or coarse grained description of the system by using a variational principle to project out the degrees of freedom of particles in y coordinates to achieve a one–dimensional diffusion equation in the longitudinal hopping time reaction coordinate. The hard disc system is an ideal model system for studying phase transitions and evaluating the existence of activated dynamic scaling. For hard discs systems, it is expected to have a divergence in hopping time at $R_p = \sigma$, as the hopping event goes to zero at this region. Their results show that the hopping time diverges as a power low with an exponent of $\eta = -3/2$, according to the following equation,

$$\tau_{hop} \sim (R_p - \sigma)^{-3/2}. \tag{1.24}$$

The key assumption in deriving this equation (based on FJ approach) is that the system rapidly reaches equilibrium in y direction and the density in the y coordinate is uniform. In order for this to be true, the dynamics of the motion must be diffusive rather than inertial. Eq. 1.24 was obtained analytically. The

key advantage of this theoretical formalism is that, even though the assumptions that are made in driving this equation are system dependent, the effects of varying systems' parameters such as particle–particle interactions and channels' size effects are still the same and can be evaluated systematically. Their results showed that the hopping time exponent ranged from $\eta = 1.97$ to $\eta = 1.42$, as the time step was decreased for a fixed range of pore radii, respectively. The shortest time steps show agreement with the FJ approximation. In their work, in addition to the FJ scheme, the TST approach approximation was explored with inertial particle dynamics simulation to study the hopping time scaling exponent. It was shown that based on the TST, the rate of a dynamical process, $1/\tau_{hop}$, where the particles' moves are mainly inertially rather than diffusively, is proportional to the probability of finding the system over an entropic barrier. For a given temperature, T, this rate is calculated using the Boltzmann weighting function [77]. Bowles *et al.* [30] showed that for the model of two hard disks in a box as the passing threshold is approached the τ_{hop} is proportional to

$$\tau_{hop} \sim Z(R_p - \sigma)^{-2}, \tag{1.25}$$

where Z is the equilibrium partition integral. In another work, Zhou and Zwanzig [86] had shown that a simple TST predicts the exponent of -2 for the hopping time scaling in the region of particles' passing threshold. This disagreement in the hopping time scaling exponent, η, changing from $-3/2$ to -2, obtained from two different approximate methods of the dimensional reduction Fick-Jacobs scheme and the transition state theory, respectively, could originate from the type of particle dynamics. As mentioned earlier, the Fick-Jacobs scheme predicts the scaling of $-3/2$ by considering diffusive motion for the articles while the transition state theory gives the scaling of -2 by considering inertial moves for the particles. However, a computational study of hopping times for a system of 2d particles in a narrow hard wall channel [32] using two different dynamics for particles' motion, stochastic kinetic MC and inertial molecular dynamic simulation, produced the exponent of $\eta = -2$ for both cases. They also performed a simulation study of hopping time for hard sphere particles confined into hard cylindrical pores and the exponent η was found to be equal to the dimensionality of the system, $\eta = -3$. A later simulation study of the hopping time using a finite difference method confirmed that the exponent $\eta = -2$ for the same system of two hard disks in a hard wall channel [31]. This suggested that the scaling law exponent for hopping time might be a universal exponent depending on the dimensionality of the system and therefore independent of the details of the system's dynamics. However, to date the reason for the disagreement in the hopping time scaling exponent obtained from the approximate methods, the reduced Fick–Jacob scheme and the transition state theory approach, remains unclear. Mon, in more recent Brownian dynamics simulations [87, 88], revisited their previously published result [30] and concluded that the scaling exponent is independent from the time step. His result also showed the TST approach is only valid when the pore radius is closed to the particles' passing threshold, and in this limit Brownian dynamic simulations always predict the exponent of -2. It

has been suggested that near the passing threshold the dimensional reduction FJ scheme may no longer be valid because in this region the projected channel geometry is varying rapidly. Sané *et al.* [66] performed a Brownian dynamics simulation to investigate the validity of Eq. 1.25 for a model of colloidal particles with a strongly repulsive potential, $U \propto 1/r^{48}$, for colloid-colloid and colloid-wall interactions. Their result was in agreement with TST. In more recent work from the Bowles group [3], the power law exponent for hopping time was investigated for systems of hard and soft spheres (with hard and LJ potentials, respectively) confined to narrow pores with hard and LJ walls. They obtained exponent $\eta = -3$ when the channel radius was close to the particles' passing threshold and the particles' interaction was purely hard. For the systems that they studied, it was also shown that the power law behavior for hopping time is no longer valid for the soft potential models, where the particles could always pass each other, except in the limit $R_p \to 0$. Comparing their result with Sané *et al.* work, it was suggested that even though τ_{hop} does not obey Eq. 1.25 for systems with no clear passing threshold, it might be possible to find an effective divergence under which the hopping events become rare on the time scale of the simulation and Eq. 1.25 is applicable. More importantly, their result shows that TST is still applicable in predicting the right type of hopping behavior for the systems with no clear passing threshold where the hopping exponent is no longer obeying Eq. 1.25. They studied a wide class of systems through soft repulsive potentials and Lennard-Jones (LJ) potential and developed a model by focusing on calculations of the free energy barrier associated with two particles passing. It was shown that there is a restriction in configuration space due to the particle-particle exclusion effect which creates a free energy barrier with a transition state located at the point that two particles are side by side in the plane perpendicular to the longitudinal axis of the channel. This suggests the key elements of the activated particle hopping should be adequately captured by a two-particle description at low densities, where the transition state should not be affected by the presence of the other particles. The reaction coordinate for the hopping process is defined is as, $x_c = x_2 - x_1$, where x_1 and x_2 are the positions of the particles along the longitudinal axis of the pore so that the transition state, x_c^*, is located at $x_c = 0$. The canonical partition function for two particles trying to pass each other along the reaction coordinate is expressed as,

$$Q_R(x_c') = \frac{1}{N!\Lambda^{3N}} \int \exp(-\beta U(r))\delta(x_c' - x_c)\, dx_c, \tag{1.26}$$

where N is the number of particles, Λ is the de Broglie wavelength, and $\beta = 1/k_B T$, with k_B being Boltzmann's constant and T the temperature. $U(r)$ is the interaction potential energy as a function of the distance between the particles, and x_c' denotes the configuration space associated with a chosen point along the reaction coordinate, and is obtained by applying the delta function,

$$\int \delta(x_c' - x_c)dx_c = \begin{cases} 1 & \text{if } x_c' = x_c \\ 0 & \text{if } x_c' \neq x_c. \end{cases} \tag{1.27}$$

The reaction coordinate dependent free energy was defined as,

$$F_R(x_c') = -k_B T \ln Q_R(x_c). \tag{1.28}$$

.

Bowles *et al.* calculated τ_{hop}, ΔF, and the diffusion coefficient, D_x, for different systems with particles interacting via hard, repulsive and Lennard-Jones (LJ) potential for a wide range of pore radii=$0.93 - 1.5$. Their results show that $\ln \tau_{hop}$ is linear in ΔF for all the system they studied, as predicted via Eq. 1.23. Yet their results were not able to provide a quantitative measure of the hopping time. They argued that the free energy barrier in Eq. 1.23 is related to the probability of finding the particles on top of each other at the TS relative to finding them anywhere else in the whole configuration space, while their simulation method calculated the probability of finding the system at the TS relative to the probability of finding the particles at $x_c = 2\sigma$. Therefore, it is necessary to correctly normalize the free energy calculations to achieve a quantitative prediction of hopping time. It was also suggested that the prefactor A in Eq. 1.23 must also be determined.

Nevertheless, the simplicity of this approach, which reduces the problem of a many body system of particles diffusing inside a single file system to the problem of two particles hopping each other at the transition state is an attractive one. The main goal of this study is developing a model which is capable of quantitative prediction of hopping time. In particular, it is worth highlighting that the caged particle is effectively contained within a fluctuating cell formed by its neighbor which suggests using a constant pressure ensemble may help resolve the issue of normalization.

1.5 The Small Isobaric–Isothermal Ensemble

In the thermodynamic limit, fluctuations away from the most probable microstates are not significant, therefore the thermodynamics of the system can be characterized by the properties of the states associated with the maximum term in the probability distribution. It can be shown that the maximum term for one ensemble can be obtained through the partition function of another ensemble. That is to say, for the purpose of calculating systems' properties all the ensembles can be alternatively used and choosing a particular ensemble is simply a matter of mathematical convenience. However, these fluctuations become increasingly significant as the system size decreases. In the nanoscale regime, considering the types of fluctuations which are available to the system is critical when choosing an appropriate ensemble. It also becomes important to consider the particulars of how the ensemble itself is formulated, as in the case of the isobaric–isothermal N, p, T ensemble, where the volume is a continuous variable [4, 89, 90, 91, 92, 93, 94].

In the case of a small constant pressure and temperature ensemble, the system is immersed in a bath which applies a constant pressure and temperature to the system. The final form of N, p, T ensemble for a small

system is determined by how the surrounding communicates with the system and how the external pressure is applied to the system. In the N, p, T ensemble, the system could be separated from the surrounding either via a physical boundary (wall) or a mathematical construct or constraint. The volume of the system is determined by the boundary and it allows the system's volume to fluctuate against the externally imposed pressure. An example of a mathematically defined boundary arrives when conserving the formation of clusters during vapor phase nucleation, where the boundary defines the volume of the cluster [95, 96, 97]. Therefore, the nature of the boundary influences the final form of the N, p, T ensemble. And again, as the surface effects are negligible in the thermodynamic limit the nature of the boundary also becomes negligible in this limit [4].

The isobaric–isothermal ensemble has been extensively used in Monte Carlo simulations as most experimental observations are performed under conditions of constant pressure and temperature. In order to compare experimental and theoretical results with each other, it is necessary to ensure a proper formulation for a small isobaric–isothermal ensemble. The original formulation of the ensemble which was introduced by Guggenheim [98] is given by,

$$\Delta(N, p, T) = \sum_{V} Q(N, V, T) e^{-pV/k_B T}, \tag{1.29}$$

where $Q(N, V, T)$ is the canonical partition function for N particles contained in a volume V at temperature T, k_B is Boltzmann's constant and p is the external pressure which is applied to the system. This equation, which is derived on analogy to the other ensembles, is mathematically correct, however, Guggenheim did not describe over which set of volumes the sum was supposed to proceed. One can neglect this problem when applying the constant pressure ensemble to systems in the thermodynamic limit because fluctuations away from the most probable microstates are not significant, and the thermodynamics of the system can be characterized by the properties of the states associated with the maximum term in the probability distribution. Therefore, as the system size increases and becomes macroscopic, Δ can be substituted by its maximum term, $Q(N, V, T)$, so that we are dealing only with the canonical ensemble at the thermodynamic limit. However, in the nanoscale regime this becomes the main unsatisfactory feature of the N, p, T ensemble as the fluctuations become increasingly important as the size of the system decreases [4, 89, 90, 91, 92, 93, 94]. For the systems where the volume is a continuous variable, the summation in Eq. 1.29 can be replaced with an integral to help to remove the conceptual difficulty related to the sum being taken over an undefined set of volumes,

$$\Delta(N, p, T) = \int_{V} Q(N, V, T) e^{-pV/k_B T} dV. \tag{1.30}$$

The partition function in Eq. 1.30 is not dimensionless and incorrectly has units of volume. Different attempts have been made to resolve the dimensionality problem associated with the partition function for the isobaric–isothermal ensemble [91, 93]. The integral must contain a volume scale, V_o, to render the

partition function dimensionless such that

$$\Delta(N,p,T) = (V_o)^{-1} \int_V Q(N,V,T) e^{-pV/k_B T} dV. \tag{1.31}$$

The question of defining an appropriate volume scale was first addressed by Attard [91], who derived a volume scale based on axioms that were developed within information theory [99]. Afterward, Koper and Reiss [93] developed a physical approach, starting with the microcanonical ensemble, to drive a new volume scale. Sack [90] showed that the choice of V_o is selected arbitrarily in the thermodynamic limit and reduces to

$$V_o = \frac{k_B T}{p}. \tag{1.32}$$

However, for systems not in the thermodynamic limit, V_o is related to the system's volume and must be taken inside the integral in Eq. 1.31. In the nanoscale regime, the values of the volume scale will be based on the systems' properties such as the number of particles and the type of the boundary which is used to define the volume. Determining the effect and the properties of the boundary is of great importance as the exact form of the volume scale is determined by the nature of the boundary that is defined for a small N, p, T ensemble. For instance, if the boundary is a physical object and is assigned by a mass and momentum, the volume scale is treated as a constant and may stay outside of the integral in Eq. 1.31. On the other hand, if the boundary is a mathematical construct with no additional degrees of freedom introduced to the system, V_o becomes volume dependent and must be placed inside the integral in Eq. 1.31 [93].

These concerns were addressed by Corti [4] who developed a rigorous approach to the isobaric–isothermal ensemble for small systems which eliminates the need to define a volume scale. A summary of Corti's derivation for a small system n, p, T ensemble is provided in the rest of this section, which highlights the detailed elements of the method.

The canonical ensemble partition function for the macroscopic system of N monoatomic particles in the thermodynamic limit, $N \to \infty$ and $V \to \infty$, is given by,

$$Q(N,V,T) = \frac{1}{N! \Lambda^{dN}} \int_V e^{-\beta U_N} dr_1 \ ... \ dr_N, \tag{1.33}$$

where Λ is the de Broglie wavelength, d is the dimensionality of the system, U_N is the total interaction energy of the N particles in the system, and the $dr_1 ... dr_N$ terms show the volume elements for all the particles. The particles' position will be integrated over the entire volume V.

Corti's analysis begins by dividing the canonical partition function for a macroscopic system of N particles, in a volume V and temperature T, into two systems which includes a small subsystem of n particles ($n \ll N$) in a sub–volume v located at a point r_0, and a surrounding system of $N - n$ particles in the remaining volume, $V - v$ (see Fig. 1.2). The potential term in Eq. 1.33 can be written as

$$U_N = U_n + U_{N-n} + U_\sigma. \tag{1.34}$$

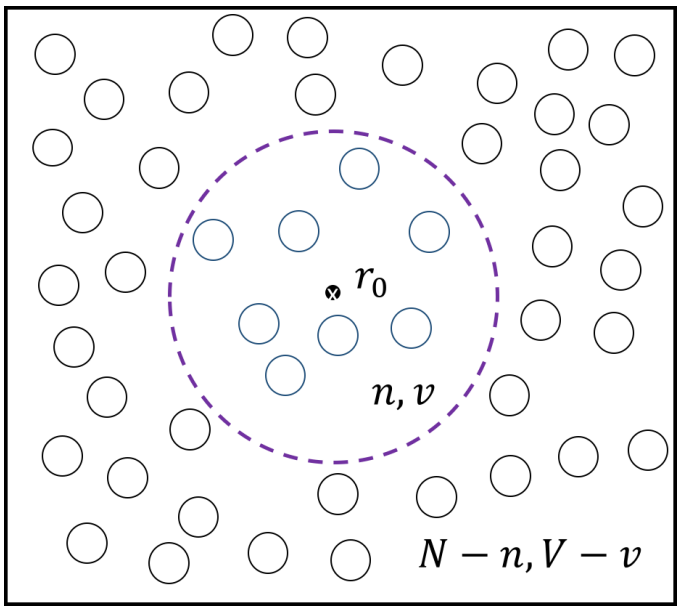

Figure 1.2: The figure illustrates division of a macroscopic canonical system into a small subsystem of n particles with volume v (inside the dashed circle) and temperature, T, with the remaining $N-n$ particles located in volume $V-v$ and temperature T in the surroundings (outside the dashed circle).

where U_n is the potential energy of the n particles in the small volume interacting with each other, U_{N-n} is the potential energy of the remaining particles in the surrounding bath interacting with each other, and U_σ is the interaction between the particles inside the small subsystem and the $N-n$ particles in the surroundings.

Since the small subsystem of n particle system is defined as a n, p, T ensemble, the volume occupied by the n particles, v, is allowed to fluctuate continuously between v and $v+dv$ such that the remaining $N-n$ particles are always outside of this sub–volume. Corti defines a partition function, $Q_N^{n,v}dv$, that represents all the possible configurations of the macroscopic system under which there are $N-n$ particles outside of $v+dv$ and n particles inside of the fluctuating sub-volume, $v+dv$, so that

$$\int Q_N^{n,v}dv = Q(N,V,T). \tag{1.35}$$

The probability of having n particles in a volume between v and $v+dv$ can be formulated as

$$P_n(v)dv = \frac{Q_N^{n,v}dv}{Q(N,V,T)}, \tag{1.36}$$

noting $Q_N^{n,v}$ is a density of states and $Q_N^{n,v}dv$ will be a pure number. Based on the Corti's analysis, the subsystem's boundary is a mathematical concept which separates the n particles from the surroundings. Since the boundary is a mathematical constraint, no additional degrees of freedom will be introduced to the system. In practice, for calculating the thermodynamic properties of the small subsystem, it is necessary to define an effective potential, without using an external potential energy, that does not allow the surrounding particles to enter the subsystem, v, and keeps the n particles inside the volume v. This is achieved by setting

the potential energy to be zero for the configurations that are allowed and infinite otherwise. When a local fluctuation in volume occurs for the subsystem, the boundary must be able to identify the new volume states of the subsystem.

The challenge is how to include the unique specifications of the exact volume of the n particles without over counting the configuration. This problem is illustrated in Fig. 1.3, which shows two volume specifications for one configuration of n particles surrounded by the same configuration of the $N-n$ particles in the surrounding bath. Therefore, it is necessary to make sure that each configuration of the macroscopic system, N particles, corresponds to only one specific volume state of the particle inside the subsystem. To define each volume state taken by the n particles, it is necessary to select a reference point in V to be the origin of the system, r_0. However, Fig. 1.4 shows that even by selecting a particular reference point, there could be several different volumes centered at the origin which correspond to the same configuration of the n particles which also result in counting the configurations redundantly in Eq. 1.35. This problem can be resolved by tying the system's volume, v, to the location of a particle inside the small system, dv, which is called the "shell particle". Therefore, any volume change inside the small system will correspond to a new configuration of the $N-$particle system (regardless of any change in the configuration of the surrounding $N-n$ particles). Since the boundary which separates the small system from its surrounding is a mathematical concept, it will not require additional degrees of freedom as it is attached to the degrees of freedom of the system. As a result, the redundant counting of configurations is eliminated, as is the need to specify a volume scale V_o. Otherwise, Eq. 1.35 will over count configurations of the N particle system.

Corti showed that based on the shell particle approach partition function, $Q_N^{n,v}dv$ can be written as

$$\begin{aligned} Q_N^{n,v}dv &= \frac{N!}{(n-1)!(N-n)!}\frac{1}{N!\Lambda^{dN}}\int_{dv} dr_1 \int_{v+dv} e^{-\beta(U_n+U_\sigma)}dr_2...dr_n \int_{V-(v+dv)} e^{-\beta U_{N-n}}dr_{n+1}\ldots dr_N \\ &= \frac{N!}{(n-1)!(N-n)!}\frac{dv}{N!\Lambda^{dN}}\int_{v+dv} e^{-\beta(U_n+U_\sigma)}dr_{12}...dr_{1n} \int_{V-(v+dv)} e^{-\beta U_{N-n}}dr_{n+1}\ldots dr_N, \end{aligned} \tag{1.37}$$

where shell particle is labeled as particle 1, and $dr_{12}...dr_{1n}$ are the relative coordination of the remaining $N-1$ particles with respect to the position of the shell molecule. In Eq. 1.37, the first binomial coefficient stands for different ways that one can arrange N particle into $n-1$, $N-n$, and the shell particle, indistinguishably. The second denominator, $N!$, is added due to the indistinguishably of all the N particles. If the particles in the surroundings, $N-n$, are fixed, in a frozen configuration, Eq. 1.37 yields

$$Q_N^{n,v}dv = \frac{dv}{(N-n)!\Lambda^{d(N-n)}}\int_{V-(v+dv)} Q^*_{n,v}\, e^{(-\beta U_{N-n})}(dr)^{N-n}, \tag{1.38}$$

where $(dr)^{N-n} = dr_{1(n+1)}\ldots.dr_{1N}$ and $Q^*_{n,v}$ is a partition function which is defined for notational convenience as,

$$Q^*_{n,v}dv = \frac{dv}{(n-1)!\Lambda^{dn}}\int_{v+dv} e^{-\beta(U_n+U_\sigma)}(dr)^{n-1}. \tag{1.39}$$

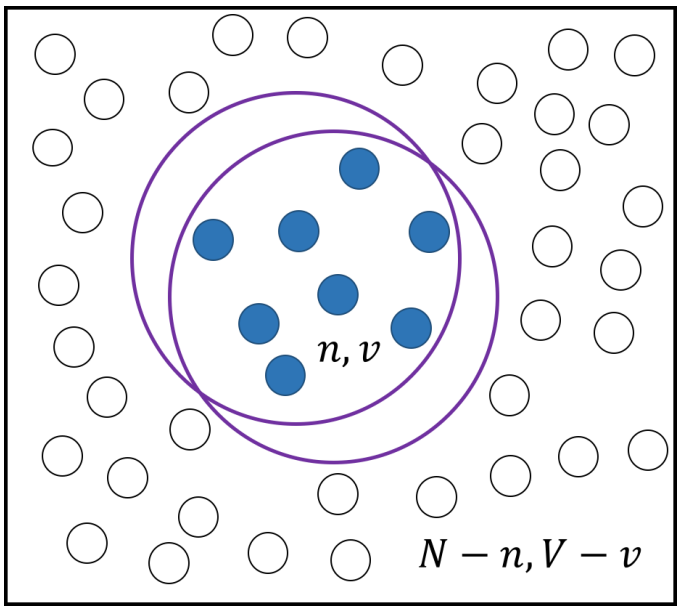

Figure 1.3: Two possible volume states of equal size (large solid circles) that correspond to the same configuration of the small system n, p, T ensemble. The blue shaded circles correspond to the particles inside the small system n, p, T ensemble and the unshaded circles represent the $N - n$ partices in the surrounding bath. Reprinted with permission from ref. [4].

Equation 1.38 can also be rewritten as [92]

$$Q_N^{n,v} dv = Q(N - n, V - v, T)\langle Q^*_{n,v}\rangle_o \, dv, \tag{1.40}$$

where $Q(N - n, V - v, T)$ denotes the partition function of $N - n$ particles in a volume $V - v$, and $\langle Q^*_{n,v}\rangle_o$ is the ensemble average of $Q^*_{n,v}$ over the configurations of the $N - n$ particles in $V - v$,

$$\langle Q^*_{n,v}\rangle_o = \frac{\int_{V-v} Q^*_{n,v} \, e^{(-\beta U_{N-n})}(dr)^{N-n}}{\int_{V-v} \, e^{(-\beta U_{N-n})}(dr)^{N-n}}. \tag{1.41}$$

Based on Eq. 1.35 the canonical partition function can be be rewritten as,

$$Q(N, V, T) = \int_0^V \, Q(N - n, V - v, T)\langle Q^*_{n,v}\rangle_o dv, \tag{1.42}$$

so that the probability of having a given configuration inside the n particle system, $P_n(v)dv$, can be expressed,

$$P_n(v)dv = \frac{Q(N - n, V - v, T)\langle Q^*_{n,v}\rangle_o dv}{Q(N, V, T)}. \tag{1.43}$$

By definition [100], the Helmoltz free energy of a system is related to the canonical partition function as

$$Q(N, V, T) = \exp(-\beta F). \tag{1.44}$$

Substituting Eq. 1.44 in Eq. 1.43 will result in [101, 102],

$$\frac{Q(N - n, V - v, T)}{Q(N, V, T)} = e^{-\beta[F(N-n,V-v)-F(N,V)]}. \tag{1.45}$$

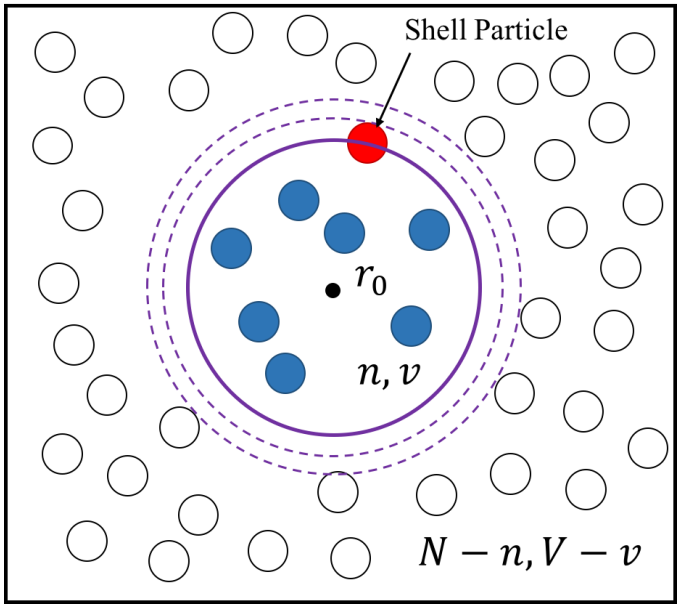

Figure 1.4: Several different volumes centered at the origin, r_0, which corresponds to the same configuration of n particles inside the small n, p, T ensemble. The exact volume of the system is defined uniquely by the shell molecule, the red shaded circle, confined to a shell of volume dv, while all the remaining particles $n-1$ are confined within v. Reprinted with permission from ref. [4].

Since the $N-n$ system is in the thermodynamic limit, $n \ll N$ and $v \ll V$, which gives [103]

$$\mu = \left(\frac{\partial F}{\partial (N-n)}\right)_{V,T}, \tag{1.46}$$

$$F(N-n, V-v) = F(N,V) - n\left(\frac{\partial F(N-n,V)}{\partial (N-n)}\right)_{V-v\approx V} - v\left(\frac{\partial F(N,V-v)}{\partial (V-v)}\right)_{N-n\approx N}, \tag{1.47}$$

where μ is the chemical potential of the bath and

$$p = -\left(\frac{\partial F}{\partial (V-v)}\right)_{N,T}, \tag{1.48}$$

is the pressure imposed by external particles on an empty cavity of size v. Using Eqs. 1.46, 1.47, and 1.48 in Eq. 1.45 gives,

$$\frac{Q(N-n, V-v, T)}{Q(N,V,T)} = e^{\beta n\mu}\, e^{-\beta p v}. \tag{1.49}$$

Substituting Eq. 1.49 into Eq. 1.43 then yields,

$$P_n(v)dv = e^{\beta n\mu}\, e^{-\beta p v} \langle Q^*_{n,v}\rangle_o dv, \tag{1.50}$$

which also satisfies the normalization condition,

$$\int P_n(v)dv = 1. \tag{1.51}$$

In this integral, $\exp(\beta\mu)$ is independent of v and can be taken out of the integral, finally allowing the partition function for the small system isobaric–isothermal ensemble, Δ, to be defined as,

$$\Delta = \int \langle Q^*_{n,v} \rangle_o \, e^{-\beta p v} dv. \tag{1.52}$$

This partition function, unlike that defined by Eq. 1.30, is dimensionless since $\langle Q^*_{n,v} \rangle_o dv$ is a pure number. Based on Corti's derivation, the volume scale in Eq. 1.31 has been absorbed inside the integral by using the shell particle approach. The implicit volume scale in Eq. 1.52 depends on v and this dependency goes away in the thermodynamic limit [93]. If the interaction between the subsystem and the surroundings are negligible, Eq. 1.52 becomes

$$\Delta = \int Q^*_{n,v} \, e^{-\beta p v} dv. \tag{1.53}$$

Corti [94] showed that the small isobaric–isothermal ensemble partition function, Δ, is related to the thermodynamic potential, $\hat{G}$, via

$$\hat{G} = -kT \ln \Delta. \tag{1.54}$$

where

$$\hat{G} = \langle U^* \rangle + p \langle v \rangle - TS, \tag{1.55}$$

where $\langle \cdots \rangle$ denotes the ensemble average and U^* is the internal energy in the presence of a shell particle. It is important to note that in this equation, $\hat{G}$ differs from the Gibbs free energy of the small system, unless it is in the thermodynamic limit, because it includes information related to the surrounding bath, such as the surroundings chemical potential, and also the volume fluctuations at thermodynamic limit will be different from the volume fluctuations sampled by the small system.

Corti also discusses the applicability of the shell particle approach for the systems where an isobaric–isothermal system's boundary is a physical object with an assigned mass rather than a mathematical constraints [4]. The nature of boundary influences the final form of the partition function for different types of systems, and when the boundary is a physical object, which is distinguishable from the n particles inside the small system, the degrees of freedom of the boundary must be taken into account. The canonical ensemble for the n particle system which includes the boundary is defined as $Q_{n,B,v} dv_B$, where B is the physical boundary with its center of mass is located within dv_B. Note that the boundary is treated as a particle within the small system but is distinguishable from the remaining n particles. A momentum partition function can be extracted from the canonical ensemble partition function as

$$Q_{n,B,v} dv_B = Q'_{n,B,v} \frac{dv_B}{\Lambda_B^3}, \tag{1.56}$$

where $Q'_{n,B,v}$ is the remaining part of $Q_{n,B,v} dv_B$ after extracting the momentum partition function of the boundary. By assuming a large system size where the interactions between the surrounding and small system,

including the boundary, is small, Eq. 1.56 reduces to

$$\Delta = \frac{1}{\Lambda_B^3} \int_{v_B} Q'_{n,B,v} e^{-\beta p v} dv_B. \tag{1.57}$$

When the boundary is distinguishable from the n particles and the surrounding and has its own degrees of freedom, the volume redundancies are not a problem anymore. However, the volume scale still appears in Eq. 1.57 which for this case is equal to the cube of de Broglie wavelength of the boundary. Corti concluded that in small systems, the choice and type of boundary affects the ensemble average, and must be chosen so that it conforms to the system's actual physical situation.

To investigate the system size effect on the ensemble average for isobaric–isothermal ensembles obtained from shell particle approach, using Eq. 1.53, and the original algorithm which uses Eq. 1.31, Corti performed multiple MC simulations using both methods and compared the results [94]. His model consists of N identical, structureless LJ particles confined to a spherical system volume, where the interactions between the small system and its surrounding are ignored. The results indicate that the ensemble averages obtained from two methods differ from each other and the differences are significant when the system size are small. For larger system sizes, these differences become negligible. This highlights the importance of correctly formulating the partition function for small isobaric–isothermal ensembles to eliminate the problem of redundancy via shell particle approach.

1.6 Scope of the Thesis

In order to understand the diffusive properties of individual tracer particles in single file fluids, and therefore use it for a variety of applications in SFD in single file systems, it is useful to develop a transition state theory which is capable of predicting τ_{hop}. The goal of this thesis is to develop a method which is capable of predicting hopping times quantitatively for various confined fluids using a simple system of two particles trying to hop each other within the confinement of the channel. This thesis will address the following questions:

- Can TST provide a quantitative measure of the hopping times in single file systems?
- How does the inter-molecular potential influence the hopping time in a single file system?
- Is there a difference in free energy barriers for enantiomers, attempting to pass each other inside a chiral carbon nanotube (CNT)?

This thesis is organized as follows:

- Chapter 2 addresses the first question by developing and testing a transition state theory for the quantitative prediction of the hopping time using a small system n, p_l, T ensemble, consisting of two

particles attempting to pass each other in a quasi–one–dimensional channel. The chapter provides a derivation of the partition function using a small system n, p_l, T ensemble for two types of systems that are analytically tractable: A two-dimensional (2d) system of ideal gas particles confined between hard walls and a two-dimensional system of hard discs confined between hard walls. This is followed by a description and application of the Monte Carlo (MC) simulation method to calculate the free energy barriers associated with two particles passing each other at the transition state and the direct measurement of hopping times in large systems for comparison. This chapter highlights the key features of the method which allows the study of diffusive properties of a single file system consisting of thousands of fluid particles by the simulation of only two particles. The results of this research have been published in Journal of Chemical Physics, titled as "Diffusion in quasi-one-dimensional Channels: A small system n,p,T transition state theory for hopping times." by S. Ahmadi and R. K. Bowles [5].

- Chapter 3 focuses on the second question and investigates the effects of the interaction potential on the diffusion for a 2d system of soft repulsive discs interacting via $[U(r_{ij}) = (\sigma/r_{ij})^{\alpha}]$ confined within a channel with hard walls over a range of different channel sizes and degrees of particles softness, $1/\alpha$. This work shows that the proposed transition state theory model is able to quantitatively predict the hopping time for the systems studied. This chapter also highlights how this approach can be used to efficiently explore and optimize particles diffusion inside single file systems. The results of this research have been published in Journal of Chemical Physics, titled as "The effect of soft repulsive interactions on the diffusion of particles in quasi–one–dimensional channels: A hopping time approach." by S. Ahmadi, M. Schmidt, R. J. Spiteri, and R. K. Bowles [1].

- Chapter 4 addresses the third question and investigates the potential application of SFD in the crossover regime for the separation of chiral molecules confined to chiral channels. Different enantiomers confined to a chiral channel may exhibit different hopping times, because they have different free energy barriers while attempting to pass each other which would lead to different hopping times for each component that could be used for separation. This idea is tested by calculating the free energy barriers for hopping of a chiral molecule confined to chiral carbon nanotubes.

- Chapter 5 includes the conclusion remarks and proposals for future studies.

1.7 Description of the Candidate's Contribution

The Ph.D. candidate is the primary lead of the current research work along with supervision of Dr. Richard K. Bowles.

For the second and third chapter of the thesis, the Ph.D. candidate performed the analytical derivation of the partition function for the systems that were studied. She performed all the simulation work and

the data analysis of the result with help provided by Dr. Bowles. The results of the second chapter have been published in Journal of Chemical Physics, titled as "Diffusion in quasi-one-dimensional channels: A small system n,p,T transition state theory for hopping times." by S. Ahmadi and R. K. Bowles [5]. The results of the third chapter have been published in the Journal of Chemical Physics, titled as "The effect of soft repulsive interactions on the diffusion of particles in quasi–one–dimensional channels: A hopping time approach." by S. Ahmadi, M. Schmidt, R. J. Spiteri, and R. K. Bowles [1]. As indicated above, the PhD candidate is the primary author of the paper, and the second author of the paper is M. Schmidt, from Dr. R. J. Spiteri's group. M. Schmidt contributed by performing the free energy optimization described in Sections 3.2.4 and 3.3.4. The Ph.D. candidate was involved in performing all the other simulation work and also analyzing and interpreting the results obtained from the simulation and optimization.

For the fourth chapter of the thesis, the Ph.D. candidate defined the model and developed all the methodology to simulate the diffusion of enantiomers. She primarily conceptualized all the result with the help provided by Dr. Bowles. The results from the fourth chapter are being prepared for publication.

Chapter 2

A Transition State Theory for Hopping Time

2.1 Introduction

The goal of this chapter is to develop a method which is capable of the quantitative calculation of hopping times, using the principles underlying transition state theory. The key element in achieving the quantitative prediction of the hopping time is the calculation of the barriers associated with particles passing each other. To evaluate the method, two relatively simple systems will be studied, a two–dimensional (2d) ideal gas system and a 2d hard discs system. These confined hard discs systems provide a simple model to study the properties of confined fluids while making the analytic calculations tractable.

In this work, it will be shown that the free energy barrier calculations, using the small n, p, T ensemble approach, provide a good estimation of the hopping times for both systems studied. For the case of the ideal gas model, the method is in agreement with the hopping time theory and can successfully predict the hopping time behavior for the entire range of channel radii. For the case of the 2d hard discs system, the model works well when the channels are sufficiently narrow, however, it breaks down when the channels becomes wider. The results of the work described in this Chapter have been published in reference [5].

The chapter is organized as follows: Section 2.2 provides a detailed description of deriving the partition functions for the systems studied in this work, the 2d ideal gas and 2d hard disc systems, using the small system n, p, T approach, and developing a transition state model for quantitative analysis of hopping times for confined fluids. The 2d ideal gas system is defined as point like particles located in a 2d channel, and 2d hard disk system is defined as disc like particles with diameter σ located in a 2d channel. Section. 2.3 gives a description of the simulation techniques used in this work to calculate the free energy barriers associated with two particles passing each other, the hopping times kinetic prefactor calculations using the two particle system, and the direct measurement of the hopping times for large systems. Section 2.4 outlines the results and application of the proposed model to both systems. Section 2.5 contains the discussion based on the obtained results.

2.2 Developing a Transition State Theory Model for Hopping Times

2.2.1 Free Energy Barrier Calculations for Hopping Times

What happens in a very small fraction of phase space is an important factor in determining the rate of activated processes like chemical reactions, which is well described by TST despite its relative simplicity. In single file diffusion when the particles are diffusing in a sufficiently narrow tube, the hopping event is the rate limiting step. Since the probability of having both particles cross each other at the transition state is a rare event, calculating the barrier–crossing rate, which is inversely related to the hopping time, with good statistical accuracy will not be feasible even in a very long simulation. Here, a Transition state theory is developed, which involves calculating the height of free energy barrier associated with the activated process of two particles, as well as determining the kinetic prefactor.

Phenomenologically, the time it takes for a hopping event to occur, by a particle jumping over the cage created by its local neighbors, is inversely proportional to the rate and is given by,

$$\tau_{hop} = \frac{1}{\vartheta \exp(-\beta \Delta G^*)} = \frac{A}{P^*} = A e^{\beta \Delta G^*}, \tag{2.1}$$

where ϑ is a kinetic prefactor (see Eq. 1.22), ΔG^* is the height of the Gibbs free energy barrier when two particle are passing each other at the TS, A is the hopping time prefactor which is defined as $1/\vartheta$, and P^* is the probability of finding the system in the transition state.

Figure 2.1(b) illustrates how the the small n, p, T system is used in this work to study the TST free energy barrier associated with particles passing each other in a quasi-one dimensional channel by hopping past one of their neighboring particles. In this study, the system consists of $n = 2$ particles confined to a long, uniform, two dimensional channel which extends longitudinally along the $x-$axis and has a radius R_p in the $y-$axis. The center of the channel is located at the point r_0 and the shell particle is located at $+L/2$ so that the total length of the cell is L. The cell's volume in two dimension is defined $v = 2R_pL$. The channel radius is kept fixed so that fluctuations in the volume will be associated to the longitudinal displacement of the shell particle and are given by [5],

$$dv = 2R_p dL. \tag{2.2}$$

The small system isobaric–isothermal partition function given by Eq. 1.53 then becomes,

$$\Delta = \int Q^*_{n,v} e^{-\beta p_l 2R_p L} 2R_p dL, \tag{2.3}$$

where p_l is the longitudinal pressure acting on both ends of the channel [104]. Particle 1 is the shell particle, the location of which determines the boundary at one end of the cell and the integration of the shell particle over its $y-$axis degree of freedom results in $2R_p$ factor in the integral.

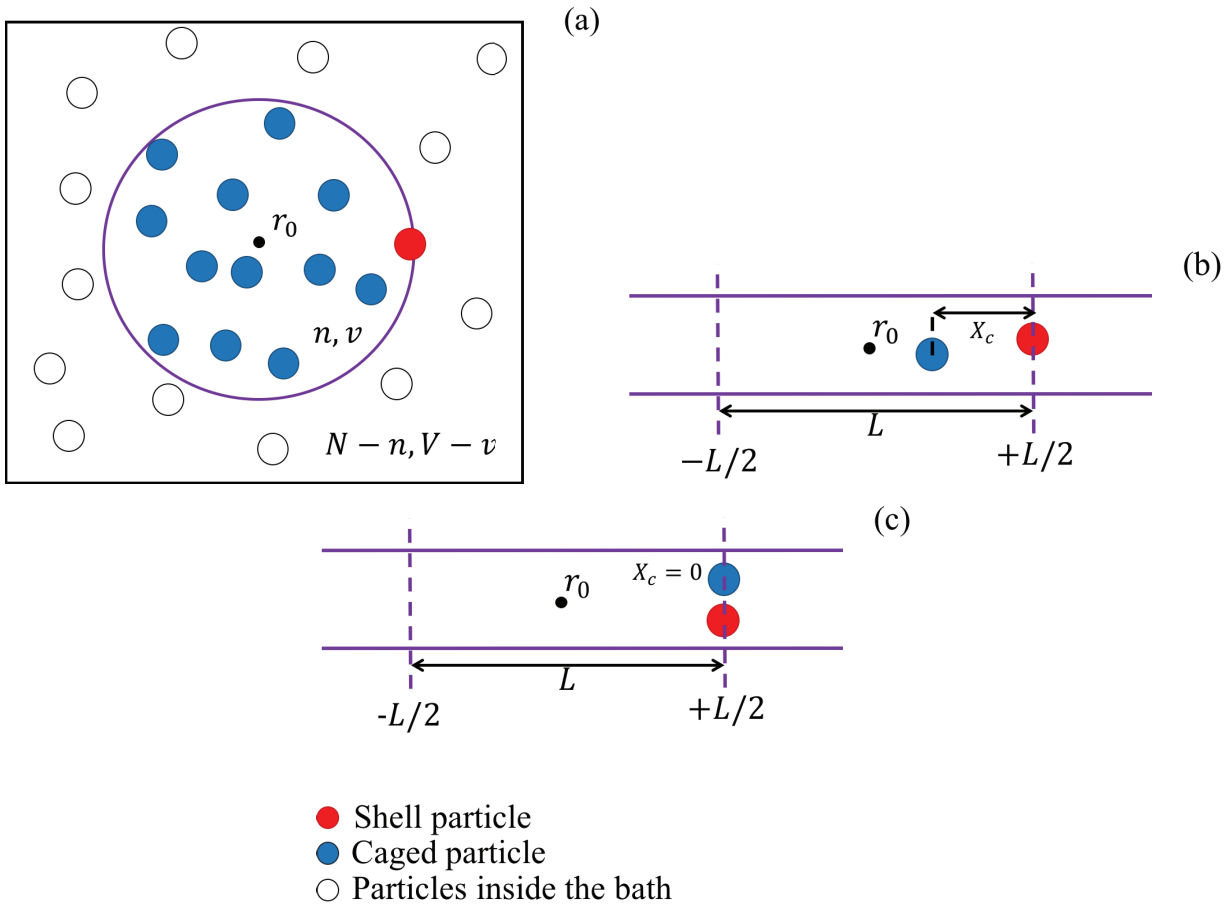

Figure 2.1: (a) A configuration of a macroscopic canonical system divided into a small subsystem of n particles with volume v and temperature T, centered at r_0, with a shell molecule, and the remaining $N-n$ particles located in volume $V-v$ and temperature T in the surroundings. (b) The two dimensional small n, p_l, T ensemble, centered at r_0, with a shell particle located at $L/2$ and the caged particle located at a longitudinal distance from the shell particle, x_c. (c) The transition state, for the hopping process, where $x_c = 0$ [5].

.

Particle 2 in our system represents the caged particle. The reaction coordinate for the hopping process is defined as the longitudinal separation of the caged particle from the shell particle along x axis, $x_c = x_1 - x_2$, and as shown in Fig. 2.1(c) the transition state occurs at $x_c = 0$. To obtain the configuration space associated with specific points, $\Delta_{x_c'}$, anywhere along the reaction coordinate, a delta function is applied to Eq. 2.3 as

$$\Delta_{x_c'}\, dx_c = \int_L Q^*_{n,v,T}\, e^{-\beta p_l 2R_p L}\, \delta(x_c' - x_c) 2R_p\, dL, \tag{2.4}$$

such that

$$\int \delta(x_c' - x_c) dx_c = \begin{cases} 1 & \text{if } x_c' = x_c \\ 0 & \text{if } x_c' \neq x_c. \end{cases} \tag{2.5}$$

The partition function for the system can be obtained via

$$\Delta = \int_{x_c} \Delta_{x_c}\, dx_c. \tag{2.6}$$

The probability of having the caged particle at x_c' is then,

$$P(x_c')\, dx_c = \frac{\Delta_{x_c'}\, dx_c}{\Delta}, \tag{2.7}$$

where $P(x_c')$ is a probability density and

$$\int_0^\infty P(x_c)\, dx_c = 1. \tag{2.8}$$

Finally, the Gibbs free energy barrier for particle hopping, ΔG^*, is directly related to the probability of finding the caged particle in the transition state by,

$$\beta \Delta G^* = -\ln P^* \tag{2.9}$$

where

$$P^* = \int_0^{x_c^*} P(x_c) dx_c, \tag{2.10}$$

and the transition state region is defined as the distance located within the range of the reaction coordinate, $x_c = 0 - x_c^*$. Since the configuration space of the transition state is a restricted subset of all the possible configurations available to the system, the work required to bring the caged particle from anywhere in the cage into the transition state will always be positive and is represented by ΔG^*. As shown in the case of heterogeneous nucleation [105], using the entire configuration space accessible to the system as the reference state in calculating the energy barrier, results in remarkable improvement in calculating rates using TST [5].

The dividing surface, TS, between two neighboring particles that are trying to pass each other occurs at $x_c = 0$, along the reaction coordinate. However, a transition region within x_c^* can be defined to ensure that the probability P^* in Eq. 2.9 remains dimensionless, rather than representing a probability density. In this work, the size of the transition region, x_c^*, was selected to be small relative to the size of the fundamental

particle motion which is responsible to move the particle from one side of the TS to another with high probability. If x_c^* is chosen to be too large, then the transition state will include the configurations that do not contribute to the barrier crossing, which would lead to poor and most likely under estimation of the hopping time [5].

It should be mentioned that the system consists of only two particles so there is only one transition state for each hopping event. It could be argued that the local cage for a central particle should be defined by two particles, one on each side, which will give rise to two transition states. However, each transition state involves two particles, and when they pass each other they both escape their cages for each hopping event. Therefore, we only need to count one transition per caged particle. In addition, adding the third particle to the system would require the use of two shell molecules to define the volume which would make the analysis more complicated. Due to the symmetry of the system, adding the third particle would also complicate the definition of reaction coordinate, which measures the longitudinal distance between the caged particle and the shell particle [5].

According to transition state theory, the hopping time is a product of two factors: (1) the hopping prefactor A and (2) the free energy barrier at transition state (see Eq. 2.1). The free energy barrier is related to the probability of finding the system in the transition state, and the hopping prefactor A is related to the rate at which two particles pass each other at the transition state, barrier crossing rate.

The Bennett–Chandler scheme [84, 106, 107] is applied to compute the crossing rate for a transition between two states, A and B, that are separated by a free energy barrier and produces a more general approach that reduces to TST. Based on the Bennett-Chandler scheme the reaction can be describes as a first-order phenomenological rate law:

$$\Delta P_A(t) = \Delta P_A(0) e^{-t/\tau}, \tag{2.11}$$

where P_A is the probability of having the system in state A and $\Delta P_A(t)$ stands for the difference between P_A and its equilibrium value at time t. To quantitatively formulate the rate, it is necessary to determine the characteristic n_A and n_B functions, which specify whether the system is in state A or state B. A reaction coordinate for the system is defined in a way that connects the two states together. Considering x_c^* as the reaction coordinate at the transition state that separates state A from state B, the characteristic function is defined as,

$$n_A = \Theta(x_c^* - x_c), \tag{2.12}$$

$$n_B = \Theta(x_c - x_c^*), \tag{2.13}$$

where Θ is the Heaviside function [108]. The following microscopic expression can be used to determine the rate constant, k_{AB} [109]:

$$k_{AB} = \frac{\langle \dot{x_c} \delta(x_c - x_c^*) \Theta(x_c(t) - x_c^*) \rangle_{eq}}{\Theta(x_c^* - x_c)} = M(t), \tag{2.14}$$

where δ is the Dirac delta function, $\dot{x_c}$ is the velocity of the tragectories at the TS , and $M(t)$ is the time correlation function and explicitly depends on time. However, k_{AB} does not depends on time so Eq. 2.14 is only valid if and when $M(t)$ reaches a constant value after an initial transitory period [84, 109].

For a Markov process, and under the assumption of a perfect reaction coordinate, and ideal crossing events, where the particles do not recross the barrier to their initial state, transition state theory can provide a good estimation for the transition rate, using the free energy and the average velocity of the particles at the top of the energy barrier [85, 109]. Under this assumption, the crossing rate can be calculated by taking the limit $t \to 0^+$ in the expression for the transition rate in Eq. 2.14 [108]:

$$\begin{aligned} k_{TST} &= \lim_{t \to 0^+} M(t) \\ &= \frac{\left\langle |\dot{x_c^*}| \right\rangle_{eq}}{2} P_0(x_c^*) \\ &= \frac{\langle |v_c^*| \rangle_{eq}}{2} P_0(x_c^*). \end{aligned} \tag{2.15}$$

and the hopping time is directly connected to the transition rate, k_{TST}, as follows

$$\tau_{hop} = \frac{1}{k_{TST}}. \tag{2.16}$$

The first contribution in the Eq. 2.15 is the average flux of the trajectories over the top of the barrier, $\langle |v_c^*| \rangle$, and the second term is the probability density of finding both particles at the top of the barrier [108]. The method for calculating the free energy barriers or probabilities was already described, using the two particle small n, p_l, T ensemble, therefore, the remaining challenge is to calculate the average flux of the trajectories over the top of the barrier. This can be achieved in simulation by considering an ensemble of configurations located in the transition state and measuring the time evolution of x_c [1].

It should be mentioned that those trajectories that recross the free energy barrier should ideally not contribute to the transition rate, k_{AB}. However, k_{TST} includes the trajectories that recross the barrier as well. Therefore, the TST approach overestimates the true crossing rate which leads to a lower predicted hopping times. The barrier recrossing is a classic problem in TST and there are many advanced methods in the literature [110, 111, 112, 113, 114, 115, 116] that are quantifying the recrossing effects.

2.3 Simulation Method

2.3.1 Free Energy Barrier Calculations

Corti [94] showed that the shape of the small system volume, which also represents the simulation cell, affects the probability of a trial MC move being accepted in the small n, p, T ensemble. In this study, the

interactions between the particles in the cell and those in the surroundings, U_σ, are neglected and only the case of n particles confined to the two dimensional channel described in Fig. 2.1(b) is considered in calculating the partition function for the system, which can be written as [5]

$$\Delta = \frac{1}{(N-1)!\Lambda^{2n}} \times \int\int\int\int e^{-\beta U_n} e^{-\beta p_l 2R_p L} dL dy_1 dx^{n-1} dy^{n-1}, \tag{2.17}$$

where degrees of freedom of the $n-1$ particles are defined by the integrals over the $dxdy$ coordinates of the $n-1$ particles within the small system, the degrees of freedom of the shell particle over the diameter of the channel is defined by the integral over dy_1, and the degrees of freedom of the shell particle associated with the volume of the cell is defined by the integral over dL. If a scale factor $x_i = L\bar{x}_i$ is introduced, then Eq. 2.17 can be expressed as [5],

$$\Delta = \frac{1}{(N-1)!\Lambda^{2n}} \times \int\int\int\int L^{n-1} e^{-\beta U_n} e^{-\beta p_l 2R_p L} dL dy_1 d\bar{x}^{n-1} dy^{n-1}, \tag{2.18}$$

where U_n becomes a function of the scaled coordinate system. There is no need to rescale the $y-$coordinates when the shell particle moves, because only changes in the longitudinal dimension of the shell particle (the cell) has an effect on the volume fluctuations. The probability of finding the system in a configuration specified by $\bar{x}^n, y^n$, in a volume with the cell length in the range L to $L+dL$, is then [5],

$$P(\bar{x}^n, y^n; L)dL \propto L^{n-1} e^{-\beta U_n} e^{-\beta p_l 2R_p L} dL, \tag{2.19}$$

and the acceptance probability for a trial move from an old to a new configuration in the MC simulation becomes,

$$\begin{aligned} \mathrm{acc}(\mathrm{old} \to \mathrm{new}) = \min(1, \exp\{ &- \beta[U_n^{\mathrm{new}} - U_n^{\mathrm{old}}] \\ &- \beta p_l 2R_p[L^{\mathrm{new}} - L^{\mathrm{old}}] + (n-1)\ln[L^{\mathrm{new}}/L^{\mathrm{old}}] \}). \end{aligned} \tag{2.20}$$

Although the analysis is applied to the two dimensional channels studied here, Eq. 2.20 can be extended for studying three dimensional, quasi-one dimensional channels, by including an appropriate geometric factor for the channel cross section in the pressure-volume term, as long as fluctuations in the volume only involve changes in L.

Using MC simulation, the probability, $P(x_c)dx$, of finding the caged particle in a volume dx at a longitudinal distance x_c from the transition state is calculated directly. The small isobaric–isothermal simulations are performed by confining $n = 2$ particles to a channel with radius, R_p, and length, L, under the condition $\beta = 1$ and $\beta p_l = 1$. The volume of the small system, with its center located at the origin, is defined by particle one, which is the shell particle, and is located at $L/2$. The second particle, caged particle, is placed within the cell between $-L/2$ and $L/2$. The MC moves for the two dimensional ideal gas and two dimensional hard discs are proceed as follows: After a random selection of a particle, it is moved randomly by a step δx and δy, up to a maximum displacement of $|\Delta x| = |\Delta y| = 0.05\sigma$. If the trial displacement of a particle results

in an overlap with another particle or causes the particle to leave the channel, the move is immediately rejected. When the shell particle is chosen, the trial move will also change the volume, by changing L by $2\delta x$ and the position of the second particle, the caged particle, needs to be rescaled to ensure it remains inside the sub–volume. At the end of each move, the probability of accepting the move is determined using Eq. 2.20. It should be mentioned that in order to have a positive volume so that $v > 0$, the position of the shell particle must remain positive during the simulation. For each state point studied, 2×10^7 MC cycles are used to obtain equilibrium and data is collected over the next $10^8 - 10^9$ MC cycles, depending on the total number of data points collected at the transition state. Each MC cycle consists of $n = 2$ MC moves. Simulation runs were sufficiently long to ensure the transition state region, $x_c < \Delta x_c$, was sampled at least 100 times. The configurations are sampled at every 1000 MC cycles to ensure that they are not correlated. The probability is calculated by building a histogram of configurations versus the reaction coordinate using bin sizes of $\Delta x_c = x_c^* = 0.005\sigma$ for the ideal gas and $\Delta x_c = x_c^* = 0.03\sigma$, and $\Delta x_c = x_c^* = 0.05\sigma$ for the hard discs. The probability densities are calculated by dividing the probabilities by the bin size, Δx_c [5].

2.3.2 Crossing Rate Calculations and Simulation Details

According to Eq. 2.15 and as mentioned earlier in Section 2.2, the crossing rate, k_{TST}, is the product of two contributions, the average velocity of the particles at the top of the energy barrier and the probability of having the system at TS. The MC simulation details for calculating the probabilities at the transition state are provided in Section 2.3.1. In order to calculate the average flux of the trajectories over the top of the barrier at the equilibrium, it is necessary to generate weighted configurations at the transition state, within x_c^*, after the system reaches equilibrium. The n, p_l, T system, is used to generate the weighted configurations. The average flux of the trajectories for the system is calculated using a N, V, T ensemble simulation for two hard discs over the range of channel radii, $R_p = 1.01 - 1.2$. In this system, the average velocity is equal to the average displacements of the reaction coordinate, and is calculated via

$$\langle v_c^* \rangle = \left\langle \frac{|x_c(t + \Delta t) - x_c(t)|}{\Delta t} \right\rangle, \tag{2.21}$$

where $x_{c(t=0)} = x_{1(t=0)} - x_{2(t=0)}$ is the particles longitudinal distance from each other before the MC moves start, and $x_{c(t=1)} = x_{1(t=1)} - x_{2(t=1)}$ is the reaction coordinate at $t = 1$. The average in Eq. 2.21 is taken over the 800 initial configurations generated by the small n, p_l, T ensemble simulation. To obtain $\langle v_c^* \rangle$, the canonical ensemble (N, V, T), simulations with two hard discs, $N = 2$, are used with the standard Metropolis MC scheme [85] and the particles are moved as a simple approximation to Brownian motion [117]. The MC simulation is performed as follows: configurations at the transition state are used as the starting configurations for the MC simulations. The unit of time for the MC simulation is defined as $N = 2$ attempted particle moves and each simulation is performed for one time step, $\Delta t = 1$. For each starting configuration,

one particle is selected randomly and is moved by a step δx and δy, up to a maximum displacement of $|\Delta x| = 0.06\sigma$ and $|\Delta y| = 0.12\sigma$. The move is immediately rejected if the trial displacement causes any of two particles to overlap with each other or with the hard wall. According to the standard Metropolis MC probabilities, the probability of accepting a trial move from an old to a new configuration is calculated by:

$$\text{acc}(\text{old} \rightarrow \text{new}) = \min\left(1, \exp\left\{-\beta[U_n^{\text{new}} - U_n^{\text{old}}]\right\}\right). \tag{2.22}$$

2.3.3 Hopping Time Calculations

The hopping time is defined as the average time that a particle requires to pass one of its caging nearest neighbors in a single file system, and can be calculated using MC simulations performed in the canonical ensemble. The hard disc system consists of $N = 500$ particles, with diameter σ, and confined to a two dimensional channel. The channel has a radius R_p along the y–axis and length L along the x direction, with periodic boundaries that are applied longitudinally. The standard Metropolis MC scheme [85], which is applied as a simple approximation to Brownian motion [117] is used to move the particles during the simulation. A MC trial move involves the random selection of a particle, which is moved by a random selection of a trial step in both the x– and y–directions up to a defined maximum step size. For hard disc system, the hopping time, $\tau_{hop}(sim)$, calculations are performed under two different dynamics (step size): one with a maximum step size of $|\Delta x| = |\Delta y| = 0.05\sigma$ and the other one with maximum step size of $|\Delta x| = 0.06, |\Delta y| = 0.12\sigma$. If the trial move causes a particle to overlap with another particle or with the wall it will be rejected, and the particle will be returned to its original position, otherwise it will be accepted. Each MC cycle is counted as a unit of time during the simulation and is comprised of N MC trial moves. For hard discs system, in order to avoid particles overlap at the beginning of the simulation, they are placed evenly along the channel and placed randomly across the tube in a way that they do not overlap, then the system is equilibrated over 2×10^7 MC cycles. Before the data collection, each particle's cage was identified as their immediate left and right neighboring particles, and the particles initial hopping times is set to zero. Each particle's hopping time is calculated by counting the number of MC cycles that it takes for the particle to escape its cage. At the end of each MC cycle, if a particle jumps out of its cage the hopping time for the particle is recorded, then is reset to zero, and the new caging neighbors for the particles are identified. Data is collected over 5×10^7 MC cycles and the average hopping time, τ_{hop}, is calculated over all hopping times recorded for all particles. The ideal gas system consists of $N = 100$ particles, with diameter $\sigma = 0$, and confined to a two dimensional channel. For the ideal gas system, the hopping time calculations are performed with a maximum step size of $|\Delta x| = |\Delta y| = 0.01\sigma$ and data is collected over 5×10^7 MC cycles [5].

The direct measurements of the hopping time, $\tau_{hop}(sim)$, obtained using the N, V, T ensemble, must be performed at a thermodynamic state point consistent with the pressure used in the free energy calculations.

To obtain the correct state point, the density associated with each system with a different radius is calculated separately using the n, p_l, T ensemble where $\beta p_l = 1.0$, $n = 1000$, and 10^8 MC cycles are used after the system reaches the equilibrium. MC simulations for the density calculations involves the random selection of a particle, which is moved by a random selection of a trial step in both the x– and y–directions up to a maximum step size of $|\Delta x| = |\Delta y| = 0.05 - 0.1\sigma$ to ensure 80% of the trial moves are accepted. The shell particle approach is used. The average volume, $\langle V \rangle$, for each system is obtained by sampling the data at every $10,000$ MC steps and the density for each system is calculated as $\rho = N/\langle V \rangle$, for both the ideal gas and hard disc systems. Table 2.1 shows the density range, $\rho = N/\langle V \rangle$, obtained for both the ideal gas and hard disc systems at the different radii. The density range calculated for the hard disc system using only two particles is $\rho = 0.54 - 0.65$, which is significantly higher than that obtained for the large system. This results from the lack of interactions with the surrounding in the two particle system, allowing the system to sample smaller volume configurations that would be inaccessible if more particles were present. When the density is calculated for a system of three particles in the n, p_l, T ensemble, the density range reduced to $\rho = 0.47 - 0.53$. This suggests that for hopping time calculations using the two–particle system could be improved by accounting for the interactions between the small system and the surroundings, i.e., by inclusion of U_σ [5].

In addition, the small n, p_l, T ensemble lacks the periodic boundary condition and the interaction of the particles are limited to those inside the sub–volume. This results in an over estimation of the densities if the system size is too small. To illustrate the importance of achieving a large enough system size for the density calculations, the equation of state is calculated for the 2d hard disc systems with different number of particles and is compared with the analytical result obtained for the same system using the transfer matrix method, with $R_p = 0.55 - 0.93$ [6]. Fig. 2.2 shows the simulation result obtained for the equation of state for the 2d hard disc system, $p_l V/nk_B T$, as a function of the occupied volume, $\phi = n\pi\sigma^2/4V$, using different numbers of particles inside the small n, p_l, T system, $n = 3 - 100$, at $R_p = 0.55$ and over a wide range of pressures, $p_l = 1 - 60$. In this figure, the solid line represents the analytical result obtained for the 2d hard disc system, using the transfer matrix method [6], developed by Kofke *et al.* [104]. To ensure good estimates of the pressure, a system size of $N = 500$ particles was used [5].

Systems	R_p/σ	ρ
2d-ideal gas	1.1-1.2	1.00
2d-Hard discs	1.01-1.2	0.27-0.30

Table 2.1: Densities for the idea gas and hard sphere systems for different radii, at $\beta p = 1.0$.

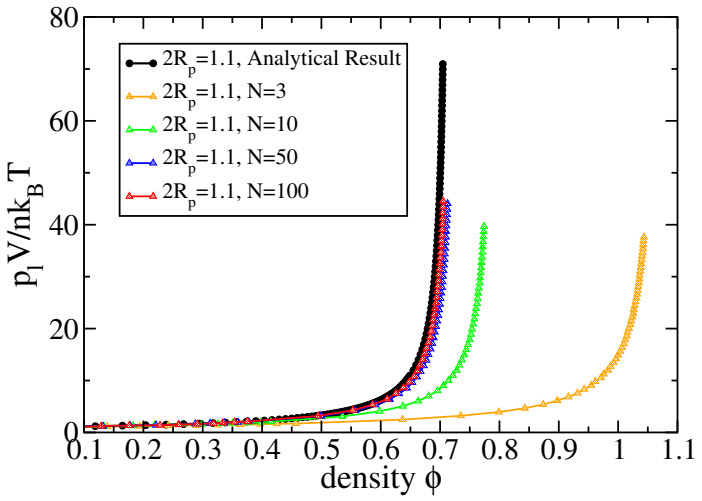

Figure 2.2: The equation of state for the 2d system of hard discs in a 2d channel with hard walls as a function of occupied volume, ϕ. The round symbols represent the analytical result obtained using a transfer matrix method [6] and the triangle symbols represent the simulation result obtained from the small n, p_l, T ensemble method.

.

2.4 Results

2.4.1 Two–dimensional Ideal Gas Systems

The hopping barrier is first calculated for a two-dimensional ideal gas system, when the particles have no interactions so that $U_\sigma = U_n = 0$. Also, the particles are confined between $-R_p$ and R_p due to their hard interaction with the walls. The reaction coordinate partition function for this system can be written as [5],

$$\Delta_{x_c} dx_c = \frac{dx_c}{\Lambda^4} \int_{-R_p}^{+R_p} \int_{-R_p}^{+R_p} \int_{x_c}^{\infty} e^{-\beta p_l 2R_p L} \, dL dy_1 dy_2. \tag{2.23}$$

In Eq. 2.23, the position of the caged particle bounds the length of the cell in its lower limit. Solving the integrals over y_1 and y_2 independently and then integrating the result over L gives,

$$\Delta_{x_c} dx_c = \frac{2R_p}{\Lambda^4} \frac{e^{-\beta p_l 2R_p x_c}}{\beta p_l} \, dx_c. \tag{2.24}$$

The full partition function for the system can then be obtained by integrating over the remaining x_c coordinate to yield

$$\begin{aligned} \Delta &= \frac{2R_p}{\beta p_l \Lambda^4} \int_0^{\infty} e^{-\beta p_l 2R_p x_c} \, dx_c \\ &= \frac{1}{\beta^2 p_l^2 \Lambda^4}. \end{aligned} \tag{2.25}$$

Calculating the system volume, using the partition function obtained in Eq. 2.25, demonstrates that the correct partition function for the system was obtained. The system's volume is given by

$$V = 2R_p \langle L \rangle = -\frac{1}{\beta}\left(\frac{\partial \ln \Delta}{\partial p_l}\right)_{n,T} = \frac{2}{\beta p_l} = \frac{n}{\beta p_l}, \tag{2.26}$$

which is the expected equation of state for an ideal gas [4].

The probability of finding the caged particle at a point x_c along the reaction coordinate is obtained by using Eqs. 2.24 and 2.25 in Eq. 2.7 as,

$$P(x_c)dx_c = \beta p_l 2R_p \, e^{-\beta p_l 2R_p x_c} \, dx_c. \tag{2.27}$$

The probability of finding the caged particle within a region dx_c of the transition state, where $x_c = 0$, is then,

$$P(0)dx_c = \beta p_l 2R_p dx_c. \tag{2.28}$$

Figure 2.3 shows that the free energy density, $-\ln P(x_c)$, increases linearly as a function of x_c, with a slope of $\beta p_l 2R_p$, which reflects the fact that increasing x_c increases the lower bound on the accessible volume fluctuations, and restricting the total number of configurations available to the system. Even though it might seem that the hopping process for an ideal gas particle is "barrier–less", it actually takes work to restrict the two particles to the transition state region relative to having the caged particle located anywhere within the small system volume. This necessarily requires a positive free energy barrier ΔG^*, given by Eq. 2.9, which includes an integral of the normalized probability over a small region of the reaction coordinate in the transition region. It can also be seen in Fig. 2.3 that the probability density obtained from the simulations match the results obtained from the exact analysis, which is not surprising for such a simple problem, but it provides a proof of principle and suggests that the simulation approach is capable of being applied to systems with more complicated particle–particle and particle–wall interactions [5].

Figure 2.4 shows a plot of $\ln \tau_{hop}(sim)$, which is obtained from $N = 100$ particle hopping time simulations, versus the analytical free energy barrier calculations for two ideal gas particles hopping at the TS over the entire range of channel radii studied, Eqs. 2.27 and 2.9 were used, with $x_c^* = 0.005$. The slope of one for this plot confirms that our TST approach, using the small system isobaric–isothermal ensemble, has a potential to be used for hopping times calculations in quasi–one dimensional systems. The intercept results in the kinetic prefactor $A = 0.90$ which is related to the velocity of the particles moving out of the transition state region. Equation 2.28, with Eq. 2.1, suggests that τ_{hop} for the two–dimensional ideal gas particles should vary linearly as R_p^{-1}, with a slope $\sim A/2\beta p_l x_c^*$ (see Fig. 2.5) [5].

2.4.2 Two–dimensional Hard Discs System

Here the free energy barriers associated with two hard discs passing each other while diffusing inside a two–dimensional channel with hard walls is calculated [5]. Due to the particle–particle exclusion effect arising

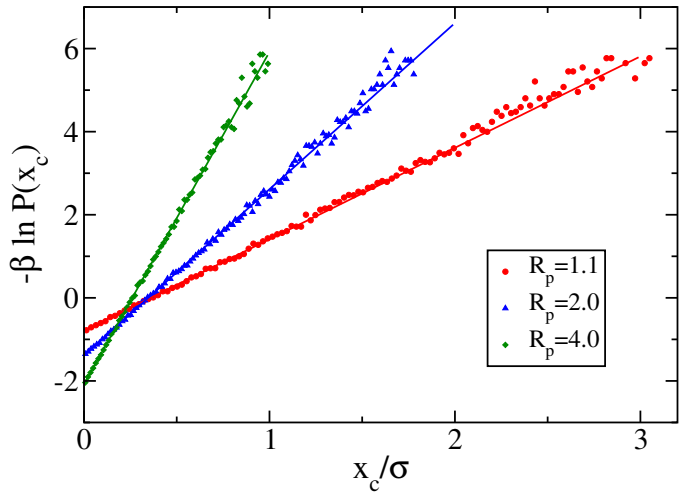

Figure 2.3: Free energy density, $-\ln P(x_c)$ as a function of the reaction coordinate, x_c, over a range of pore radii at fixed pressure, $\beta p_l = 1.0$, for the 2d ideal gas system. The solid lines represent results from the theory (see Eq. 2.27). The points represent the data obtained from simulation (see Section 2.3 for details) [5].

.

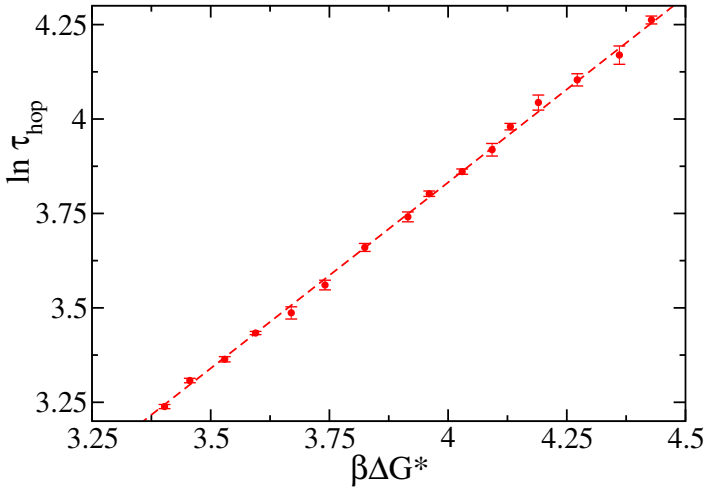

Figure 2.4: ln τ_{hop} as a function of $\beta\Delta G^*$ for the 2d system of ideal gas particles for different pore radii, $R_p = 1.1 - 4.0$, obtained from simulation. The dashed line is the best linear fit to the data and has a slope of 0.98. The error bars represent the standard deviation in the measured hopping times [5].

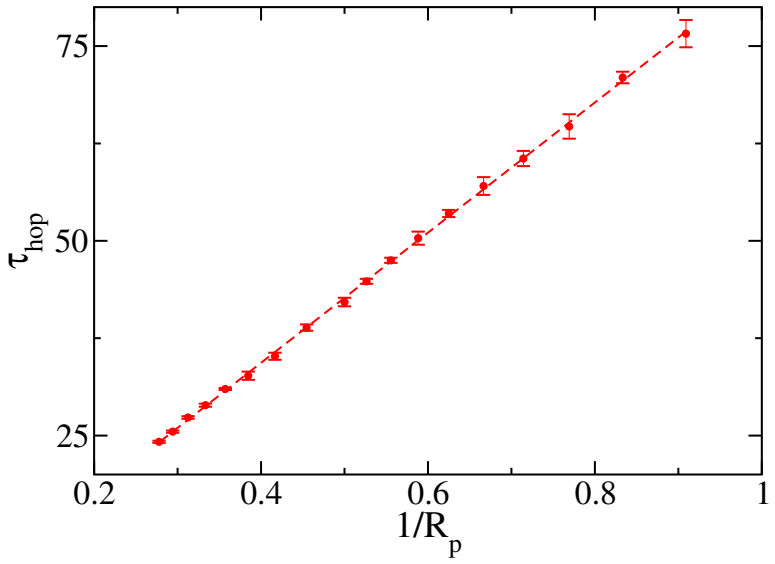

Figure 2.5: τ_{hop}, as a function of the inverse channel radius $1/R_p$, for the 2d system of ideal gas particles. The dashed line is a linear fit to the data with a slope of 83.6. The error bars represent the standard deviation in the measured hopping times [5].

from the hard interaction between the particles, it will be more difficult for the particles to escape their cage when the channel width becomes narrower. For this system, the particle–particle interaction is defined as

$$U_{HD}(r_{ij}) = \begin{cases} 0 & \text{if } r_{ij} \geq \sigma, \\ \infty & \text{if } r_{ij} < \sigma, \end{cases} \tag{2.29}$$

where σ is the diameter of the hard particles and $r_{ij} = |\mathrm{r}_i - \mathrm{r}_j|$ is the the distance between two particles. The particle–wall interaction is given by,

$$U_{WHS}(\hat{r}_{ij}) = \begin{cases} 0 & \text{if } |y_i| \leq R_p - \sigma/2, \\ \infty & \text{if } |y_i| > R_p - \sigma/2, \end{cases} \tag{2.30}$$

where y_i is the y–coordinate of the particle. The low pressure cases are considered in this work, where the interactions between the particles inside the sub–volume and those in the surrounding can be neglected. Setting $U_\sigma = 0$ then makes the solution to the small system n, p_l, T partition function analytically tractable. The reaction coordinate partition function for this system is then given by [5],

$$\begin{aligned} \Delta_{x_c} dx_c &= \frac{2dx_c}{\Lambda^4} \int_{x_c}^{\infty} e^{-\beta p_l 2R_p L} dL \int_{-R_p+\frac{\sigma}{2}+\sigma_2}^{R_p-\frac{\sigma}{2}} dy_1 \int_{-R_p+\frac{\sigma}{2}}^{y_1-\sigma_2} dy_2 \\ &= \frac{(2R_p - \sigma - \sigma_2)^2}{\Lambda^4 \beta p_l (2R_p - \sigma)} e^{-(2R_p-\sigma)\beta p_l \ x_c} dx_c, \end{aligned} \tag{2.31}$$

where,

$$\sigma_2 = \begin{cases} \sqrt{\sigma^2 - x_c^2} & \text{if } |x_c| \leq \sigma, \\ 0 & \text{if } |x_c| > \sigma. \end{cases} \tag{2.32}$$

The factor of two appears in the reaction coordinate partition function to count the configurations for which the order of particle 1 and 2 in the y–coordinate is reversed. Integrating Eq. 2.31 over x_c and considering the pairwise nature of σ_2 yields [5],

$$\Delta = \frac{1}{\beta^2 p_l^2 \Lambda^4} \left[1 + \frac{2e^{-\beta p_l (2R_p - \sigma)} \left[\beta p_l \sigma (2R_p - \sigma) + 1 \right] + \beta^2 p_l^2 \sigma^2 (2R_p - \sigma)^2 - 2}{(2R_p - \sigma)^4} - \frac{\pi \sigma [I_s(z) - L_s(z)]}{2R_p - \sigma} \right], \tag{2.33}$$

where $I_s(z)$ is the modified Bessel function of the first kind, and $L_s(z)$ is the modified Stuve function, both with $s = 1$ and $z = \beta p_l \sigma (2R_p - \sigma)$ [118].

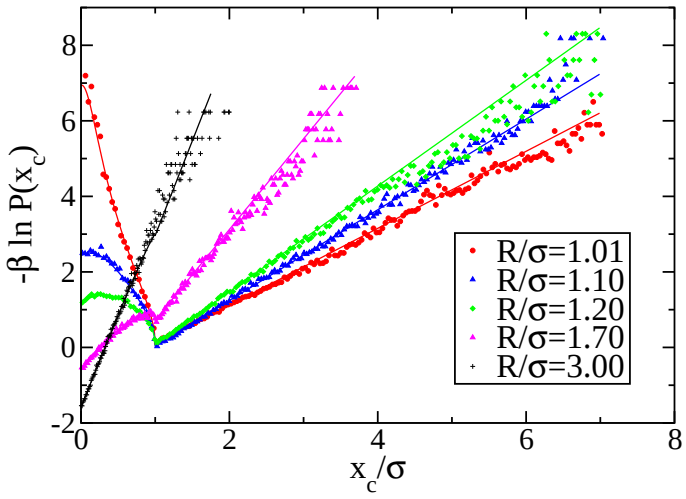

Figure 2.6: Free energy density, $-\ln P(x_c)$ as a function of x_c, at fixed pressure, $\beta p_l = 1.0$, over radius of $R_p/\sigma = 1.01 - 3$ for the 2d hard disc system. The solid lines represent results from the theory and the points represent the data obtained from the simulation [5].

.

Figure 2.6 shows the probability density, $-\ln P(x_c)$, as a function of x_c for the channels with radius in the range $R_p/\sigma = 1.01 - 3$. For all the radii, where $x_c > \sigma$ the two discs behave like the particles in the ideal gas system because in this region they do not exclude volume with respect to each other. When $x_c < \sigma$, the volume exclusion of the two discs results in a restriction in configuration space. However, the volume exclusion effect becomes negligible when the channel diameter is wide and the free energy density behaves close to linear in the region $x_c < \sigma$. By decreasing the channels diameter, in the region where $x_c < \sigma$, there

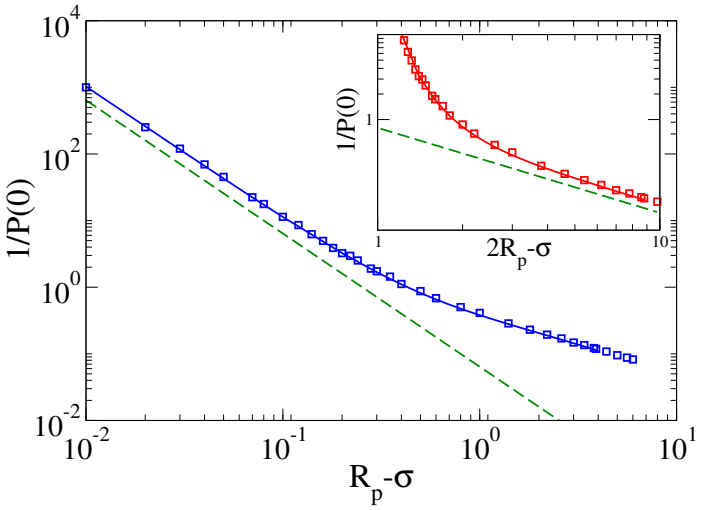

Figure 2.7: Log–Log plot of $1/P(0)$ as a function of the discs passing threshold, $R_p - \sigma$. The solid line shows the theoretical results obtained from Eq. 2.34, the points are the free energy results for the free energy simulations and the dashed line is a guide to show the limiting slope of -2. Insert: Log–Log plot of $1/P(0)$ as a function of $2R_p - \sigma$ shows the wide channel scaling behavior for hopping times obtained from the theory, Eq. 2.34, (solid line) and the simulation (points). The dashed line is a guide to highlight the limiting slope of -1 [5].

is a maximum which is located near $x_c = 1$ and moves toward $x_c = 0$ as $R_p \to \sigma$. This unexpected behavior arises because of two competing factors. When the diameter of the channels decreases, due to the increase in the excluded volume interaction between the two discs, the number of accessible configurations available to the system decreases which results in higher free energy density as the two discs get closer to the transition state. On the other hand, when $x_c < \sigma$, the number of accessible configurations increases because less work needs to be performed against the external pressure (the pressure–volume work) [5]. The free energy profile, using the small system isobaric–isothermal ensemble, significantly differs from that obtained using the canonical ensemble where the free energy maximum is always located where the particles are passing each other at $x_c = 0$ [3]. Instead, the free energy maximum in the system is not located at the transition state, i.e. at $x_c = 0$, which represent where the particles are passing each other and exchanging their position as part of the hopping process.

Based on Eq. 2.32, at the transition state $\sigma_2 = \sigma$, and by replacing Eq. 2.31 and Eq. 2.33 in Eq. 2.7 one can obtain the probability of finding the caged particle at the transition state, $P(0)dx_c$, as [5]

$$P(0)dx_c = \frac{4(R_p - \sigma)^2 dx_c}{\Lambda^4 \beta p_l (2R_p - \sigma)\Delta}. \tag{2.34}$$

Based on TST, the hopping time is inversely proportional with the probability of finding the system at the TS, $\tau_{hop} \sim 1/P(0)$, and Eq. 2.34 confirms that the hopping time diverges with the exponent $\eta = -2$.

In the hard disc model, when the channel radius approaches the passing threshold for the particles, $R_p \to \sigma$, the excluded volume interaction restrains the particles from passing each other. In this region, the hopping time is expected to diverge as a power law, $\sim (R_p - \sigma)^{\eta}$, for the systems with hard particle–particle and particle–wall. Once the channel radius reaches the passing threshold, $R_p = \sigma$, and becomes smaller, the discs will be permanently caged between their neighbors. The Fick–Jacobs analysis [70], which uses a reduced dimensionality approach by projecting the diffusion of the two discs on to a one–dimensional reaction coordinate [71, 72] predicts $\eta = -3/2$, while TST [30] predicts $\eta = -2$. Simulation studies of hopping time predicts the scaling factor of $\eta = -2$, which is in agreement with the TST result. However, the scaling factor is predicted only when the channels are verry narrow [32, 87]. Figure 2.7 also illustrates the hopping times behavior for hard discs diffusing in very narrow channels compared to the wider channels. The figure shows that the hopping times scaling factor approaches to $\eta = -2$ for the very narrow channels, $R_p = 1.01 - 1.2$, and it crosses over to the wide channels scaling, $\eta = -1$, for the wider channels, $\sim (2R_p - \sigma)^{-1}$, which is consistent with the ideal gas system results, under conditions where $2R_p \gg \sigma$ [5].

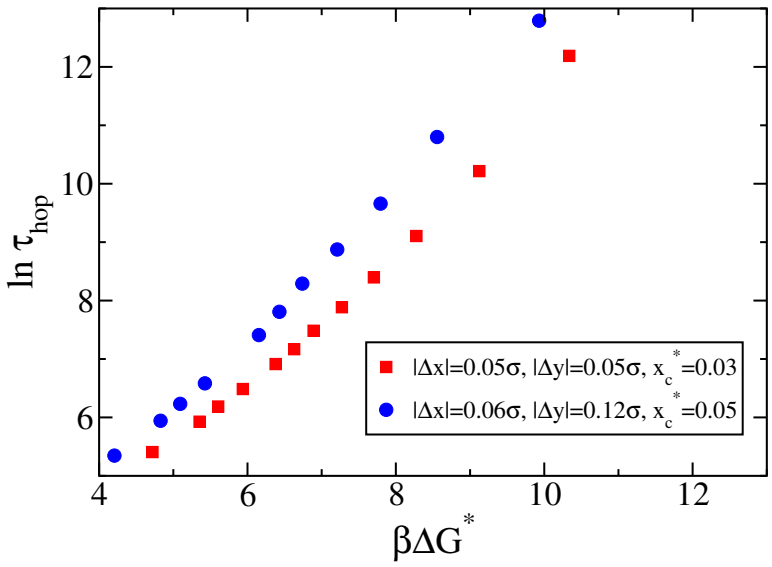

Figure 2.8: ln τ_{hop} versus $\beta\Delta G^*$ for hard discs inside different size 2d channels with radii, $R_p = 1.01 - 1.20$. The points represent the data obtained from the simulation with $x_c^* = 0.03$ and $x_c^* = 0.05$.

Figure 2.8 shows ln τ_{hop} as a function of $\beta\Delta G^*$ for hard discs inside different size channels with $R_p = 1.01 - 1.2$. The hopping times were calculated under two different dynamics, with maximum step sizes of $|\Delta x| = |\Delta y| = 0.05\sigma$, and $|\Delta x| = 0.06\sigma$ and $|\Delta y| = 0.12\sigma$. The free energy barriers at the TS were obtained for two different choices for the transition state width, $x_c^* = 0.03$ and $x_c^* = 0.05$. This figure shows how the

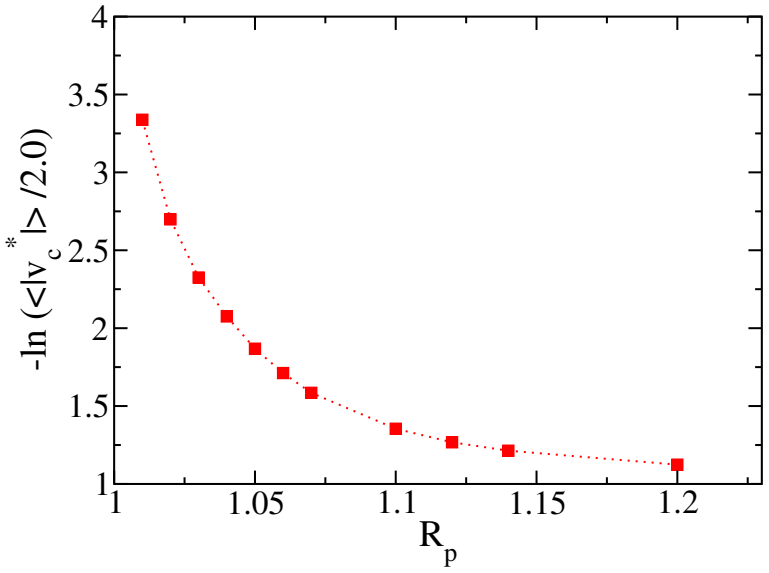

Figure 2.9: The prefactor term as a function of channel's radii, $R_p = 1.01 - 1.2$, with $x_c^* = 0.05$, $\Delta x = 0.06$, and $\Delta y = 0.12$. The squares represent the data obtained from the simulation and the dashed line provides a guide to the eye.

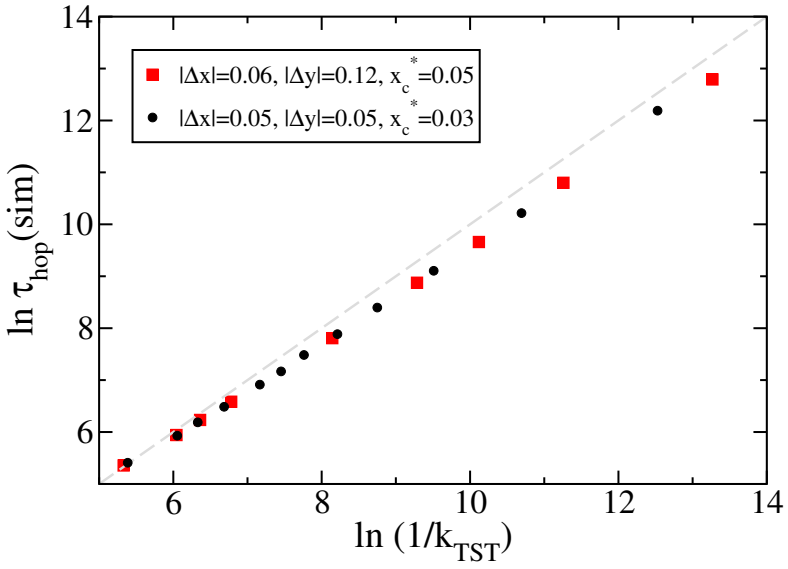

Figure 2.10: $\ln\tau_{hop}(sim)$ versus $\ln(Ae^{-\beta\Delta G^*})$ for hard discs inside different size 2d channels with radii, $R_p = 1.01 - 1.20$. The points represent the data obtained from the simulation with $x_c^* = 0.03$ and $x_c^* = 0.05$. The dashed line has a slope of 1 and provides a guide to the eye.

hopping behavior of the particles changes based on their dynamics and how $\beta\Delta G^*$ varies by changing x_c^*. The dependency of the hopping time on the particles dynamics is more dominant for the narrower channels than it is for the wider channels. However, the free energy calculation is independent of the dynamics but it depends on the choice for the transition state region, x_c^*. The non–linear dependency between the hopping times and the free energy barriers suggests that the kinetic prefactor (see Eq. 2.1) has a dependency on R_p as well and the prefactor calculations must be taken into account in order to achieve a useful formalism for the hopping time calculations. Fig. 2.9 shows how the kinetic prefactor varies by changing the channels radii and clearly reflects the dependency of the hopping time on the dynamics.

Finally, Fig. 2.10 shows ln $\tau_{hop}(sim)$ as a function of $1/k_{TST}$ for hard discs inside different size channels $R_p = 1.01 - 1.2$. Including the kinetic prefactor calculations, which accounts for the dynamics of the hopping times and also depends on the transition state region choice, x_c^*, and R_p, results in a good quantitative prediction of hopping times for both cases.

2.5 Discussion

The diffusion behavior of fluids confined to single file systems can be understood using the hopping time approach. The attractive feature of this approach is that all the effects that might influence the motion of tracer particles inside narrow channels are contained within a single parameter, τ_{hop}, which measures the average time that it takes for a particle to to hop one of its immediate neighbors. A hopping event in a single file system can be considered as an activated process and therefore are amenable to the application of TST. The calculation of the height of the free energy barrier for hopping for a small size system with volume fluctuations is the challenge that needed to be solved. For a system with volume fluctuations the appropriate ensemble to use is the isobaric–isothermal ensemble, however, the bulk thermodynamics results are only applicable to a systems in the thermodynamic limit, but not for a nanoscale size system. This is due to the system size dependency of the volume scale for the isobaric–isothermal ensemble [5].

It was shown that that the small system isobaric–isothermal ensemble introduced by Corti, can overcome the problem of overcounting the configurations when considering the volume fluctuations for a finite size isobaric–isothermal ensemble. In this work, the small system isobaric–isothermal ensemble combined with the TST was used to develop a method which only requires the simulation of two particles to measure the free energy barrier for particles hopping [5]. This method provides an accurate prediction of the hopping time for large size systems, which consist of hundreds of particles, and require expensive simulation time.

As noted earlier, the method calculates the power law exponent of $\eta = -1$ for the 2d ideal gas system, $\tau \sim 1/R_p$, and $\eta = -2$ for the 2d hard discs model with narrower channels, $\tau \sim (R_p - \sigma)^{-2}$, as predicted by TST. Based on the TST assumption, the trajectories that recross the barrier to their initial state do not contribute to the rate. This results in an over estimation of the rate and consequently underestimation of

the predicted hopping times. However, when the channels are narrower the proposed method overestimates the hopping times. One possible explanation of this could be related to the assumption that was made in defining the partition function for the small n, p_l, T ensemble, which neglects the interaction between the small system and its surroundings. How the interaction between the small system and its surroundings affects the crossing barrier is not clear and it will depend on the type of interactions between the small system and its surroundings and also the nature of the wall. As a result, it is expected for the model to work well where the interactions between the sub–system and the surroundings are minimal such as low pressure cases [5].

The presented method can effectively predict the hopping time and therefore the dynamics of diffusion, in the crossover regime, for fluids confined to sufficiently narrow channels. In the crossover regime, the hopping time is proportional to the diffusion coefficient through Eq. 1.20, where the hopping barrier is relatively high. However, Mon and Percus [28] showed that Eq. 1.20 might be applicable to predict the hopping behavior for the wider channels, where the barrier is only a few $k_B T$, but with a different hopping time exponents. In this work, it was shown that for the case of hard discs confined to wider channels the hopping exponent follows the wide channels scaling behavior with $\eta = 1$. To apply this model for the wider channels it is essential to account for the interactions between the small system and the surroundings [5].

Chapter 3

Hopping Times Calculations for Repulsive Fluids

3.1 Introduction

In quasi–one–dimensional channels particles are arranged in a single file and within confined local cages which are formed by each particle's left and right nearest neighbor along the channel. In the long time limit, when particles can jump out of their local cages by passing their neighbors, normal Fickian diffusion is observed. For the tracer particle, particle–particle exclusion effects and the relatively narrow structure of the channel, which restricts the available configuration space for the particles when they attempt to pass each other, produces a free energy barrier. When the barrier is high, hopping is a rare event and can be considered as an activated process that can be addressed using TST. As mentioned earlier in Chapter 2, the hopping time is inversely related to k_{TST} and can be obtained via Eqs. 2.15 and 2.16 [84, 106, 108, 119].

The small system isobaric–isothermal (n, p, T) ensemble developed by Corti *et al.* [4, 92] is used to calculate the free energy barrier required for a particle when it is escaping its local cage by hopping past one of its neighbors. The detailed description of this approach can be found in Sections 1.5 and 2.2. In summary, the method considers the isobaric–isothermal ensemble for a small system of n particles with a volume, v, which is immersed in a larger system with $N - n$ particles with a fixed volume, $V - v$. Both systems have a fixed temperature, T. The volume of the small system is defined by a shell particle, one particle of the n particle system, and is limited to a region dv, located at the boundary of the small system. Tying the volume of the small system to the location of the shell particle helps to avoid the over counting of configurations associated with the volume fluctuations of the small system. The volume fluctuation of the small system is integrated over the degrees of freedom of the surrounding $N - n$ system and creates a small system isobaric–isothermal ensemble without a need for introducing a system size dependent volume scale.

The previous chapter developed a method which is capable of the quantitative prediction of the hopping times for two–dimensional hard discs model [5]. This chapter aims to address the second question posed in this thesis and quantitatively and qualitatively studies particle–particle interaction effects on diffusion in confined fluids. To achieve this, the hopping times obtained for a system of repulsive discs confined to a hard walled channel, using the TST and a small system ensemble consisting of two particles, are compared to the

hopping times which are measured directly from simulation of a large system, consisting of 500 particles. In addition, the hopping times are obtained for different degrees of particle softness and provide information about the repulsion effect of the interaction potential on hopping times, and hence diffusion. In this work, it will be shown that both the free energy barriers and the kinetic prefactor are important elements in achieving a good qualitative and quantitative estimation of hopping time and the proposed transition state theory method is a useful approach for obtaining both elements. In addition, this highlights the benefits of using the TST approach as an effective tool for diffusion optimization.

This chapter is organized as follows: Section 3.2 describes the model and outlines the simulation methods used to calculate the hopping times using the TST method and direct measurement of the hopping time for large systems. This section will finish by a description of the hopping time optimization method. Section 3.3 outlines the simulation result and discussion, and the conclusions are summarized in Section 3.4.

3.2 Model and Methods

3.2.1 Model

To study the effect of the interaction potential on diffusion behavior a two–dimensional system of repulsive discs confined to a narrow two–dimensional channel with hard walls is considered. The channel has a radius of R_p, which extends in the $y-$axis, and length of L, along the $x-$axis. The center of the channel is chosen to define the origin of the coordinate system. The particles interact through an inverse–power–law potential,

$$U(r_{ij}) = \epsilon(\frac{\sigma}{r_{ij}})^{\alpha} : \alpha = 5 - 100, \tag{3.1}$$

where $r_{ij} = |\mathbf{r}_i - \mathbf{r}_j|$ is the distance between particles i and j, α is the power-law exponent that describes the repulsion strength of the potential, ϵ is the interaction strength and the interaction potential is cut off at $r_c = 2.5\sigma$. The larger the α value the harder the repulsive potential. The quantity $1/\alpha$ identifies the softness of the interacting potential, and $1/\alpha = 0$, with $\alpha \to \infty$, describes the hard sphere potential. The interaction potential between the particles and the wall is chosen to be hard and is given by,

$$U_W(y_i) = \begin{cases} 0 \ \text{ if } |y_i| \leq R - \sigma/2, \\ \infty \text{ if } |y_i| > R - \sigma/2, \end{cases} \tag{3.2}$$

with y_i being the y–coordinate of a particle. All the simulations are performed using reduced units. In addition to the repulsive system which is defined above, the simulations are carried out for the equivalent two dimensional hard sphere system, under the same conditions used to study the soft particles, to provide a direct comparison between the result obtained from the repulsive discs system with the result obtained from the hard discs system in Chapter 2.

3.2.2 Free Energy Calculations

Monte Carlo simulation is used to calculate the free energy barriers for particles hopping using a small isobaric–isothermal ensemble, n, p, T. The small system ensemble simulations are performed by confining $n = 2$ particles to a channel with radius, R_p, and length L, under conditions with $\beta = 1$ and $\beta p_l = 1.0$. The volume of the small system, with its center located at the origin, is defined by the location of particle one, which is the shell particle, and is placed at $L/2$. Particle two, the caged particle, is located within the cage between $-L/2$ and $L/2$. The MC moves proceed as follows: After a random selection of a particle, it is moved randomly by a step δx and δy, up to a maximum displacement of $|\Delta x| = 0.06\sigma$ and $|\Delta y| = 0.12\sigma$. If the trial displacement of results in an overlap with the wall or if it puts particle two outside the cage the move is immediately rejected. When the shell particle is chosen, the trial move will also change the cell length by $2\delta x$ and the position of the caged particle is rescaled to ensure it remains within the volume. As the volume of the small system is defined by the location of the shell particle, its position remains positive during the simulation to ensure $v > 0$ [1]. The MC acceptance probability for a trial move from an old to a new configuration is given by,

$$\begin{aligned} \mathrm{acc}(\mathrm{old} \rightarrow \mathrm{new}) = \min(1, \exp\{ &- \beta[U^{\mathrm{new}} - U^{\mathrm{old}}] \\ &- \beta p_l 2R_p[L^{\mathrm{new}} - L^{\mathrm{old}}] + (n-1)\ln[L^{\mathrm{new}}/L^{\mathrm{old}}] \}). \end{aligned} \tag{3.3}$$

For each system, the ΔG^* values are obtained from 20 independent runs. For each run, 2×10^7 MC cycles are used to obtain equilibrium and data is collected over the next 8×10^8 MC cycles, where each MC cycle includes $n = 2$ MC moves. The configurations are sampled every 1000 MC cycles to ensure that they are not correlated. The probability is calculated by building a histogram of configurations versus the reaction coordinate using bin sizes of $\Delta x_c = x_c^* = 0.05\sigma$. The free energy along the reaction coordinate is calculated using the probabilities, $\beta\Delta G = -\ln P$. The error bars represent the standard deviation of ΔG^* over the 20 runs. Systems with $\alpha = 5 - 100$ and $R_p/\sigma = 1.01 - 1.10$ are considered. It is required to use probability density to calculate the transition rate, according to Eq.2.15, which is obtained by dividing the transition state probability at TS, P^*, by the bin size, Δx_c.

The average velocity, $\langle v_c^* \rangle$, at which the system crosses the barrier is obtained from Eq. 2.21. To obtain the velocities, the canonical ensemble (N, V, T) simulations, with $N = 2$ particles, are used with the standard Metropolis MC scheme [85] being used to move particles, as a simple approximation to Brownian motion [117]. The MC simulation is performed as follows: A transition state configuration is used as starting the initial condition and satisfies $x_c < 0.05$. Each MC cycle, which represents the unit of time, is defined as $n = 2$ attempted particle moves and each simulation is performed for one MC cycle, $\Delta t = 1$. For each initial configuration, one particle is selected randomly and is moved by a step δx and δy, up to a maximum displacement of $|\Delta x| = 0.06\sigma$ and $|\Delta y| = 0.12\sigma$. The move is immediately rejected if the trial displacement

causes any of two particles to overlap with the hard wall; otherwise the probability of accepting the trial move is calculated according to the standard Metropolis MC probabilities. The transition state configurations were taken from free energy barrier simulations which performed in the small n, p_l, T ensemble. The average velocity for each system is calculated over 1000 distinct initial configurations. The hopping time is then obtained from the transition rate according to Eq. 2.16 [1].

3.2.3 Hopping Time Calculations

The hopping times are directly measured for all the systems studied using canonical (N, V, T) simulations for systems of $N = 500$ repulsive discs confined to channels with radius, R_p, and length, L. The results obtained from direct hopping time measurements, $\tau_{hop}(sim)$, are used as a test to compare against the result, produced by the TST method. The dynamics used for the MC simulations, to achieve a direct measurement of hopping time, are the same as that described for the free energy calculations. Periodic boundary condition are applied along the channels longitudinal direction for the (N, V, T) simulations. Each MC move consists of the random selection of a particle and moving it in a random direction by step size of δx ad δy and up to a maximum displacement of $|\Delta x| = 0.06\sigma$ and $|\Delta y| = 0.12\sigma$. Each MC cycle, defined as $N = 500$ attempted particle moves, representing the unit of time, t, for the simulation. Initially, particle positions are distributed evenly along the channel and randomly across the width of the channel. Before collecting data, 3×10^7 MC cycles are performed to ensure the system has reached equilibrium and data is collected over the next 5×10^7 to 3×10^8 MC cycles, depending on the system, to ensure the average hopping time converges. At the beginning of collecting data, the initial hopping time is set to zero and each particle's cage is defined as their immediate left and right neighbors. The number of MC cycles that each particle takes to jump outside of their local cages is counted as their hopping time. After a particle jumps outside its cages, its new cage is identified and the particle's hopping time is reset back to zero. The hopping time, $\tau_{hop}(sim)$, is obtained as the average over all the hopping times recorded for each particles is calculated. To check the system size effect on the calculated hopping times, different simulations were performed with $N = 100 - 800$. The result confirmed $N = 500$ is sufficiently large to account for system size effects [1].

The direct measurement of the hopping time in large system is performed in the canonical ensemble, rather than the constant isobaric–isothermal ensemble, because volume fluctuations at constant p cause particle positions to be rescaled, which can lead to error in the hopping time estimation. To ensure the N, V, T ensemble simulations are performed at the correct state point the appropriate linear density, $\rho_l = N/L$, for each system (R_p, α) is calculated using the n, p_l, T ensemble where $\beta p_l = 1.0$, $n = 500$. The shell particle approach is used for the density calculations, as it has been shown that for the large system sizes, the standard isobaric isothermal ensemble and the small shell particle method provide the same result at low pressures [5]. The MC trial moves are the same as that outlined in Section 3.2.2 for the free energy

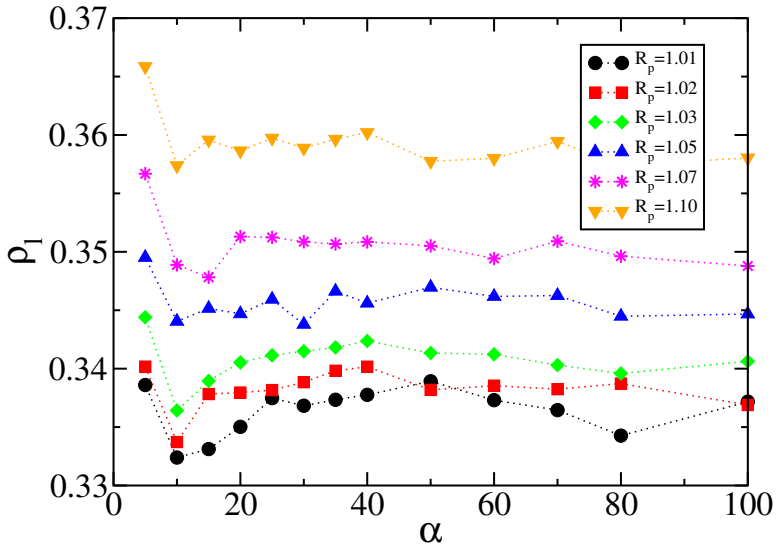

Figure 3.1: Linear density, ρ_l, vs α for different channel radii. The densities are calculated using n, p_l, T ensemble and shell particle method [1].

.

calculations (Eq. 3.3). The maximum displacement of $|\Delta x| = 0.06\sigma$ and $|\Delta y| = 0.12\sigma$ results in an MC acceptance ratio of $85 - 92\%$. The system is equilibriated over 10^7 MC cycles before collecting data, and then the average density for each system is obtained by sampling the data every $10,000$ MC cycles over the period 5×10^7 MC cycles. Figure 3.1 shows that the density increases with increasing channels diameter, but remains relatively constant as α varies [1].

3.2.4 Optimization Method

To highlight the possible application of this approach, the pythOPT global optimization problem–solving software environment [120] was used to search for the interaction parameters, $1/\alpha$ values, that would result in the highest hopping barrier and therefore the slowest diffusion rate for the systems studies here. The pythOPT environment offers multiple global optimization solvers as well as a suite of benchmark problems and routines for performance analysis [1]. The Guaranteed Convergence Particle Swarm Optimization (GCPSO) solver [121] was used in this study. During the optimization, the MC free energy simulation method outlined in Section 3.2.2 is used to calculate the free energies corresponding to different values of α. The prefactor calculations is not included during the optimization process, but can easily be included for quantitative analysis. A total of 50 swarm particles and 10^6 function evaluations were used for each GCPSO

simulation. The total optimization process, for a single radius, takes approximately five central processing unit (CPU)–days.

3.3 Simulation Results and Discussion

3.3.1 Hopping Times

To study how particle–particle interactions influence their diffusion properties, the result obtained from direct measurements of hopping times from the large system simulations are investigated [1]. Figure 3.2 shows that $\tau_{hop}(sim)$ initially increases for all the channel radii as the potential moves from softer particles (larger $1/\alpha$ values) toward harder interactions (smaller $1/\alpha$ values). The initial increase in the hopping times is greater for the narrower channels than it is for the wider channels. For a fixed channel size, this behavior is consistent with the expectation that it will be harder for particles to pass each other if it is energetically more difficult to bring them together. Furthermore, in the limit of $R_p \to \sigma$ and when the particle–particle interaction becomes harder ($1/\alpha \to 0$), the hopping time must diverge [30], causing their dynamics to switch from normal diffusionl to SFD. However, Fig 3.2 shows the hopping times go through an unexpected maximum, initially increasing as the particles' hardness increases and then decreasing to the hard disc interaction at $1/\alpha = 0$. The existence of this maximum suggests that for each channel size there is a range of α values where softer particles find it harder to diffuse than the harder particles. As the channels diameter become narrower this maximum sharpens and its location moves toward the lower values of $1/\alpha$ [1].

3.3.2 Gibbs Free Energy and Hopping Prefactor

The rest of this section examines how the free energy barrier required for two particles to pass each other can quantitatively predict the large system hopping time behavior [1]. Figure 3.3 shows the Gibbs free energy profile as a function of separation of the two particles along the reaction coordinate for both hard discs system, $\alpha = \infty$, and repulsive discs systems with $\alpha = 5$ and $\alpha = 100$. For all the cases, at larger x_c values, the interaction between the particles become negligible so they are able to move freely across the entire diameter of the channel. The ΔG increases linearly as it did for the ideal gas system (see section 2.4). The free energy exhibits a minimum at $x_c \approx \sigma$ and starts to increase again with decreasing x_c because the repulsive interaction between the particles restricts the available configuration space for the particles, and increases the energy of interactions. The free energy minimum is sharp for the hard disc system and it becomes shallower as the interactions become softer. Decreasing x_c results in a fast increase in the free energy barrier for the harder interaction and it shows a slower increase for the softer case, $\alpha = 5$. When the channels are very narrow, as shown in Fig. 3.3, the maximum in the free energies is located at the geometrically defined transition state, where particles are located on top of each other, $x_c = 0$. However, for

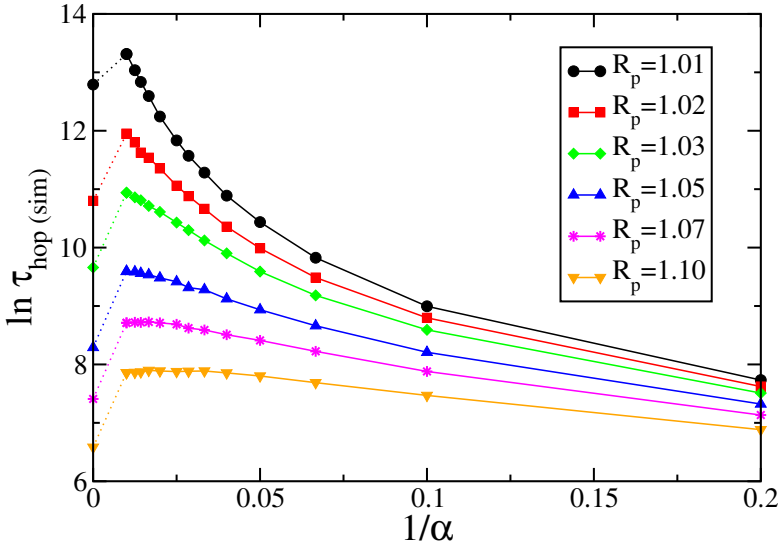

Figure 3.2: $\ln \tau_{hop}(sim)$ as a function of $1/\alpha$ for different channel radii. $\ln \tau_{hop}(sim)$ indicates the hopping times directly measured from simulation [1].

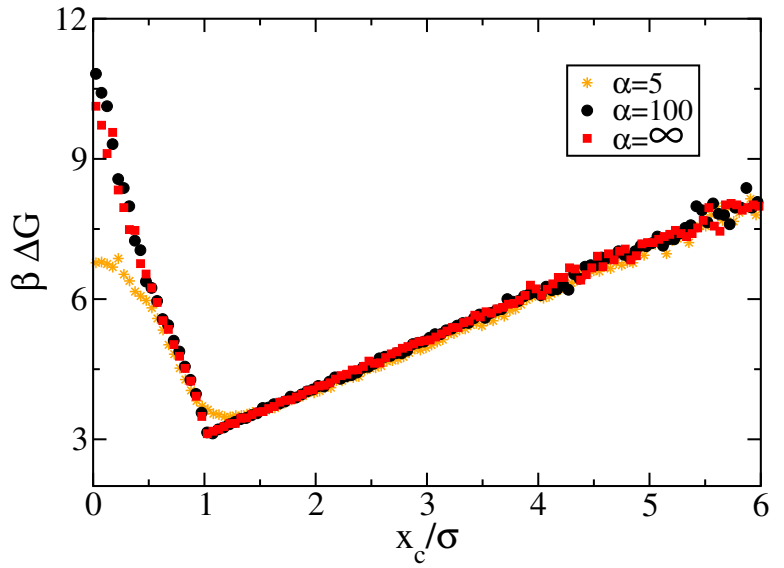

Figure 3.3: Gibbs free energy profile vs the reaction coordinate, x_c, for repulsive systems with $\alpha = 5$ and $\alpha = 100$ and the hard disc system with $\alpha = \infty$ with $R_p/\sigma = 1.01$ [1].

the wider channels the competing effects between the pressure–volume work and the restriction in available configuration space moves the maximum between $x_c = 0$ and $x_c = 1$. Nevertheless, it is important to note that because each hopping event is associated with particles exchanging their position at $x_c = 0$, it is the probability of being at the geometric transition state that determines the hopping time and the diffusion coefficient [1].

Figure 3.4 shows the height of the free energy barriers at the transition state, ΔG^*, as a function of particles' softness for all the systems studied. When compared, the measurements of the TST successfully predict the hopping time general trends that were obtained via the direct hopping time simulations, $\ln \tau_{hop}(sim)$ (see Fig. 3.2). In addition, the position of the free energy barrier maximum can be located for all channel radii using this result. Figure 3.5 shows the kinetic prefactor term as a function of α for all the channel radii. The strong dependency of the prefactor on α for the narrower channels could be the reason for disappearance of the maxima in the hopping time calculations by outweighing the effect of the decreasing free energy (compare Fig. 3.2 and Fig. 3.4). For wide channels the dependency of the prefactor on α becomes negligible and this allows the hopping time trend to follow the free energy behavior. This result emphasizes the importance of including the properties of prefactor even for the narrow channels where the free energy barriers is the dominating factor in hopping times calculations. Figure 3.5 also illustrates the strong dependency of the prefactor on the channel width when the interaction are relatively hard. This dependency on the channels diameter decreases when particles are softer [1].

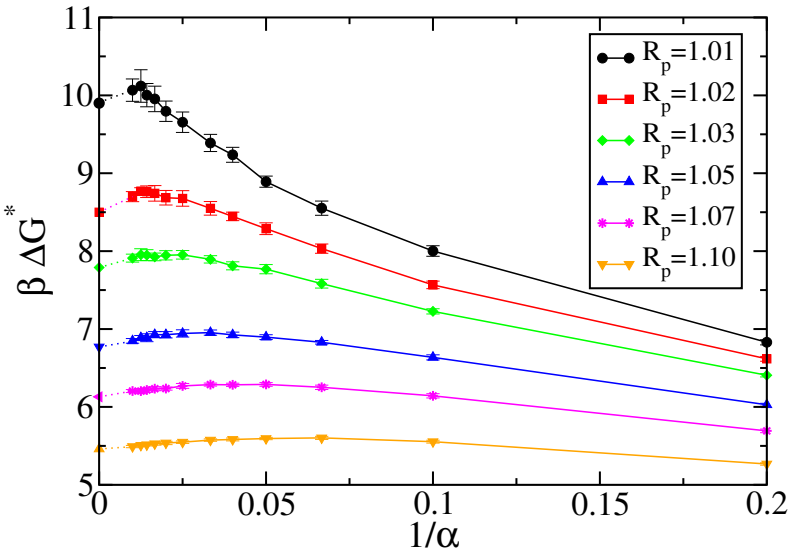

Figure 3.4: Gibbs free energy barrier at the transition state, $\beta\Delta G^*$, as a function of $1/\alpha$ for different channel radii [1].

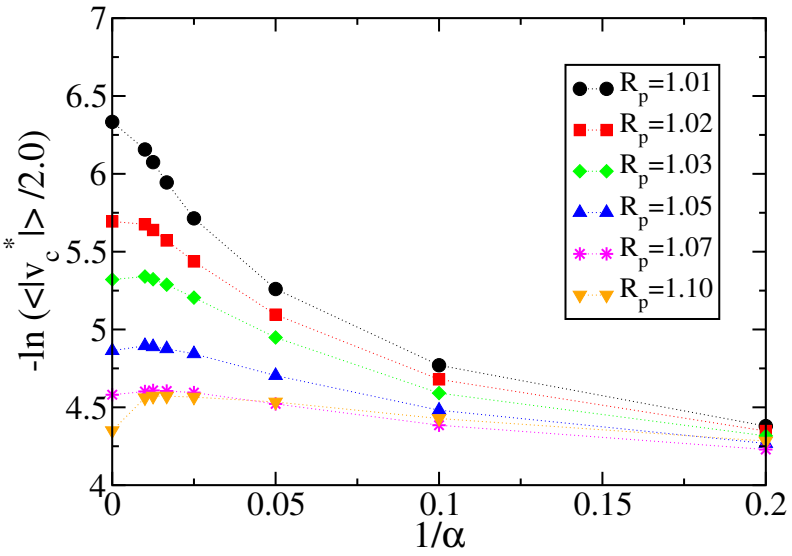

Figure 3.5: The prefactor term, $-\ln(\langle|v_c^*|\rangle/2.0)$, as as a function of $1/\alpha$ for different channel radii [1].

Figure 3.6 shows the ratio of $\tau_{hop}(TST)$, obtained from the theory, and the direct hopping time measurements as a function of channels radii for different interaction potentials. The result indicates that there is a factor of two difference between the theory and the actual hopping time calculations over the range of channel radii studied. The theory underestimates the hopping times for the wider channels and it overestimates it for the narrower channels. Our plot also suggests the error could potentially increase further as the channel becomes narrower. Transition state theory is expected to underestimate the hopping time for all the cases because it neglects trajectory recrossing, which is consistent with the result for narrow channels. To achieve improved predictions of the hopping time in this regime, it is necessary to perform calculations that account for the recrossing effects and help to correct terms associated with the kinetic prefactor. It is also important to note that the proposed method, which uses the two particle approach, makes an additional assumption by which it neglects the interactions between the small system and its surrounding bath. The theory would be exact if these interactions were included in the calculation of the small n, p_l, T partition function. This assumption results in errors in the free energy calculations, and in particular, in the free energy barrier calculations for softer particles and wider channels where the the long range interaction between the small system and its surrounding bath may become more important. For example, it is expected that the accuracy of the method improves for the narrower channels because the fluid structure becomes more single file and as a result the effect of the long range interactions decreases. Nevertheless, the simplicity of the method in capturing the general features of the hopping times for confined fluids makes it a useful

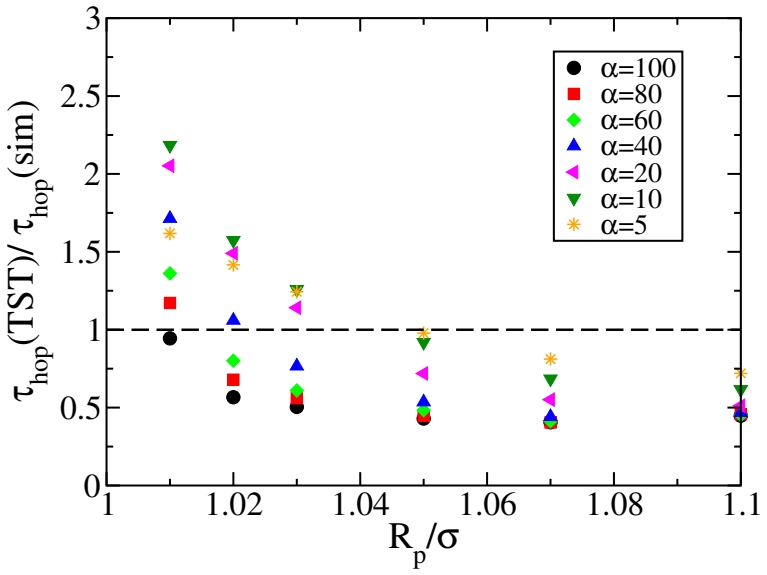

Figure 3.6: Comparison of the predicted hopping time obtained from the theory, $\tau_{hop}(TST)$, with the directly measured hopping time via simulation, $\tau_{hop}(sim)$, for different values of α and R_p. The dashed line represents the perfect agreement [1].

method in determining factors that might influence diffusion behavior in highly confined fluids [1].

3.3.3 Transition State Partition Function

To analyze the origin of the maximum in the free energy barrier height as a function of particles softness, observed in Fig. 3.4, a transition state partition function is defined for the two particle system. The analytical derivation of the full partition function for the 2d system involves the integration of the repulsive potential over multiple variables, so a simplified analysis is carried out to calculate the partition function for the system when it is located at the transition state. This system can be characterized by a partition function for two particles in one-dimensional line (see Fig. 3.7). The one-dimensional transition state partition function for the system can be written as [1],

$$Q_{1d} = \frac{2}{2!\Lambda^2} \int_0^{2R_r} dr_1 \int_0^{2R_r - r_1} e^{-\beta U(r_{ij})} dr_{ij}, \tag{3.4}$$

where $\Lambda = (h^2/2\pi m k_B T)^{1/2}$ is the thermal de Broglie wavelength for a particle with mass m, h is Plank constant, $R_r = R_p - \sigma/2$ is the reduced channel radius which is defined as the accessible channel width for the center of the discs due to the hard wall interaction, $r_{ij} = r_2 - r_1 > 0$ is the distance between two particles, $U(r_{ij})$ is the interaction potential defined earlier via Eq. 3.1. The factor of two appears in Eq. 3.4 in order to account for both possible particle orders on the line. The Helmholtz free energy for the transition

state, relative to two ideal gas particles, is then given by [1],

$$\beta \Delta F_{1d}^{*} = -\ln\left(Q_{1d}/Q_{ig}\right), \tag{3.5}$$

where $Q_{ig} = (1/2!\Lambda^2)(2R_p)^2$ is the ideal gas partition function. It should be mentioned that due to ideal gas particles point like nature they can sample the entire width of the channel, $2R_p$ [1]. The energetic, E, and entropic, S, contributions to the free energy, $F = E - TS$, can then be obtained using the usual canonical ensemble expressions, $\langle E \rangle = k_B T^2 (\partial \ln Q/\partial T)_{N,V}$ and $S = k_B \ln Q + \langle E \rangle /T$, respectively.

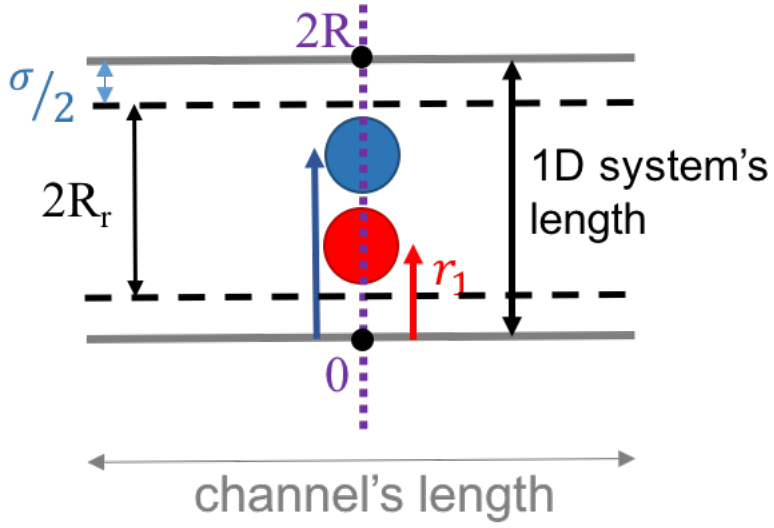

Figure 3.7: A schematic representation of the one-dimensional transition state [1].

Figure 3.8 shows that the one–dimensional partition function, defined for the system when it is located at the transition state, can be used to capture the general effects of the interaction potential parameter and the channel radius on the hopping free energy barriers. Even though, in the one–dimensional model, the location of the maximum in the free energy barrier height differs from that in the actual system it still is able to show how the maximum evolves with changes in the channel radius. However, the transition state partition function cannot be used to estimate the hopping time because it does not provide information about the probability of finding the system at the transition state.

The model also can be used to examine how the energetic and entropic contributions to the free energy barrier at the TS relate to the maximum in the free energy barrier as a function of particles softness. Figure 3.9 shows the entropic and energetic variations at the transition state as a function of particles softness for a fixed channel radius, $R_p = 1.01$. For the hard disc case, with $1/\alpha = 0$ and $E = 0$, the barrier is entirely entropic in nature and the particle–particles interaction creates a restriction in accessible configuration space for two particles. As the interaction becomes softer, by increasing $1/\alpha$, it allows particles to overlap with

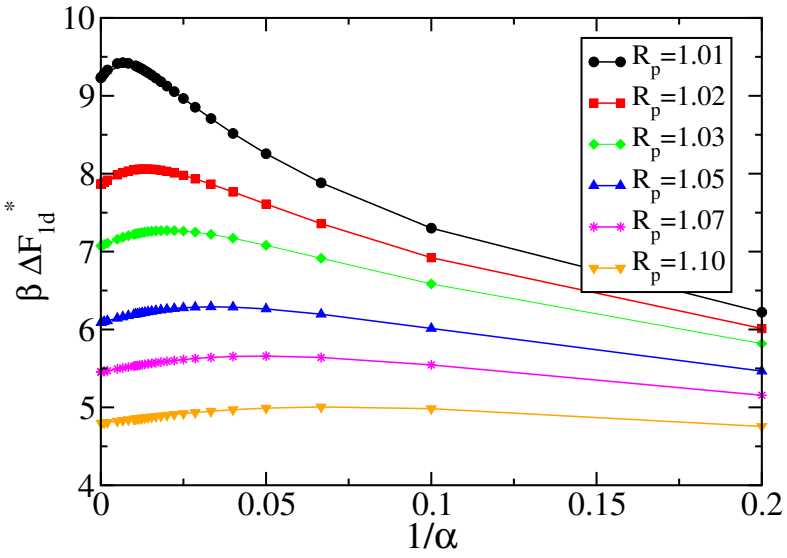

Figure 3.8: Helmholtz free energy for the one-dimensional transition state ensemble as a function of $1/\alpha$ for different channel radii [1].

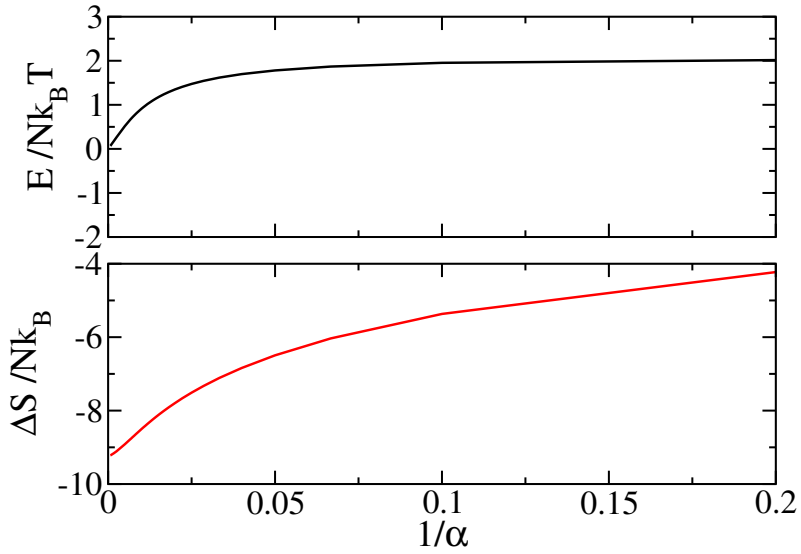

Figure 3.9: The energy, E/Nk_BT, and entropy relative to an ideal gas, $\Delta S/Nk_B$ of the one-dimensional transition state ensemble as a function of particle softness for a channel with $R_p = 1.01$ [1].

each other, causing their energy and entropy relative to ideal gas system to increase. However, for small values of $1/\alpha$ the energetic cost increases more rapidly than the entropy, leading to an increase in $\beta\Delta F^*$. Increasing $1/\alpha$ further causes the energy to plateau while the entropy continues to increase which leads an overall decrease in the hopping barrier, and the formation of a maximum in $\beta\Delta F^*$.

3.3.4 Optimization

The hopping time approach is a useful tool for studying diffusion in single file systems as all the factors that influence the fluids diffusion are captured within a single parameter, τ_{hop}. This suggests τ_{hop} could be used as a target for the optimization of diffusion in these systems. Considering the fact that the proposed TST model is capable of capturing the overall hopping time behavior and only requires simulation of a two particle system, it is used in this work to evaluate τ_{hop} as a part of optimization scheme.

	Global Optimization		Quadratic fit	
R	$1/\alpha$	$\beta\Delta G^*$	$1/\alpha$	$\beta\Delta G^*$
1.01	0.0107	10.095	0.0104	10.084
1.03	0.0123	7.978	0.0165	7.947
1.05	0.0215	6.957	0.0292	6.950
1.07	0.0429	6.294	0.0425	6.289
1.10	0.0585	5.603	0.0626	5.601

Table 3.1: Values of $1/\alpha$ and $\beta\Delta G^*$ at the maximum in the hopping free energy barrier obtained from GCPSO simulation and by quadratic fit to the data in Fig. 3.4 [1].

The pythOPT global optimization problem–solving software environment method was used to obtain the interaction parameters, $1/\alpha$ values, for which the system exhibits the highest hopping barrier and therefore the slowest tracer particle diffusion. The goal is to identify the location of the maxima in Fig. 3.4 under which the τ_{hop} will be longest.

To compare the optimization result with the simulation result, a quadratic polynomial was fit, using the five points around the maximum, for each of the free energy curves in Fig. 3.4, to obtain the free energy maxima. Table 3.1 compares the result obtained from the optimization with the systematic simulation result for $\beta\Delta G^*$. The result show that despite to the sensitivity of optimization problems [122] due to having a noisy function for the free energy barriers with considerably large standard deviations in the result obtained for $\beta\Delta G^*$, i.e. for $R_p = 1.01$, the agreement is relatively good.

This example demonstrates the potential application of the method in either obtaining a desired tracer diffusion rate in various engineering devices. In practice, the optimization could include a variety of parameters that might influence the diffusion such as particle–particle and particle–wall interaction parameters,

channel size or particle size.

3.4 Conclusions

The hopping time is an interesting phenomenological parameter because it contains information about the system factors, such as the density and particle-particle and particle-wall interactions, that determine the dynamic behavior of quasi–one–dimensional fluids. It was shown that the quantitative prediction of hopping time can be achieved using the proposed TST method which uses an small isobaric–isothermal ensemble to calculate the free energy barriers associated with two particles passing each other at the transition state. Studying the hopping time behavior of a 2d system of repulsive particles shows that kinetic prefactor is potential dependent and must be included in hopping time calculations. It was shown that combining these two factors, the free energy barrier and the kinetic prefactor, gives a good estimation of hopping time for all the potential and channel radii studied in this work. In addition, the TST method can be used as a tool for studying the interparticle interaction effect in the dynamics of single file systems.

Chapter 4

Hopping Barriers of Enantiomers inside Carbon Nano–Tubes

4.1 Introduction

Molecules that contain the same molecular formula and the sequence of the bonded atoms but with different spatial arrangements of their atoms are known as stereoisomers. Chiral compounds are classified as a specific type of stereoisomers. Chiral and chirality were used for the first time in a footnote of a lecture given by Sir William Thomson at Oxford University Junior Scientific Club on May 16, 1893. In the first sentence of the famous footnote he says [123] "I call any geometrical figure, or group of points, chiral, and say that it has chirality, if its image in a plane mirror, ideally realized, cannot be brought to coincide with itself". And based on the most recent IUPAC definition [124], chirality is defined as a geometric property of a rigid molecule, with a non deforming geometrical figure, which is not superimposable on its mirror image. Chirality of an object is related to its symmetry which is determined using certain symmetry operations such as rotational, mirror, inversion, and translation symmetry. A molecule that has a plane of symmetry or other symmetry elements, such as inversion center, is usually achiral. Thus, a molecule that has no symmetry element of the second kind is called chiral.

One way to distinguish between two enantiomers of a chiral molecule is the direction of rotation of plane–polarized light. The molecule is called dextrorotatory ((d) or (+)) if the rotation of plane–polarized light is clockwise or to the right; and the molecule is called levorotatory ((I) or (-)); if the rotation of plane–polarized light is counterclockwise or to the left. The second method distinguishes between enantiomers based on their absolute chemical configuration. When a special configuration of atoms around a chiral center is clockwise, the enantiomer is defined right–handed or type R, otherwise it is S-enantiomer (left–handed). When R and S enantiomers of a molecule within a mixture are presented in equimolar amounts, the mixture is called a racemic mixture. Racemic mixtures are optically inactive, because the left and right rotations of plane–polarized light are counterbalanced due to the equal concentrations of each enantiomer. Additionally, enantiomers exhibit almost the same physical and chemical properties when they are located in an achiral

environment. However, their behavior changes when they are located in a chiral environment or when they interact with other chiral components [7].

Natural properties of amino acids and sugars, as the building blocks of peptides, proteins, and polysaccharides are determined by their chirality. It has been shown that because of chirality, living organisms exhibit different responses to each enantiomer found in drugs, agrochemicals, food additives, flavors or fragrances components, and waste compounds [125, 126]. Often one isomer will be responsible for the intended action (eutomer), while the other (distomer) can elicit a very different and, for the most part, unwanted response [127, 128]. For example, different enantiomes of chiral pesticides may result in different environmental activities, durability and strength, or final products when they are broken down under enzymatic pathways [129, 130, 131]. Also, enantiomers of a racemic drug may show different pharmacological activities in biological systems, such as differences in their distribution, metabolic, and excretion behavior [132]. Examples of stereoselectivity for various receptors can also be found in the human body. S-asparagine to the human tongue produces a bitter taste, while R-asparagine transmits a more pleasant sweet quality. The human nasal membrane also demonstrates this with S-carvone smelling like caraway, and R-earvone smelling like mint [133]. These example illustrate the importance of using the appropriate enantiomer and developing methods for synthesizing enantiopure components [134]. It should be noted that the selective synthesis of one enantiomer, asymmetric synthesis, and development of new strategies for asymmetric synthesis is a continuing challenge [135].

The separation of chiral molecules is of considerable interest because of the chiral nature of living systems such as bio–organic molecules. Chiral separation traditionally has been known as some of the most challenging analytical separation. Enantiomers display the exact same physical and chemical properties when interacting with achiral environments, leaving a large part of traditional separation methods (e.g., distillation and liquid-liquid extraction) that operate on the assumption of difference in solubilities or boiling points unable to leverage those disparities [136].

Louis Pasteur was the first to successfully resolve a racemic mixture into its individual enantiomers and to discover steriochemistry [137]. He showed that the sodium ammonium salt of racemic acid or paratartaric acid (PTA) crystallized as a mixture of two crystal type with left–handed and right–handed properties, and he separated these crystals, using a pair of tweezers. When he dissolved them separately he observed that each crystal has the same optical activity in magnitude as the other, but opposite in directions. Pasteur concluded that PTA is a 1:1 mixture of *dextro*−tartaric, (+)-TA, and *levo*−tartaric acid, (−)-TA. He related the opposite optical activity of these substances to the chirality of their molecules, he also concluded that the chirality effect of these molecules might be as a result of helical arrangements of the atoms in their structure [138]. Since then many different strategies have been developed for the separation of enantiomers, though different racemic mixtures respond with varying degrees to the same strategy. Fig. 4.1 produces a

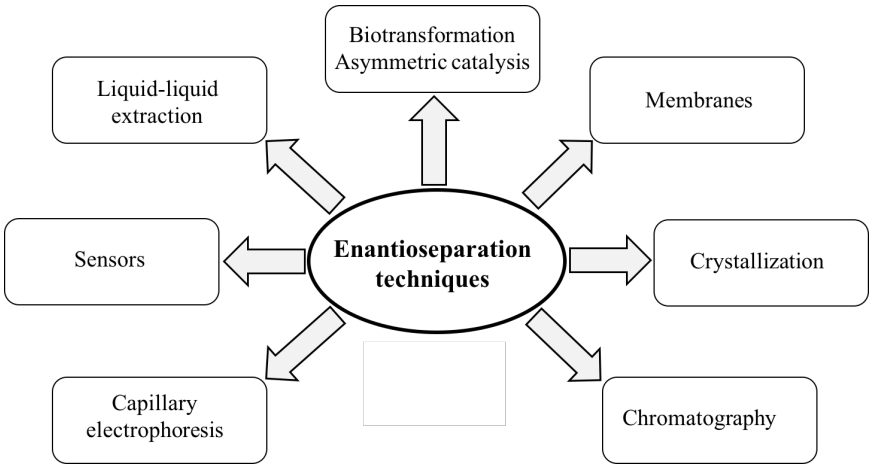

Figure 4.1: Analytical and preparative techniques that are used for separation of enantiomers. Reprinted with permission from ref. [7].

.

schematic representation of the primary groups of methods for enantiomeric separation. The majority of techniques are inefficient and costly due to combinations of time intensive procedures, such as crystallization and chromatography, and/or the requirement of large amounts of organic solvents [7]. The prevalent method for obtaining enantiomeric pure drugs is chiral chromatography. In achiral chromatography, the relative net differences in analyte interactions with the mobile-phase and stationary-phase environments is the driving factor for separation. In chiral separation, the ability of the enantiomers to interact stereospecifically with a chiral environment is the crucial factor [136]. With this technique, the stationary phase should be chiral and the enantiomers should have easy access to the molecules of the stationary phase, a challenging objective to accomplish [139].

Another approach involves selectively transporting the target enantiomer into a receiver solution on the other side of a synthetic enantioselective membrane [140, 141, 142]. In some physiological processes, the translocation of chiral components across biological membranes is important, such as the passage of sugars and antibiotics through cell membranes or the outer membrane of bacteria [143]. Lee *et al*. [144] introduced an enantiomeric separation method of a chiral drug by using an innovative bio–nanotube membrane design, utilizing alumina films with cylindrical pores of monodisperse nanoscopic diameters e.g., 20 nm. By attaching an antibody that stereospecifically binds with a particular enantiomer in the drug to the inner walls of the nanotubes translocation of the enantiomer was achieved. Meanwhile the enantiomer with less of a propensity to bind with the antibody does not translocate, there by separating the two.

In general, enantioseparation factors are quite limited in a large number of instances, reducing the amount of mechanistic models that can be identified through experimental techniques. This suggests, molecular modeling can be a worthwhile tool, for advancing the understanding of chirality and chiral separation. In

a Molecular Dynamics (MD) simulation study [145], the possibility of selective transportation of a pair of enantiomers (R– and S–phenylglycine) was studied, using a modified silica nanotube with amino acids attached to the pore wall. The nanotube mimics the structure of an artificial protein channel in a cell membrane. They showed that the enantioselectivity of their modified channel could be due to different interaction of the enantiomers with the immobilized amino acids on the wall. It was demonstrated that the different average dipole orientations and also the translational-rotational motion of the chiral molecules result in selective chiral transportation inside the nanotube.

The goal of this chapter is to address the third question posed on this thesis: Is there a difference in free energy barrier to hopping for enantiomers in a chiral nanotube that could potentially lead to enantiomeric separation? To address this question, the following hypothesis is proposed: Different enantiomers confined into a chiral channel exhibit different free energy barriers while attempting to pass each other.

The proposed hypothesis is tested by calculating the free energy barriers for hopping for a pair of enantiomers confined to a chiral carbon nanotube where the free energy profiles are obtained for $(R-, R-)$, $(S-, S-)$, and $(S-, R-)$ pairs of a chiral molecule, using the TST approach developed in Chapter 2. In this chapter, it is shown that under certain circumstances different enantiomers of a chiral molecule may exhibit different free energy barriers when passing each other within a chiral tube.

This chapter is organized as follows: Section 4.2 gives a brief introduction about carbon nanotubes as ideal pore models for studying the unique properties of confined fluids. Section 4.3 describes the model defined in this work for simulation studies of enantiomers inside carbon nanotubes. This section also includes computational details in defining the pair interaction potential and the interaction parameters. Section 4.4 gives a detailed description of the Monte Carlo simulation techniques used in this work to calculate the free energy barriers associated with the different pairs of enantiomers passing each other within the confinement of the nanotubes. Section 4.5 contains the simulation results and discussion, and the conclusions are summarized in Section 4.6.

4.2 Structures and Properties of Carbon Nanotubes

According to classical fluid mechanics, as the radius of a nanoscale channel decreases the work demanded to move fluid through it increases greatly, thus the energy necessary for nanoscale pumping mechanisms becomes impractically great. These energy requirements can be vastly reduced when using channels with enhanced fluid flow. Researchers have demonstrated both numerically [146, 147, 148, 149] and experimentally [150, 151, 35] that CNT based membranes benefit from a mechanism which enhances fluid flow in these channels dramatically. It has also being shown that CNTs have the ability to mimic natural protein channels. When using CNTs as biomimetic channels, they have shown the capability to increase the efficiency of fluid transfer considerably. Applications for these channels include drug delivery, water purification, chemical separation,

sensing and in nanofluidic and gating devices [151, 150, 152]. Therefore, greater insight into the control of liquid transport and in manufacturing liquid transfer devices could be gained by understanding the diffusion of fluids and flow rates in nanoscale channels. The properties of carbon nanotubes, specifically their simple periodic and clearly defined atomic structure, their large length to diameter ratio, and their chemical stability, allow for them to be ideal models for studying single file fluids in simulation studies.

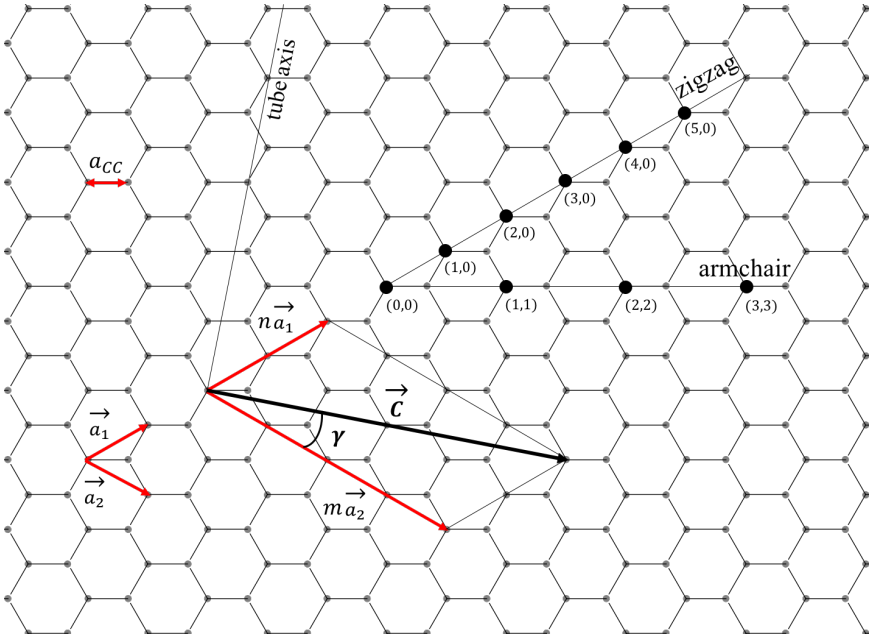

Figure 4.2: Definition of chiral vector and chiral angle on a graphene sheet for CNT(2,4). a_1 and a_2 are the unit cell vectors of the two-dimensional lattice formed by the graphene sheet. Reprinted with permission from ref. [8].

Currently there are two general types of nanotubes produced, single walled (SWNT) [153, 154] and multi-walled (MWNT). As the name suggests, SWNTs are made up of a single sheet of graphene rolled to form a seamless cylinder consisting of a diameter in the order of 1 nm and lengths that reach in to centimeters. MWNTs consist of an arrangement of SWNTs, nested concentrically, with a separation of 0.35 nm, which resembles the basal plane separation in graphite [155]. The diameters of MWNTs can range from 2 to 100 nm with lengths in tens of microns. The way in which a graphene sheet is rolled directly affects many of the characteristics of the resulting nanotube. The process of rolling establishes a specific axial direction, because it breaks the symmetry of the planar system. The axial direction is defined by the relative direction of the hexagonal lattice. The nanotube can be metallic, semi–metallic, or semi–conducting depending on the relation between the axial direction and the unit vectors which describe the hexagonal lattice. Semi–conducting nanotubes have band–gaps that are inversely proportional with the diameter of the tube, which varies between $0.18 - 1.8\ eV$ for the widest to narrowest SWNTs that are stable at the given diameters [156].

Single walled nanotubes are classified using a single chiral vector, $\vec{C}$, which connects a chosen origin

atom to a second atom, (see Fig. 4.2), and follows the equation [8]

$$\overrightarrow{C} = n\overrightarrow{a_1} + m\overrightarrow{a_2}. \tag{4.1}$$

Here n and m are integer numbers, and $\overrightarrow{a_1}$ and $\overrightarrow{a_2}$ are the unit cell vectors of the two–dimensional lattice formed by the graphene sheets. The direction of the nanotube length, the nanotube axis, is perpendicular to this chiral vector (see Fig. 4.2). The circumference of the nanotube which is defined by the length of the chiral vector $\overrightarrow{C}$ and is given by [8]

$$c = |\overrightarrow{C}| = a\sqrt{(n^2 + nm + m^2)}, \tag{4.2}$$

where the value a is the length of the unit cell vector $\overrightarrow{a_1}$ and $\overrightarrow{a_2}$. The length a can be used to calculate the carbon–carbon bond length, a_{cc}, and it follows the equation [8]

$$a = |\overrightarrow{a_1}| = |\overrightarrow{a_2}| = a_{cc}\sqrt{3}. \tag{4.3}$$

For graphite, the carbon–carbon bond length, $a_{cc} = 0.1421\ nm$, and the same value is usually used for nanotubes [157]. However, due to the curvature of the tube, the actual bond length is expected to be slightly larger and a value such as $a_{cc} = 0.144\ nm$ should be a better approximation [158, 159, 160]. The diameter of the carbon nanotube is thus given by the equation,

$$r = \frac{a_{cc}\sqrt{3}}{\pi}\sqrt{(n^2 + nm + m^2)}. \tag{4.4}$$

The chiral angle, (shown in Fig. 4.2), is defined as the angle between the chiral vector and zigzag nanotube axis and is given by,

$$\gamma = \tan^{-1}(\frac{m\sqrt{3}}{m + 2n}). \tag{4.5}$$

The pair of integers (n, m), which is related to the chiral vector, is used to describe nanotubes. Three types of CNTs are introduced using (n, m) values: "armchair" type tubes with $n = m$, and $\gamma = 30°$, "zigzag" type tubes with $m = 0$, and $\gamma = 0°$, and "chiral" tubes with $n \neq m$ where γ takes a value between $0°$ and $30°$. The chirality of the nanotube affects the optical, mechanical, and electronic properties of the nanotubes and is determined by (n, m) values, such that with $|n - m| = 3q$ the nanotubes are metallic and those with $|n - m| = 3q \pm 1$ are semiconducting (q is an integer) [8].

4.3 Model Description

A simple rigid model of a chiral molecule is used to study the hopping barriers of enantiomers inside CNTs. The model consists of a central atom bonded to four different atoms in tetrahedral coordination. The properties of molecules confined to narrow carbon nanotubes are mainly controlled by the van der Waals

interactions. In this study, the Lennard–Jones (LJ) potential (see Eq. 4.6) is used to describe the pair potential interactions between the molecules, and also between each chiral molecule and the carbon nanotubes. The CNT structures are considered rigid as well. The pair interactions are defined such that each site "a" on the molecule "i" interacts with all the other sites "b" on the other molecule "j", so the energy of interaction is given by

$$U_{ij}^{(a,b)} = 4\varepsilon_{ij}^{(a,b)} \left[\left(\frac{\sigma_{ij}^{(a,b)}}{r_{ij}^{(a,b)}} \right)^{12} - \left(\frac{\sigma_{ij}^{(a,b)}}{r_{ij}^{(a,b)}} \right)^{6} \right], \tag{4.6}$$

where i and j are used for molecules and a and b are for sites on each molecule, $r_{ij}^{(a,b)} = |\mathbf{r}_i^a - \mathbf{r}_j^b|$ denotes the distance between two interacting sites located on two molecules, $\varepsilon_{ij}^{(a,b)}$ is the LJ potential's well-depth, and $\sigma_{ij}^{(a,b)}$ is the cross collision diameter. The Lorentz–Berthelot [161] rules were used to obtain the cross interaction parameters so that σ_{ij} and ε_{ij} are given by

$$\sigma_{ij}^{(a,b)} = \frac{\sigma_i^{(a)} + \sigma_j^{(b)}}{2}, \tag{4.7}$$

$$\varepsilon_{ij}^{(a,b)} = \left[\varepsilon_i^{(a)} \varepsilon_j^{(b)} \right]^{1/2}. \tag{4.8}$$

atom	x	y	z	l_{Ci}(Å)
C	0.0	0.0	0.0	0.0
H	0.618342137	–0.618342137	–0.618342137	1.071
F	–0.763834405	0.763834405	–0.763834405	1.323
Cl	–1.015559122	–1.015559122	1.015559122	1.759
Br	1.113708668	1.113708668	1.113708668	1.929

Table 4.1: The list of coordinates for atoms in molecule $R-CHFClBr$. l_{Ci}(Å) is the bond length between the central atom, C, and the surrounding atoms, i.

It is well known that carbon with four different substituent atoms forms a chiral molecule. In this study, Bromochlorofluoromethane ($CHFClBr$) is chosen as a basic chiral molecule with two optical enantiomers denoted as $R{-}CHFClBr$ and $S{-}CHFClBr$. The chemical criteria for labeling the $R-$ and $S-$ enantiomers is as follows: The surrounding four atoms (all attached to the cental C atom) are labeled from (1) to (4) according to their molecular mass, $Br \rightarrow (1)$, $Cl \rightarrow (2)$, $F \rightarrow (3)$, and $H \rightarrow (4)$. The central atom is visualized to be located in the plane of the paper and the lightest molecule, in this case $H \rightarrow (4)$ is placed perpendicular to the plane of the paper and pointing away from the viewer. If the rotation from atom (1) to (3) is clockwise, the enantiomer is labeled as $R-$, and if the rotation is counterclockwise the enantiomer will be denoted as $S-$ [162], (see Fig. 4.3). The x, y, and z coordination of the atoms forming the $R-$ and $S-CHFClBr$ are included in Tables 4.1 and 4.2.

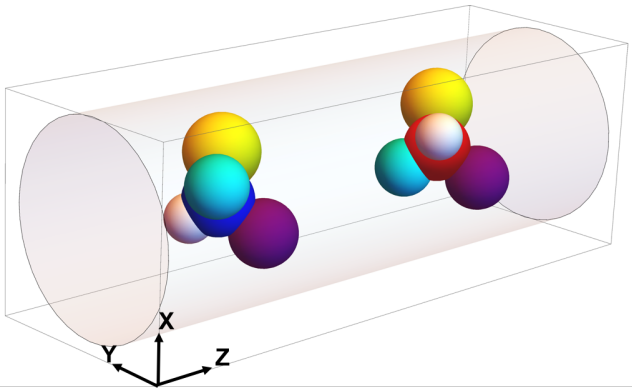

Figure 4.3: A schematic of the tetrahedral model for $S-$ and $R-$ enantiomers inside a cylindrical tube. The central of mass for the $S-$ enantiomer, the shell molecule, is located at $+L/2$ (the enantiomer with the central atom in red color) which defines the volume. The caged molecule, $R-$ enantiomer in this case, is randomly placed within the cage (the enantiomer with the central atom in blue color).

atom	x	y	z	l_{Ci}(Å)
C	0.0	0.0	0.0	0.0
H	–0.618342137	0.618342137	–0.618342137	1.071
F	0.763834405	-0.763834405	-0.763834405	1.323
Cl	–1.015559122	–1.015559122	1.015559122	1.759
Br	1.113708668	1.113708668	1.113708668	1.929

Table 4.2: The list of coordinates for atoms in molecule $S-CHFClBr$. l_{Ci}(Å) is the bond length between the central atom, C, and the surrounding atoms, i.

Each molecule consists of a central LJ sphere, C atom, attached to the four LJ spheres, H, F, Cl, and Br atoms, in a tetrahedral coordination with a bonding angle of 109.5°. The LJ interaction parameters, obtained from reference [163], are summarized in Table 4.3. In reference [163], Quantum Mechanics (QM) calculations are applied at the Hartree–Fock level using the GAUSSIAN 94 program [164] and the $6-311+G^*$ basis set ($6-311+G^*//6-311+G^*$) to obtain the optimized geometry and the energy of $CHFClBr$. The bond lengths and the angles are calculated using the SPARTAN'14 [165] at the Hartree–Fock level and the $6-311+G^*$ basis set.

In very narrow CNTs, SFD behavior is observed where the hopping time is infinite and molecules' motion is restricted to one dimension [146, 166, 167]. Sufficient increase in the channel width will allow transverse motion and will reduce the hopping time and free energy barrier associated with the molecules passing each other. However, a large increase in the channel width will let the particles to easily pass, leading to normal diffusion, so the system is no longer located at its transition region from SFD to normal diffusion. To avoid this problem, different width CNTs are examined to find the appropriate channel size where hopping events

atom	σ(Å)	$\varepsilon(kJmol^{-1})$
C	3.60	0.209
H	2.50	0.125
F	2.75	0.339
Cl	3.47	1.112
Br	3.65	1.647

Table 4.3: Lennard–Jones interaction parameters for molecule $CHFClBr$.

are finite but infrequent enough for the enantiomers to show SFD for a long time between their hops. The CNT(10,6) is chosen as the reference CNT with radius= 5.47Å.

To investigate the effect of structural changes to the enantiomers and the wall, on the hopping barriers, a modified chiral molecule is defined as $R{-}C'H'F'Cl'Br'$ and $S{-}C'H'F'Cl'Br'$, where the atoms have smaller radius, σ, compared to the reference molecule, and a modified CNT is defined with increased interaction parameters, and different carbon diameters on the wall. Tables 4.4 shows the new radii defined for the modified chiral molecule. For the modified molecule, the bond lengths are mainly kept the same, except for the bond length for $C' - H'$ which is increased from 1.071 Å to 1.171 Å. Table 4.5 contains the interaction parameters and carbon diameters on the wall defined for the reference and modified CNTs.

atom	σ(Å)	$\varepsilon(kJmol^{-1})$
C'	2.0	0.209
H'	0.65	0.125
F'	1.4	0.339
Cl'	1.9	1.112
Br'	2.44	1.647

Table 4.4: Lennard–Jones interaction parameters for molecule $C'H'F'Cl'Br'$.

nanotube	σ_C^{wall}(Å)	$\varepsilon_C^{\text{wall}}(kJmol^{-1})$
Reference CNT	3.6	0.209
Modified CNT	2.0-2.5	5.209

Table 4.5: Carbon diameters on CNT walls, and Lennard–Jones interaction parameters chosen for the reference CNT models and modified CNTs .

4.4 Simulation Methods

4.4.1 Free Energy Barrier Calculations

To calculate the free energy barriers associated with two enantiomers passing each other inside a CNT, Monte Carlo simulations are performed using the small n, p_l, T ensemble, described in Section 2.2, with $T = 298.15K$ and $p_l = 100\ atm$.

Because of the relatively high free energy barriers around the TS ($\approx 20\ k_BT$) the direct MC sampling method is not feasible, as this will result in a poor data sampling around the transition state. Therefore, to lower the statistical error in sampling data around the TS, the Umbrella Sampling technique [85, 168], with a harmonic biasing potential and multiple window sampling, is used to obtain the free energy barrier profiles along the reaction coordinate, x_c. A spring constant of $k = 5k_BT$ and a total of 45 independent overlapping simulation windows separated by 1Å were used to calculate the free energy profile along the reaction coordinate in the region, $x_c = 0 - 45$Å. For each biasing window, the weighted free energy barrier calculations for hopping is carried out as follows: one of the enantiomers, is selected as the shell molecule and its center of mass is initially located at $L/2 = 10.0$Å and the second enantiomer is chosen to be the caged particle and is placed randomly within the cage, $-L/2$ and $+L/2$. For each chosen umbrella window, a total of 10^7 MC cycles are performed before collecting data, to ensure the equilibrium, and a total of 2×10^8 MC cycles are performed to collect data, with configurations being sampled every 25000 MC cycles. Each MC cycle includes $n = 2$ trial moves. The trial move for each molecule could either be a translational or a rotational move. The trial moves are conducted with equal frequency. The translational moves are performed with maximum step size of $|\Delta x| = |\Delta y| = |\Delta z| = 0.1 - 0.12$Å. The rotational moves for the molecules are characterized by two angles in the intervals $[0 - \pi]$ and $[0 - 2\pi]$. The rotational moves are performed with a maximum change in both rotational angles of 45°. When the shell molecule is chosen, the trial move will also change the cell length by $2\delta x$ and the position of the caged molecule is rescaled to ensure it remains within the cell, $-L/2$ and $+L/2$. As the volume of the small system is defined by the location of the shell molecule, its position must remain positive during the simulation to ensure $v > 0$. The total energy, U, is the sum of the pair interactions between the sites on one molecule and all the sites on the second molecule, and also between all sites on both the molecules and the carbon atoms on the CNT wall, located within the longitudinal distance of $x_c = \left[2.5 \times (\sigma_i^a + \sigma_C^{\text{wall}})/2.0\right]$ Å from each molecule. In the translational move, the new position of the molecular centers of mass for the chosen molecule is selected and then the new potential energy U^{new} for the system is calculated. The MC acceptance probability for a trial translational move is

calculated using the equation,

$$\begin{aligned}\text{acc}(\text{old} \rightarrow \text{new}) = \min(1, \exp\{ &- \beta[U^{\text{new}} - U^{\text{old}}] \\ &- \beta p_l 2R_p[L^{\text{new}} - L^{\text{old}}] + (n-1)\ln[L^{\text{new}}/L^{\text{old}}] \ \}).\end{aligned} \tag{4.9}$$

In the rotational move, the chosen molecule is rotated and the new energy, U^{new}, for the system is calculated in the same way that is done for the translational move. If the rotational move leads to a configuration of lower energy, $\Delta U < 0$ where $\Delta U = U^{new} - U^{old}$, the move is accepted. Otherwise, the possibility of accepting the rotational move is calculated via the equation

$$\text{acc}(\text{old} \rightarrow \text{new}) = \min\left(1, \exp\left\{-\beta[U_n^{\text{new}} - U_n^{\text{old}}]\right\}\right). \tag{4.10}$$

The Multistate Bennett Acceptance Ratio (MBAR) [169] is used to reconstruct the free energy profile from the weighted probabilities obtained from the simulation. The free energies are normalized and the final ΔG values are obtained as an average over 5–15 independent runs and the error bars are calculated as the standard deviation from the average in ΔGs.

4.5 Simulation Results and Discussion

4.5.1 Free Energy Barriers for Pairs of $CHFClBr$ Enantiomers inside CNT(10,6)

The free energy barriers are calculated for three pairs of $CHFClBr$ enantiomers confined to CNT(10,6):

- A pair of (R)– and (R)– enantiomers, (RR)
- A pair of (S)– and (S)– enantiomers, (SS)
- A pair of (S)– and (R)– enantiomers, (SR)

The high free energy barriers associated with the two molecules attempting to pass inside the relatively narrow CNT, results in poor sampling of the configuration space around the TS. As explained in Section. 4.4, Umbrella Sampling methods are used in this work to enhance the sampling around the TS. To construct a good sampling distribution around the TS, it is necessary to make sure the molecules are able to rotate and sample different orientations. Increasing the value of spring constant, used for the umbrella potential, increases the number of sampled configurations around the TS, however, due to the non-spherical structure of the molecules it also restricts their relative orientations at the TS. Special care was taken into account to find an optimal spring constant, $k = 5k_BT$, and maximum rotational angle, 45°, which enhances the sampling and at the same time does not restrict the orientation of the molecules. Figure 4.4 illustrates the unit vectors which are defined for each molecule to obtain the relative orientation of two molecules with respect to each other. Vectors $\vec{f}$ and $\vec{g}$ represent the direction of $C - Br$ and $C - H$ bonds on each molecule and $\vec{V_1}$ and

$\vec{V_2}$ are defined as the cross product of $\vec{f}$ and $\vec{g}$ for each molecule, $\vec{V_1} = \vec{f_1} \times \vec{g_1}$ and $\vec{V_2} = \vec{f_2} \times \vec{g_2}$. The angle between $\vec{V_1}$ and $\vec{V_2}$ is denoted by θ, and is used to represent the relative orientation of two enantiomers.

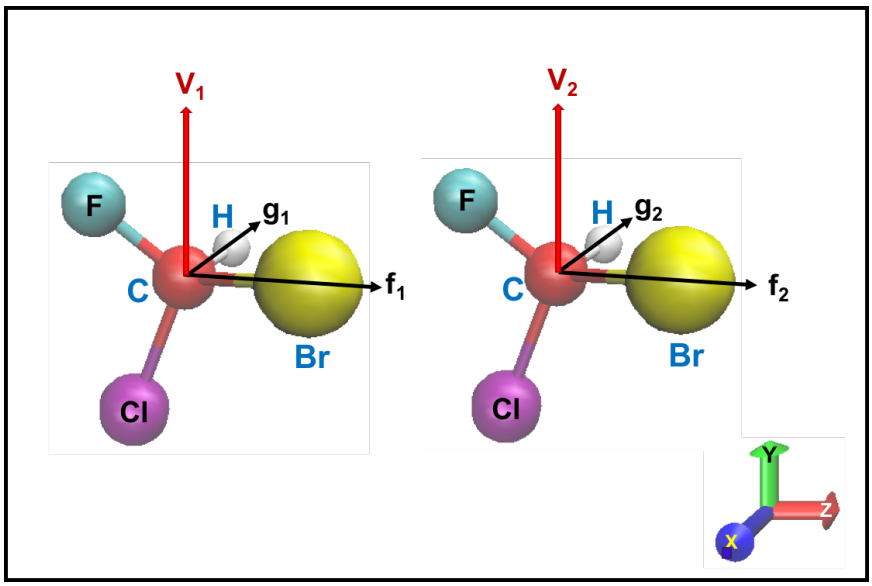

Figure 4.4: The schematic picture shows the unit vectors, V_1 and V_2, which θ angle between them, $\cos(\theta) = \vec{V_1}.\vec{V_2}$, which is used to show the relative orientation of two molecules. $\vec{V_1} = \vec{f_1} \times \vec{g_1}$ and $\vec{V_2} = \vec{f_2} \times \vec{g_2}$.

.

Figure 4.5 shows θ obtained for different pairs of $CHFClBr$ enantiomers inside a CNT(10,6), when their center of mass is located around the TS region, $x_c \sim 0.0$Å. The result shows that there is two equally preferred angles that two enantiomers take with respect to each other and it also indicates that the enantiomers are able to rotate and switch between these two angles within the confinement of the tube. These two angles are energetically equally favorable. It should be noted that θ only gives information about the angle between V_1 and V_2 vectors of two enantiomers and not their absolute orientation that would determine the exact structural orientation of the enantiomers with respect to each other and the nanotube. Therefore, this angle by itself is not sufficient enough to give insights about the absolute orientation of two enantiomers within the tube. Studying the enantiomers' orientations at the TS and its relation to their free energy barrier when they are passing each other is an interesting subject to be investigated, however, it is outside the scope of the current work.

Figure 4.6 shows the free energy profile obtained for the pairs of $S-CHFClBr$ and $R-CHFClBr$ enantiomers inside the CNT(10,6) with Radius= 5.47Å. ΔG^* is located at $x_c = 0$ and the result shows that a pair of $S-CHFClBr$ enantiomers passing each other inside a CNT(10,6) exhibit no significant difference in the free energy barrier compared to a pair of $R-$enantiomers. Hovever, the failure of the carbon nanotube to effectively distinguish between the two enantiomers of $CHFClBr$ does not rule out the possibility that

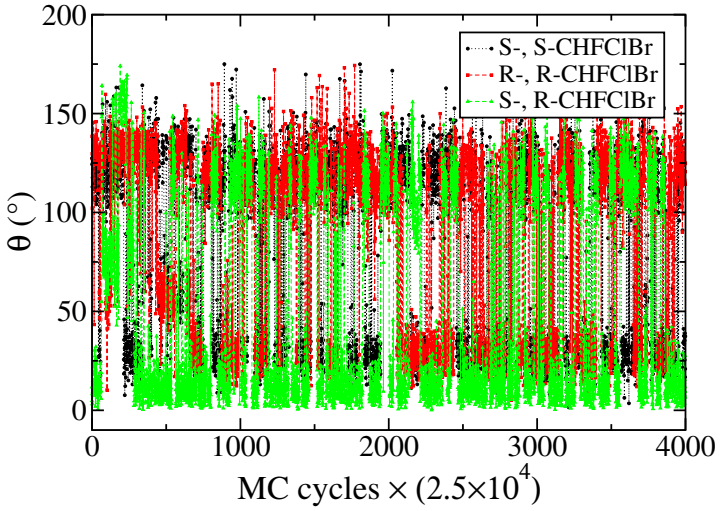

Figure 4.5: The relative orientation of two enantiomers, (θ), when $x_c \sim 0.0$Å as a function of MC cycles for two pairs of $S-CHFClBr$ and $R-CHFClBr$ enantiomers inside a modified CNT(10,6).

.

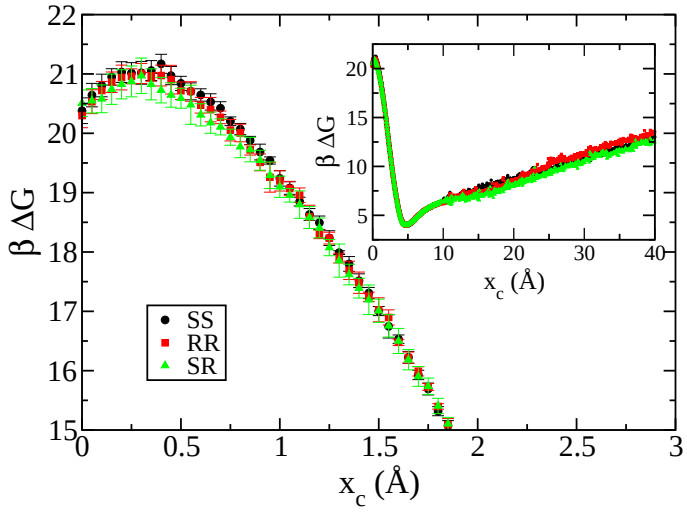

Figure 4.6: Gibbs free energy profile, ΔG, as a function of $x_c = (0-3)$Å for three pairs of $S-CHFClBr$ and $R-CHFClBr$ enantiomers inside a CNT(10,6) with radius=5.47 Å. Inset: Free energy as a function of whole reaction coordinate: $x_c = (0-40)$Å for three pairs of $R-CHFClBr$ and $S-CHFClBr$ enantiomers inside a CNT(10,6). ΔG values in $x_c = (0-10)$Å region are obtained from 10 independent runs and in $x_c = (10-40)$Å region are obtained from a single run.

.

chirality can affect diffusion in single file systems in all cases. It may be that the chiral interaction between the enantiomers and the CNT is too weak in this case [144, 145, 170]. Or the diameter of the CNT(10,6) is still too wide to have an effect. The spherical–like structure of the enantiomers could also make it hard for the chiral tube to pick the difference between the two enantiomers and therefore results in similar free energy barriers for the enantiomers. The combination of all the factors must be considered to effectively investigate their combined effects on the diffusion behavior of the enantiomers inside the chiral tubes.

4.5.2 Free Energy Barrier Calculations for Pairs of $CHFClBr$ Enantiomers inside Modified CNTs

To examine the chiral interaction effect on the free energy barriers associated with two enantiomers passing each other, the LJ interaction parameters defined for C atoms on the CNT(10,6), $\varepsilon_C^{\text{wall}}$, is increased from $\varepsilon_C^{\text{wall}} = 0.209 kJmol^{-1}$ to $\varepsilon_C^{\text{wall}} = 5.209\ kJmol^{-1}$, to define the modified CNT(10,6), and the free energy barriers are calculated for the pairs of $CHFClBr$ enantiomers. Fig. 4.7 shows the free energy profile obtained for three binary pairs of $S-CHFClBr$ and $R-CHFClBr$, inside the modified CNT(10,6). Increasing the LJ interactions of C atoms on the wall with the enantiomers (with all the atoms present in each enantiomer's structure), results in higher energy barrier required for passing within the same size CNT(10,6). Stronger interactions between the wall and enantiomers creates some differences in the free energy profile between a pair of $S-$ and $R-$ enantiomers at $x_c = 0.5 - 3.0$Å. However, the difference goes away in the transition state region where $x_c = 0.0$Å.

Figure 4.8 shows θ between each pair of enantiomers for two pairs of $S-CHFClBr$ and $R-CHFClBr$ enantiomers inside the CNT(10,6), when their center of mass is located around the TS region, $x_c \sim 0.0$ Å. Unlike the two equally preferred angles that the two enantiomers take when they were placed inside a reference CNT(10,6), an unmodified CNT(10,6), (see Fig. 4.5), in this case, the enantiomers prefer one orientation ($\theta = 125°$) over the other ($\theta = 25°$) when they are placed inside the modified CNT(10,6), (see Fig. 4.8). Figure 4.9 shows the interaction energy between the enantiomers and the CNT wall when they are placed inside a CNT(10,6) and a modified CNT(10,6) with increased LJ interaction parameters. The result shows when the enantiomers are placed within a CNT(10,6) they take two angles with respect to each other, $\theta \simeq 25°$ and $\theta \simeq 125°$, (see Fig. 4.5) and since both these angles are energetically the same (see Fig. 4.9 (a)) they are able to switch back and forth between both orientations when located at the TS region. However, when they are placed inside the modified CNT(10,6), $\theta \simeq 125°$ is energetically preferred over the other orientation (see Figs. 4.8 and 4.9 (b)). Therefore, when each pair of enantiomers are passing each other inside the modified CNT(10,6) they are limited to fewer possible orientations, giving rise to the higher free energy barrier, $\beta\Delta G^* \simeq 31$ (see Fig. 4.7).

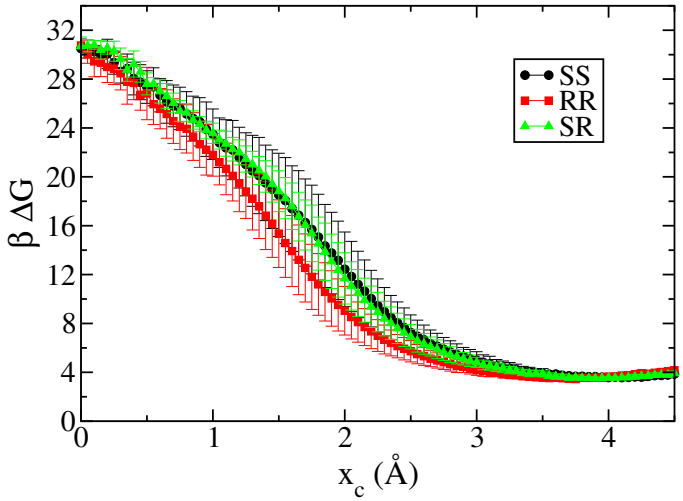

Figure 4.7: Gibbs free energy, ΔG, as a function of $x_c = (0-4.5)$Å for three pairs of $S-CHFClBr$ and $R-CHFClBr$ enantiomers inside a modified CNT(10,6) with increased LJ interaction parameter for C atoms on the wall, $\varepsilon_C^{\text{wall}} = 5.209\ kJmol^{-1}$. ΔG values are obtained from 5 independent runs.

.

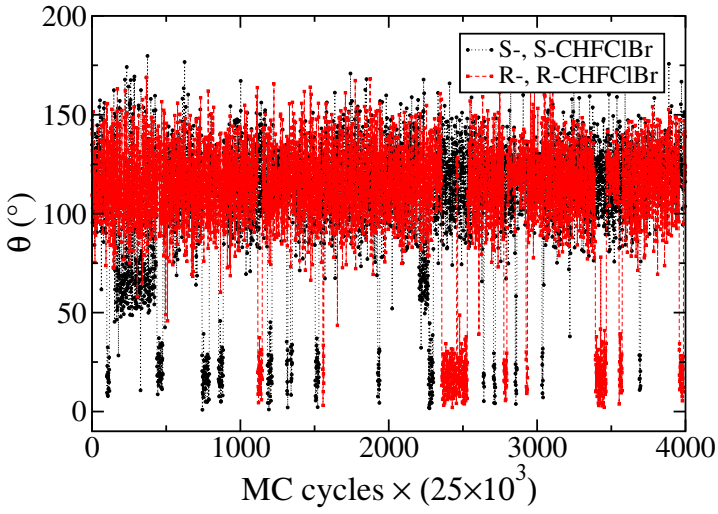

Figure 4.8: The relative orientation of two enantiomers (θ) as a function of MC cycles, when $x_c \sim 0.0$Å, for two pairs of $S-CHFClBr$ and $R-CHFClBr$ enantiomers inside a modified CNT(10,6) with increased LJ interaction parameter for C atoms on the wall, $\varepsilon_C^{\text{wall}} = 5.209 kJmol^{-1}$.

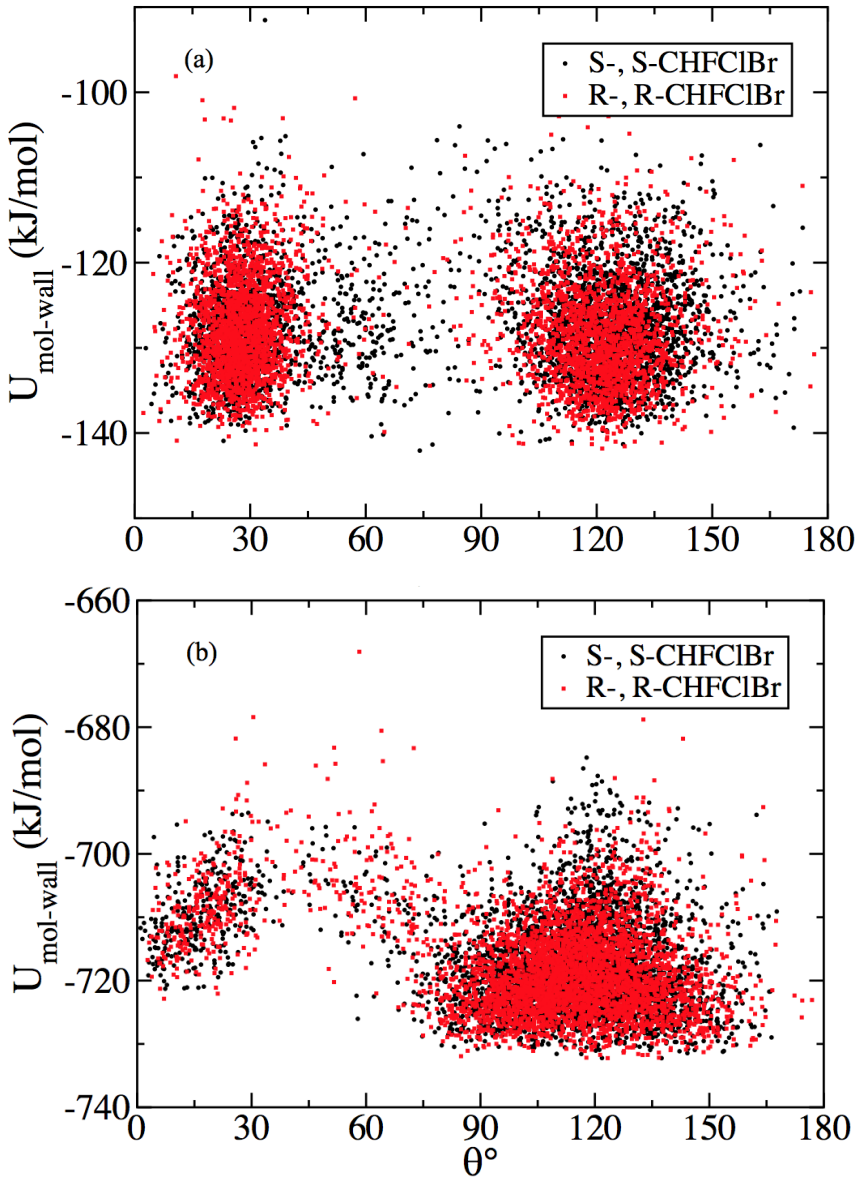

Figure 4.9: (a) $S-, S-CHFClBr$ and $R-, R-CHFClBr$ enantiomers LJ interaction with CNT(10,6) walls as a function of θ when they are located around the transition state, $x_c \sim 0.0$Å. (b) $S-, S-CHFClBr$ and $R-, R-CHFClBr$ enantiomers LJ interaction with modified CNT(10,6) walls with increased LJ interaction parameter for C atoms on the wall as a function of θ when they are located around the transition state, $x_c \sim 0.0$Å.

.

4.5.3 Free Energy Barrier Calculations for Pairs of Modified $C'H'F'Cl'Br'$ Enantiomers inside Modified CNTs

This section investigates how changing the structure of the enantiomers and also controlling the radius of the channel can affect their hopping barriers inside the modified chiral CNTs. A modified molecule, $C'H'F'Cl'Br'$, and modified CNTs are defined using the parameters listed in Tables. 4.4 and 4.5. To build the structure of the modified enantiomers, the bond lengths are kept the same as the reference molecule, $CHFClBr$, except for the $C'-H'$ length, but the diameters of the atoms were reduced, which provides a less spherical structure for the molecules. Figure 4.10 provides a schematic comparison between the reference, $CHFClBr$, and the modified, $C'H'F'Cl'Br'$ molecules.

CNTs can be considered as single sheets of graphite which is rolled at different angles (which depends on n and m index of CNTs). Choosing different rolling angles results in different nanotube properties and different diameters for nanotubes. Therefore, changing the n and m indexes to obtain wider or narrower tubes will result in tubes with different chirality and also one cannot incrementally change the diameter of the tube as the diameter is determined based on the chosen n and m indexes. To keep the chirality fixed and have a control over the diameter of the CNTs, the size of the carbon atoms diameters on the modified CNT(8,3) walls are varied between $\sigma_C^{\text{wall}} = 2.0 - 2.5$Å. Therefore, a modified CNT(8,3) with $\sigma_C^{\text{wall}} = 2.0$Å results in the widest tube, and a modified CNT(8,3) with $\sigma_C^{\text{wall}} = 2.5$Å results in the narrowest tube.

Figure 4.11 shows the free energy profile obtained for three pairs of modified $S-CHFClBr$ and $R-CHFClBr$ enantiomers inside a modified CNT(8,3) with $\sigma_C^{\text{wall}} = 2.0$Å and Radius = 3.85Å. This is the widest tube and the result shows that there is no difference between the hopping barrier for different mixtures of $S-$ and $R-$ enantiomers. However, there is a significant drop in the hopping barrier for the modified enantiomers inside the modified CNT(8,3), $\beta\Delta G^* \simeq 5.1$, compared to hopping barrier for $CHFClBr$ enantiomers inside the CNT(10,6), $\beta\Delta G^* \simeq 31$ (see Fig. 4.7). One possible explanation could be that the relative diameter of CNT(8,3) to the size of modified enantiomers is wider than that of CNT(10,6) to $CHFClBr$ enantiomers. Another explanation could be related to the modified molecule's structure which is less spherical. As a result the modified enantiomers can take orientations under which the hopping becomes more likely. Figure 4.12 shows the interaction energy between the modified enantiomers and the modified CNT(8,3) wall. The result shows that both enantiomers can take all the possible orientations which is reflected by θ. Figure 4.12 also indicates that all these angles are energetically the same, which suggest the enantiomers are free to take any orientation which would make their hopping easier. As a result the enantiomers are encountering a smaller barrier to overcome when they are passing each other.

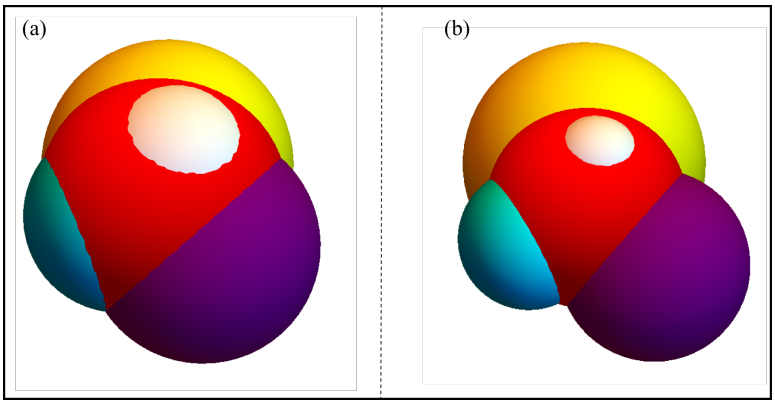

Figure 4.10: (a) Reference molecule $CHFClBr$ structure (b) Modified molecule $C'H'F'Cl'Br'$ structure.

.

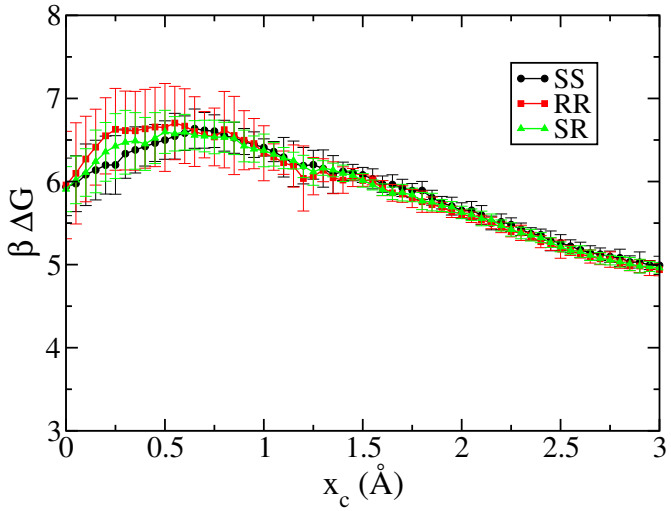

Figure 4.11: Gibbs free energy profile, ΔG, as a function of $x_c = (0 - 3.0)$Å for three pairs of modified $S - C'H'F'Cl'Br'$ and $R - C'H'F'Cl'Br'$ enantiomers inside a modified CNT(8,3) with increased LJ interaction parameter for C atoms on the wall, $\varepsilon_C^{\text{wall}} = 5.209\ kJmol^{-1}$ and $\sigma_C^{\text{wall}} = 2.0$Å. ΔG values are obtained from 15 independent runs.

.

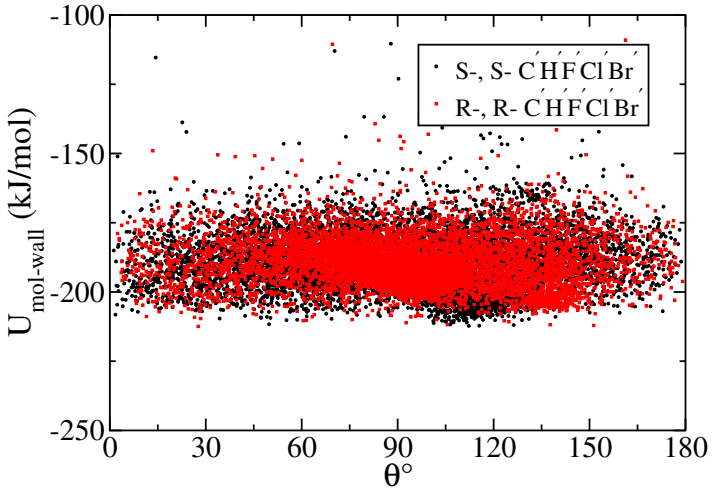

Figure 4.12: (a) $S-, S-C'H'F'Cl'Br'$ and $R-, R-C'H'F'Cl'Br'$ enantiomers LJ interaction with modified CNT(8,3) walls, with $\sigma_C^{\text{wall}} = 2.0$Å, as a function of θ when they are located around the transition state, $x_c \sim 0.0$Å.

.

4.5.4 Chirality Effect on the Hopping Barrier

In order to investigate the chirality effect on the hopping barrier for different pairs of enantiomers of the modified $C'H'F'Cl'Br'$, it is necessary to have access to a sufficiently narrow tube to ensure the SFD to normal diffusion region is long enough to observe single file diffusion behavior in the system. Fig. 4.13 (a), (b), and (c) shows the free energy profile obtained for three pairs of modified $S-C'H'F'Cl'Br'$ and $R-C'H'F'Cl'Br'$ enantiomers inside a modified CNT(8,3) with σ_C^{wall} adjusted to: (a) $\sigma_C^{\text{wall}} = 2.3$Å, (b) $\sigma_C^{\text{wall}} = 2.4$Å, and (c) $\sigma_C^{\text{wall}} = 2.5$Å. The result indicate that there is a difference in the free energy barrier for the different pairs of enantiomers inside modified CNT(8,3) for all the chosen radii. Fig. 4.13 (a), (b), and (c) shows that the pairs of $R-C'H'F'Cl'Br'$ enantiomers represent higher hopping barrier compared to the pairs of $S-C'H'F'Cl'Br'$ enantiomers for all the channel radii. Also, it can be seen, from Fig. 4.13, that the free energy gap between the enantiomers increases by decreasing the nanotube diameter. If the chirality of the nanotube plays a role in the diffusion behavior of the two enantiomers it would be expected that the free energy barriers flip by reversing the chirality of the tube. Therefore, the same free energy calculations were performed for the modified enantiomers inside the nanotubes with reversed chirality, CNT(3,8)s. Figure 4.13 (d), (e), and (f) shows the free energy profile obtained for three pairs of modified $S-CHFClBr$ and $R-CHFClBr$ enantiomers inside a modified CNT(3,8) with σ_C^{wall} adjusted to: (d) $\sigma_C^{\text{wall}} = 2.3$Å, (e) $\sigma_C^{\text{wall}} = 2.4$Å, and (f) $\sigma_C^{\text{wall}} = 2.5$Å. The result shows that there is a difference in the free

energy barrier for the different pairs of enantiomers for all the chosen radii for a modified CNT(3,8). This behavior is similar to that is observed for a modified CNT(8,3), however, when the enantiomers are placed inside a modified CNT(3,8) the pair of $S - C'H'F'Cl'Br'$ enantiomers exhibit a higher hopping barriers. The results clearly show that the free energy barriers flip when the chrality of the tube is reversed. This suggests that the chirality has an effect in deriving the free energy gap between two enantiomers of modified $CHFClBr$ enantiomer.

4.5.5 Free Energy Barrier Calculations for Pairs of Modified $C'H'F'Cl'Br'$ Enantiomers inside Modified CNT(6,6)

Figure 4.14 provides the free energy profile obtained for three pairs of modified $S - C'H'F'Cl'Br'$ and $R-C'H'F'Cl'Br'$ enantiomers inside an achiral modified CNT(6,6) with increased LJ interaction parameter for C atoms on the wall, $\varepsilon_C^{\text{wall}} = 5.209\ kJmol^{-1}$, $\sigma_C^{\text{wall}} = 2.4$Å, and Radius = 4.06Å. In this case, the height of the free energy barrier at the transition state, $\Delta G^* \simeq 6.5\ kJmol^{-1}$, is similar to the height of the barrier for the modified CNT(8,3) and CNT(3,8), with $\sigma_C^{\text{wall}} = 2.3$Å. This suggests that the relative size of the channels to the enantiomers are comparable. Observing no difference in the hopping barriers for two enantiomers obtained for the achiral CNT(6,6) to the difference in their hopping barriers for the modifed CNT(8,3) and CNT(3,8) indicates that the difference in the hopping barrier for two enantiomers could originate from the chirality effect of the nanotubes, modified CNT(8,3) and CNT(3,8).

4.5.6 Periodic Wall Interaction Effect

In the partition function analysis for the the small n, p_l, T ensemble introduced by Corti, and explained in Sections 1.5 and 2.2, it is assumed that the small system ensemble is restricted to a uniform spherical, or a symmetrical shape volume and therefore choosing the location of the center of the tube is arbitrary. However, in the current Chapter, the free energy barriers were investigated for different pairs of enantiomers confined to carbon nanotubes, where the wall which defines the volume of the small system is no longer symmetrical. To address these concerns, the interaction of the two pairs of a modified enantiomers with a confining modified CNT(8,3) is calculated while they are located on top of each other and moving across the nanotube. Figure 4.15 shows the two pair of modified $S-, S - C'H'F'Cl'Br'$ and $R-, R - C'H'F'Cl'Br'$ interaction with the the modified CNT(8,3) wall, while both enantiomers are located on top of each other and are gradually shifted along the longitudinal direction of the nanotube. The result indicates that the energy fluctuations varies very rapidly so that the periodicity of the tube is very short compared to the big fluctuations in the channels' volume. Therefore, it could be concluded that the location of the center of the tube and where it is chosen probably does not affect the free energy calculation result.

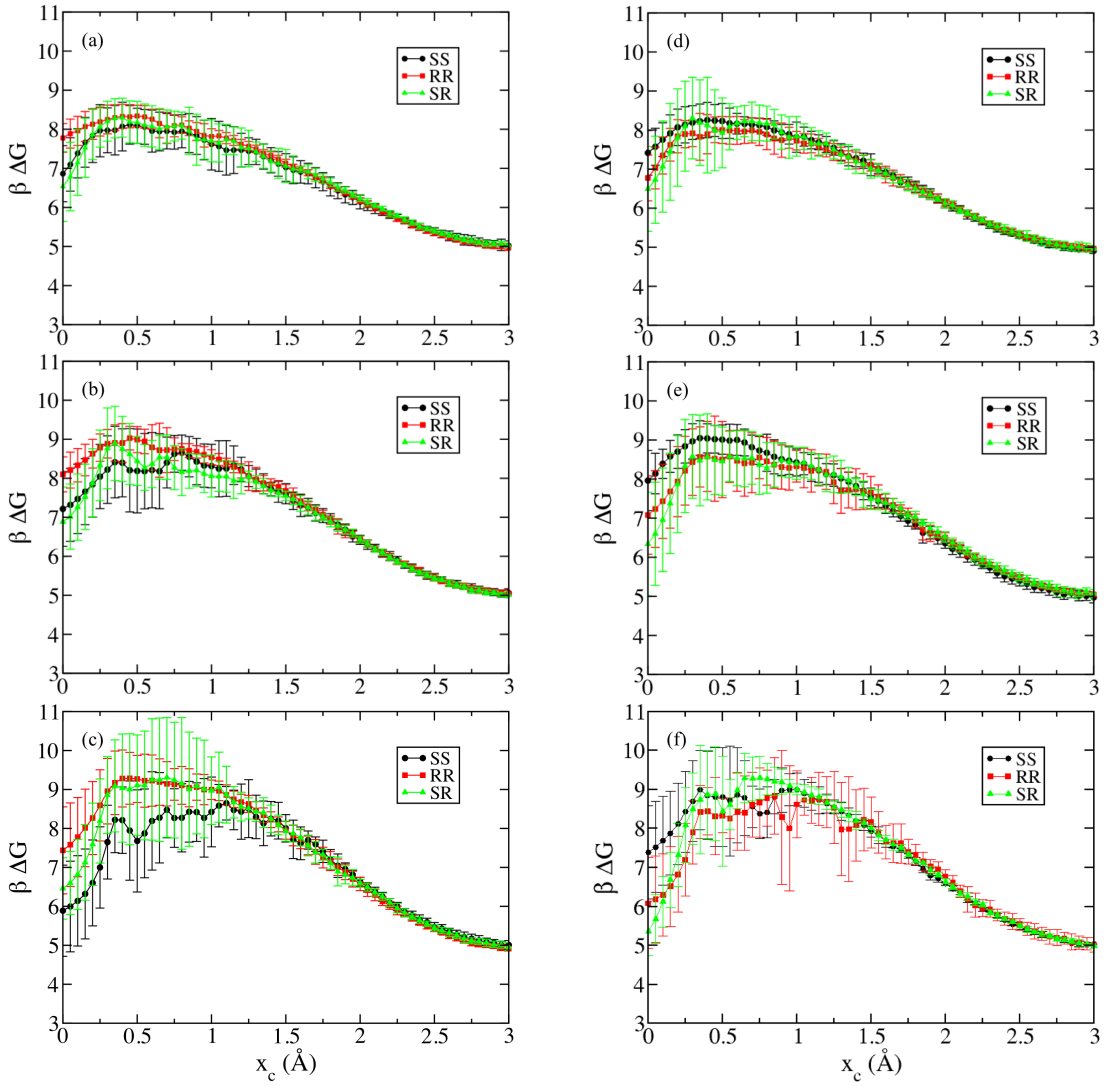

Figure 4.13: Gibbs free energy profile, ΔG, as a function of $x_c = (0 - 3.0)$Å for three pairs of modified $S - C'H'F'Cl'Br'$ and $R - C'H'F'Cl'Br'$ enantiomers inside a modified CNT(8,3), ((a), (b), and (c), and modified CNT(3,8), (d), (e), and (f), with increased LJ interaction parameter for C atoms on the wall, $\varepsilon_C^{\text{wall}} = 5.209\ kJmol^{-1}$ and σ_C^{wall} adjusted to: (a) and (d) $\sigma_C^{\text{wall}} = 2.3$Å, (b) and (e) $\sigma_C^{\text{wall}} = 2.4$Å, and (c) and (f) $\sigma_C^{\text{wall}} = 2.5$Å. ΔG values for each case are obtained from 15 independent runs.

.

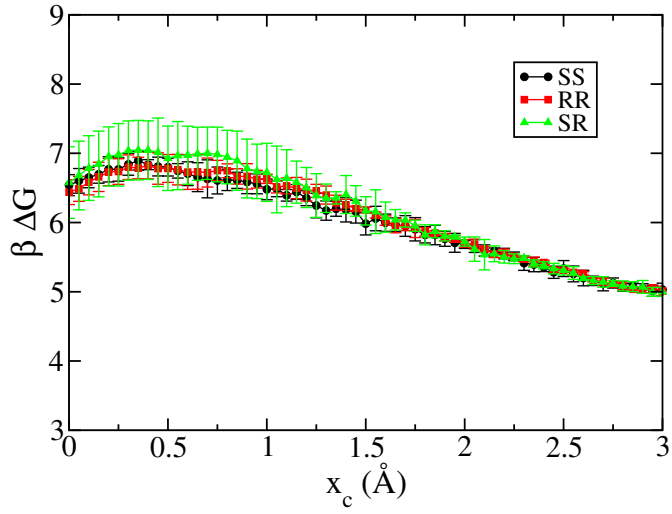

Figure 4.14: Gibbs free energy profile, ΔG, as a function of $x_c = (0 - 3.0)$Å for three pairs of a modified $S-C'H'F'Cl'Br'$ and $R-C'H'F'Cl'Br'$ enantiomers inside a modified and achiral CNT(6,6) with increased LJ interaction parameter for C atoms on the wall, $\varepsilon_C^{\text{wall}} = 5.209\ kJmol^{-1}$ and σ_C^{wall} on the wall adjusted $\sigma_C^{\text{wall}} = 2.4$Å. ΔG values are obtained from 15 independent runs.

.

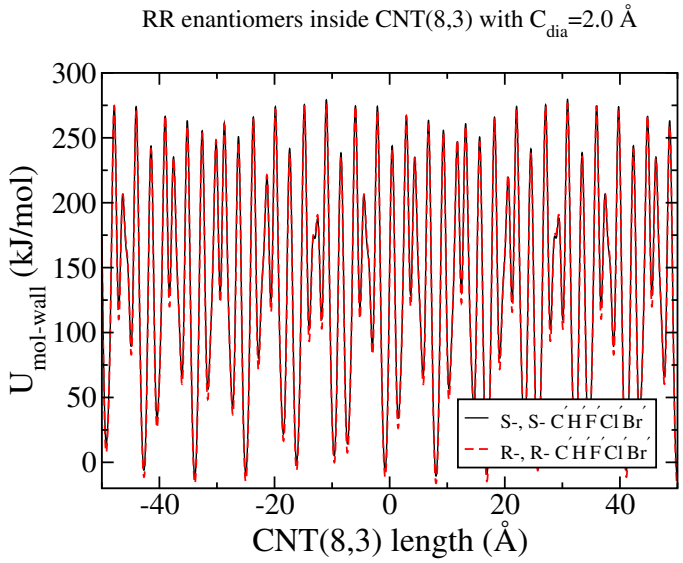

Figure 4.15: (a) $S-, S-C'H'F'Cl'Br'$ and $R-, R-C'H'F'Cl'Br'$ enantiomers LJ interaction with a modified CNT(8,3) walls, with $\sigma_C^{\text{wall}} = 2.0$ Å, as a function of the CNT(8,3) length.

.

4.6 Conclusion

It was shown that by choosing an effective interaction parameter between the enantiomers and CNTs and also relatively narrow nanotubes, chiral effects become apparent and enantiomers exhibit different free energy barriers while attempting to pass each other. The existence of different free energy barriers suggests different hopping times for two enantiomers of a chiral molecule and therefore different tracer particle diffusion behavior. It remains an open question as to whether differences in tracer diffusion in multicomponent systems influences the long time transport properties of the system, but if the hopping times play a role in the transport, then SFD could be used as a useful tool for separation of racemic mixtures and it suggests that the methods developed here can be used to explore separation in the systems that the chirality plays a significant role in diffusion of enantiomers inside nanotubes. As a result, the proposed approach can be used as an effective tool in investigating the chirality effect on the diffusion of enantiomers inside narrow chiral channels and also separation of mixtures. Despite its simplicity, this method provides a qualitative description of hopping time for the systems studied here. For a quantitative prediction of hopping time, the kinetic prefactor must also be determined. It is important to note that, confirming the existence of different diffusion behaviors for two enantiomers inside chiral nanotubes requires direct measurements of hopping times as well.

Chapter 5

Discussion, Conclusions, and Future Work

5.1 Discussion and Conclusions

The subdiffusive behavior of a tagged particle confined into a narrow channel is the key feature of Single File Diffusion. This results in a slowdown in tracer diffusion rate inside single file systems compared to the bulk diffusion behavior [43, 44]. When the channel is wide enough, the particles can pass each other which leads to normal diffusion in the long time limit. In the crossover regime between SFD and normal diffusion, hopping events are rare and the particles perform SFD on intermediate time scales, before eventually passing[66, 67]. Percus and Mon [28] developed a simple phenomenological approach that connects the longtime diffusion coefficient to a hopping time that measures the average time required for a particle to escape its local cage. The hopping time theory is an attractive approach to understanding diffusion in single file systems because it is able to describe the long time dynamic behavior of the tracer particle in terms of a single, short time parameter. Furthermore, the hopping time contains information about all the system parameters, such as particle–particle, particle–wall interaction and density, that influence diffusion[3, 28, 29, 31]. The main goals of this thesis were addressing a few interesting questions that relate to the dynamics of fluids in single file systems and its potential applications. The first goal of this thesis was to provide a quantitative measure of the hopping times in single file systems, using transition state theory. The second goal of this work was to investigate the inter–molecular potential influence on the hopping time in a single file system. The final focus of the thesis was exploring the possibility that different enantiomers of a chiral molecule interact differently with a chiral tube, creating a difference in their hopping barrier, which could be used to control the tracer particle diffusion of different components of a mixture.

The activated nature of hopping process in these systems makes transition state theory a good candidate for the calculation of the hopping time, τ_{hop}. Based on TST, the rate at which two particles pass each other is proportional to the probability of finding the system at the top of the transition barrier[30, 31]. The challenge here is to correctly calculate the probability of being in the transition state for a system consisting of a particle caged between its neighbors, which is not in the thermodynamic limit, and exhibits volume fluctuations. Formulating the statistical ensemble for describing nano–scale systems has been a challenge,

because such systems are strongly influenced by their surrounding medium. For the case of the N, p, T ensemble, the system is immersed in a surrounding bath which imposes a fixed external pressure to the system via a physical or mathematical boundary that defines the system's volume and allows it to fluctuate. For a N, p, T ensemble, where the volume is considered as continuous variable, the partition function defined by Eq. 1.31 requires a volume scale, V_o, to ensure it remains dimensionless. In the thermodynamic limit, the choice of the volume scale is arbitrary, however, for small systems the volume scale is system size dependent and therefore must be taken inside the integral.

In this work, the issue of the volume scale is overcome by applying Corti's shell particle approach[4, 94, 92] to a system of two particles confined to a single file channel [5, 1, 4]. The shell particle defines the volume of the system, as described by Corti, but it also acts as the caging neighbor particle that must be passed in order for a hopping event to occur. The reaction coordinate for the hopping process can then be defined as the longitudinal distance between the shell particle and the cage particle.

To test the validity of the TST approach, the free energy barriers and hopping times were calculated for a two dimensional ideal gas system and a two dimensional hard disc system, where the results can be analytically calculated. The hopping times obtained from the theory were also compared to τ_{hop} measured directly in the simulation of large systems. The linear relationship between $\ln\tau_{hop}$ and ΔG^* with the slope of unity for all the radii studied for ideal gas system (Section 2.4), confirms that the probabilities are correctly normalized, using the TST method with a shell particle.

In deriving the partition function for the small n, p_l, T system (see Section 2.2), an assumption is made by which the potential interactions between the small system and its surroundings are neglected. This assumption is correct for the ideal gas system, however, it is not correct for other systems, where the particles are interacting with each other and their surrounding media. As a result, the method is restricted to narrow channels and low pressure conditions, where the interaction between the small system and its surrounding is negligible. The results of this work confirm the validity of the proposed method for the quantitative measure of hopping times for the systems studied (Chapter 2 and Chapter 3). However, for the cases where the interactions between the small system and its surrounding are not negligible, such as systems with soft, longer range potentials, including the interaction potential term in partition function, U_σ, can improve the accuracy of the method. Nevertheless, the simplicity of the proposed method in capturing the general trends in hopping time, by determining the factors that influence diffusion, makes it a great tool for studying diffusion in such systems. Comparing Figs. 3.2 and 3.4 confirms that TST method, which only relies on free energy barrier calculations associated with two particles passing each other at the TS, is capable of predicting the general trends in hopping time for the systems studied here.

In addition, it was shown that the kinetic prefactor, which appears in the hopping time calculations, has a dependency on the channels' diameter, and also on the particles' interaction parameters. Because of

this dependency, the inclusion of the prefactor term to the free energy calculations is necessary in achieving a quantitative prediction for hopping time. This effect is clearly demonstrated for both hard discs and repulsive discs systems confined between hard wall channels. For hard discs systems, the prefactor has a dependency on the channel width that becomes more dominant as the channel becomes narrower. The same effect is observed for the repulsive particles. For the narrower channels and with relatively harder interactions, smaller $1/\alpha$ values, the prefactor is strongly potential dependent. However, this dependency becomes negligible for the softer particles and wider channels.

Investigating particle softness effect on their hopping time behavior reveals an unexpected maximum for both the free energy barrier and hopping times as a function of particles softness for the 2d system of repulsive discs. Transition state theory developed here allows the position of this maximum to be determined and investigates how it is influenced by varying the system parameters. It was shown that the presence of the hopping barrier maximum as a function of particles softness originates from a competition between the energy and entropy in the transition state as the interaction parameters are varied. Unlike the hard particle interactions, when the particles are soft they are allowed to overlap with each other, which results in an increase in the energy and the entropy of the system relative to the ideal gas. Studying the 1d ensemble of states associated with the transition state shows that the entropy gradually increasing when the particles softness increases, moving from $1/\alpha = 0$ to $1/\alpha = 0.2$. However, the energy grows more rapidly for small $1/\alpha$ before it finally plateaus as the $1/\alpha$ value is increased. This results in an initial increase in the height of the barrier followed by a decrease as the particles become softer, i. e. for larger $1/\alpha$ values.

Chapter 3, demonstrates that the two particle n, p_l, T ensemble can successfully predict the influence of the particle–particle interaction potential on the long time diffusion behavior of the interacting repulsive discs system. In particular, the method is capable of the quantitative prediction of the hopping time to within a factor of two. However, the method does overestimate the hopping time for the narrower channels and underestimates it for the wider channels. This could originate from a few assumptions that were considered in the developing the method using TST and small system ensemble. It is expected for the TST to underestimate the hopping time as it does not consider the barrier recrossing effects that can lead to a higher free energy barrier. In addition, in constructing the small system n, p_l, T ensemble the interaction effects between the particles within the small system and their surrounding bath was not included in the derivation of the partition function for the system. This can result in errors in the free energy calculations, being more dominant for the wider channels and for the systems with longer range potentials and more negligible for the narrower channels and harder potentials. In addition, in the kinetic prefactor calculation, only two particles were considered, which neglects the role of second neighbors in particle transition rate, that may have influence on the escape of a particle from its cage. Including the interaction potential between small system particles and its surrounding, U_σ, and improvements that account for trajectory recrossing at

the transition state, which lead to a better estimation of the prefactor term, should enhance the accuracy of the method. However, despite all the assumptions made, the simplicity of the proposed method and its accuracy which predicts the hopping times within a factor of two, makes it a useful tool in understanding diffusion in highly confined fluids.

The simplicity of the method also makes it ideal for the prediction of the dynamics properties of particles confined to narrow channels and is a good candidate to be used for determining the optimal pore radius, interaction parameters between the particles, and the type of particle–wall interaction for diffusion in single file systems. To demonstrate the general principles, the hopping time approach and TST method were used to obtain the interaction parameter that corresponded to the slowest diffusion rate for the particles in the systems of repulsive discs studied in Chapter 3. This highlights the attractive feature of the hopping time approach, which can be used as a tool to optimize and influence dynamics and mobility of tracer particle in single file systems. Because of the TST's simplicity, and efficiency in predicting hopping time trends, it was used for the hopping time evaluations during the optimization process. It was shown that the result obtained from the optimization were in agreement with the result predicted by TST method.

It has long been suggested that single file diffusion in the cross over regime could be used to separate mixtures of different sized particles [29, 33, 34, 35]. For example, choosing the right sized channel can lead to dual mode diffusion, where the large particles are unable to pass and diffuse slowly performing SFD while the smaller particles can hop, allowing them to diffuse quickly. The final goal was to explore the possibility that subtle differences in the potential interaction of a mixture would be sufficient to cause the particles of a mixture to exhibit different hopping times, that may lead to differences in diffusion. If so, this approach could be used to control the diffusion of different components of a mixture for the purpose of separation. In particular, it was proposed that enantiomers of a chiral molecule might interact differently with a chiral channel which could result in differences in their hopping barrier when passing each other inside a chiral nanotube. To shed light on this hypothesis, the free energy profile for different pairs of two enantiomers of a chiral molecule, $CHFClBr$, inside a chiral carbon nanotube, CNT(10,6), were calculated. The initial results showed that there is no notable difference between the hopping barrier for a pair of $R-CHFClBr$ enantiomers compared to a pair of $S-CHFClBr$ enantiomers.

However, this does not rule out the possibility that the chirality can affect the hopping behavior of enantiomers inside chiral nanotubes in general, altering the interactions of the system, it was found that beside the chirality of the channel, the structure of the chiral molecule, and the interaction parameters between the channel and the molecules inside the system play an important role in determining the height of the hopping barrier for the different enantiomer pairs. A modified $C'H'F'Cl'Br'$ molecule, with a less spherical structure compared to the reference $CHFClBr$ molecule, and a modified CNT(8,3), which provides a control over the diameter of the channel while keeping the chirality of the channel fixed, were defined. The free energy

profiles show that the hopping barrier is higher for the pair of modified $R-C'H'F'Cl'Br'$ enantiomers than the pair of modified $S-C'H'F'Cl'Br'$ enantiomers when confined to the modified CNT(8,3). The existence of the free energy gap confirms that the modified chiral tube, modified CNT(8,3), is able to differentiate between the two enantiomers of the modified chiral molecule. Furthermore, reversing the chirality of the tube results in a flip in the hopping barriers for the enantiomers, such that inside a CNT(3,8), with reversed chirality, the pair of $S-C'H'F'Cl'Br'$ enantiomers exhibit a higher hopping barrier. This confirms that the chirality of the tube plays an important role in creation of the hopping barrier gap between two enantiomers.

In addition, the effect of the channel width on the hopping barrier gap between two enantiomers under the same chirality effect was investigated. The result shows that the difference between the hopping barrier for two pairs of the enantiomers increases by decreasing the channel diameter, while keeping the chirality of the tube fixed. This finding is in agreement with the previous result [29], which indicates reducing the channel size increases the relative height of the hopping barrier.

The difference in the free energy barriers between two different pairs of enantiomers passing each other inside a chiral tube, is an interesting result, that suggests that different enantiomers may exhibit different rate of diffusion that can be used for enantiomeric separation if a suitable chiral channel can be found.

5.2 Future Outlook

5.2.1 Improvements to the Transition State Theory Calculations

The small system isothermal-isobaric partition function, developed by Corti [4] is a key element of the of barrier calculations developed in this thesis. It provides a rigorous formulation of the partition function without the need for a system size dependent volume scale and accounts for the volume fluctuations associated with the motion of particles forming the cage. In defining the partition function for a small n, p_l, T ensemble, considered here, it was assumed the interactions between the small system and its surrounding, U_σ, are negligible. Although the assumption is valid for very narrow channels and for the systems exposed to low external pressure, it becomes more complicated for the systems with longer range interaction potentials or systems with wider channels. For the purpose of quantitative prediction of hopping time, neglecting the small system's interaction with its surrounding bath results in errors as the hopping time is sensitive to the height of free energy barrier. Therefore, the inclusion of U_σ in the partition function and a deeper understanding of how it can influence the free energy barrier associated with particles passing each other inside the small system becomes important and needs to be addressed. The challenge in inclusion of the U_σ in the partition function is associated with the average term, $\langle Q^*_{n,v} \rangle_o$, which appears in the calculation of the partition function and is stated via Eq. 1.52. This term indicates ensemble averaging of the small system over all the configurations of the remaining particles, $N - n$, in the surrounding bath. In a study performed by Bowles *et al.* [171], they studied the interaction of clusters with their surroundings and they used a strategy that separates out the interactions between two systems, a cluster consists of n particles and its surroundings system consists of $N - n$ particles. This approach can be used to decouple the small n, p_l, T ensemble from its surrounding bath, which includes the U_σ calculations only in the surrounding system, and obtain a partition function which deals with each system separately. The advantage of using this approach is that decoupling the two systems won't require simulation of a large size system for the free energy calculations and U_σ can be calculated separately and simply added to the whole partition function.

In addition, to achieve a quantitative prediction for the hopping time, the kinetic prefactor calculation is added to the free energy barrier calculations. However, calculating the prefactor uses a two particles system simulation, ignoring the other particles presence and their interaction effect on the transition rate. Tracking the transition rate for a chosen particle within a larger system could result in a more accurate estimation for the kinetic prefactor and can improve the overall accuracy of the proposed model.

5.2.2 Understanding Molecular Orientation and Channel Effects on the Hopping Barrier

It was demonstrated in Chapter 4 that increasing the interaction parameters between the carbon nanotube and enantiomers changes the preferred angles, θ, that the molecules take with respect to each other. This gives rise to a few questions: How does changing or increasing the chirality of the tube affect the molecules orientation inside the tube? How can the orientation of the molecules at the transition state affect their hopping barrier? Can an increase in the difference in the free energy barrier between two enantiomers be used as a tool to quantify the chirality effect of the channel?

One way to approach these questions is to build a well defined channel, where the chirality and structure of the channel could be changed while keeping the other parameters of the channel fixed, such as the radius. Investigating the structural effect of the channel (chirality effect) on the difference between two molecules hopping barrier and also their orientation at the transition state can be analyzed in such models. For example, changing the helicity of the tube, adding different chiral functional groups to the outside of the pore, and varying the inner diameter of the tube while keeping the chirality fixed and studying their effect on the molecules hopping barrier can be studied. The result would give insight into the effect of the channel on the molecules orientation, and their hopping barrier, and how this can be controlled by changing the chirality of the tube or its interaction parameters with the molecules. In addition, it could be verified how changing the structure of a given molecule can affect their chirality. For example, adding or removing a functional group to the structure of a chiral molecule or adding chiral proteins to the outer wall of a nanotube might increase or change the chirality effect. Furthermore, using the tubes where the degree of the chirality can be easily manipulated and controlled while keeping the other parameters fixed can lead to more effective separation techniques.

It is important to investigate the channels structural effect on particles hopping barrier as well. For example, it was shown that the periodicity of the CNTs used in Chapter 4, might not influence the hopping barriers for the enantiomers. However, predicting the free energy barriers for the molecules confined to the channels with variable diameters, which is a common challenge in experimentally synthesizing channels, is still an open question that needs to be addressed. It will be interesting to know, how the hopping time and the dynamics of diffusion in these channels change. For example, does the average free energy barrier or the slowest barrier determine the diffusion rate?

5.2.3 Achieving a Measurable Separation

The dynamics of molecules in single file systems are connected to their hopping time and tracer diffusion coefficient which suggests the TST approach has the potential to be used as an effective tool for optimizing

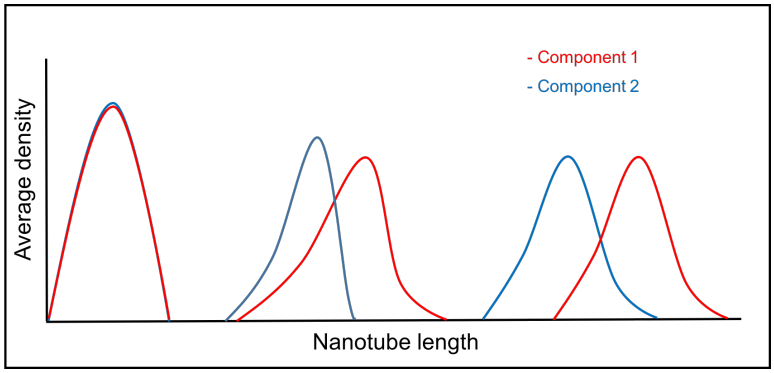

Figure 5.1: A schematic illustration for separation of enantiomers, showing the density profile for each components of a mixture along the longitudinal axis of a nanopore.

the separation of mixtures. For example, dual mode diffusion has been observed in binary mixtures of small molecules diffusing inside the molecular sieve zeolite $AlPO_4 - 5$, which depends on the size ratio between the diameter of the component and diameter of the channel [62, 64, 65]. It was also established in this thesis that the different pairs of enantiomers of a simple chiral molecule exhibit differences in their free energy barrier when they are confined to a narrow chiral channel. The existence of a free energy gap between two enantiomers of a chiral molecule suggests different hopping time for each component when they are present as a mixture, which should lead to different rates of tracer diffusion. However, the question of how big of a difference in the free energy barrier is required for achieving an effective and measurable separation is still open.

One way to approach this question is to estimate the ratio between two component's diffusion coefficients, using their hopping times such that,

$$\frac{D_{x1}}{D_{x2}} = \sqrt{\frac{\tau_{hop2}}{\tau_{hop1}}} = \sqrt{\frac{A_2}{A_1}\, e^{\beta\,(\Delta G_2^* - \Delta G_1^*)}}, \tag{5.1}$$

where D_{x1} and D_{x2} are diffusion coefficients for component 1 and 2 in a binary mixture, τ_{hop1} and τ_{hop2} are their hopping times, A_1 and A_2 are their kinetic prefactors, and ΔG_1^* and ΔG_2^* are each components' free energy barrier at the transition state. Eq. 5.1 provides a measure of the difference between each component's tracer diffusion coefficient based on their hopping time which is ultimately based on their hopping barrier. The difference in diffusion coefficient between two component of a mixture suggests that separation could be achieved as long as it is possible to choose a long enough channel length. However, based on the nature of the pore and the application, it might not be easily feasible. For example, Eq. 5.1 suggests that a difference of 2 k_BT in the barriers leads to a D_{x1}/D_{x2} of 2.82 in their tracer diffusion coefficient, assuming $A_1 = A_2$.

To obtain detailed information about achieving measurable separation in the time scale of a simulation and determining a desirable pore length for the separation, it would be necessary to perform a direct separation simulation. For example, for the case of enantiomers, in order to determine weather the free energy gap

obtained between two enantiomer is sufficient enough to achieve a separation, a simulation process can be performed as follows: at the start of the simulation, a large size system consists of both enantiomers in a $1:1$ ratio is placed at the opening of a long chiral nanotube and let the system to be equilibrated at a chosen constant temperature. A biased step size in the forward direction of the tube is applied to make sure the motion is in the direction of the nanotube axis. In analyzing the simulation result, the average density profile for each component that crosses a certain area within the nanotube axis can be used as a measure of separation. If the separation process is successful and it can be achieved within the simulation time and chosen nanotube length, the density profile is expected to be similar to the one illustrated in Fig. 5.1.

References

[1] S. Ahmadi, M. Schmidt, R. J. Spiteri, and and R. K. Bowles. The Effect of Soft Repulsive Interactions on the Diffusion of Particles in Quasi-one-dimensional Channels: A Hopping Time Approach. *J. Chem. Phys.*, 150:224501, 2019.

[2] S. N. Wanasundara, R. J. Spiteri, and R. K Bowles. Single file and normal dual mode diffusion in highly confined hard sphere mixtures under flow. *J. Chem. Phys.*, 137(10):104501–104505, 2012.

[3] S. N. Wanasundara, R. J. Spiteri, and R. K. Bowles. A transition state theory for calculating hopping times and diffusion in highly confined fluids. *J. Chem. Phys.*, 140(2):024505, 2014.

[4] D. Corti. Isothermal-isobaric ensemble for small systems. *Phys. Rev. E.*, 64(1):016128, June 2001.

[5] S. Ahmadi and R. K. Bowles. Diffusion in quasi-one-dimensional channels: A small system n, p, T, transition state theory for hopping times. *J. Chem. Phys.*, 146:154505, 2017.

[6] M. Z. Yamchi, S. S. Ashwin, and R. K. Bowles.

[7] P O. Carvalho, Q. B. Cass, S. A. Calafatti, F. J. Contesini, and R. Bizaco. Review – alternatives for the separation of drug enantiomers: Iboprofen as a model compound. *Braz. J. Chem. Eng.*, 23(03):291, 2006.

[8] T. Belin and F. Epron. Characterization methods of carbon nanotubes: a review. *Mater. Sci. Eng. B.*, 119:105–118, 2005.

[9] E. L. Cussler. *Diffusion: Mass Transfer in Fluid Systems.* Cambridge University Press, 1997.

[10] A. Finkelstein. *Water movement through lipid bilayers, pores, and plasma membranes: theory and reality.* Wiley, New York, 1987.

[11] Volker Kukla, Jan Kornatowski, Dirk Demuth, Irina Girnus, Harry Pfeifer, Lovat V C Rees, Stefan Schunk, Klaus K Unger, and Jorg Karger. NMR studies of Single-File diffusion in unidimensional channel zeolites. *Science.*, 272(5262):702–704, 1996.

[12] J. Kärger, M. Petzold, H. Pfeifer, S. Ernst, and J. Weitkamp. Single-file Diffusion and Reaction in Zeolites. *J. Catal.*, 136(2):283–299, 1992.

[13] A. V. A. Kumar. Crossover from normal diffusion to single-file diffusion of particles in a one-dimensional channel: LJ particles in zeolite zsm-22. *Mol. Phys.*, 113(11):1306–1310, 2014.

[14] A. Das, S. Jayanthi, H. S. M. V. Deepak, K. V. Ramanathan, A. Kumar, C. Dasgupta, and A. K. Sood. Single-File Diffusion of Confined Water Inside SWNTs: An NMR Study. *ACS Nano*, 4(3):1687–1695, March 2010.

[15] R. Valiullin and J. Kärger. Comment on "Single-File Diffusion of Confined Water Inside SWNTs: An NMR Study". *ACS Nano*, 4(7):3537–3537, 2010.

[16] Q. Chen, J. D. Moore, Y. Liu, T. J. Roussel, Q. Wang, T. Wu, and K. E. Gubbins. Transition from single-file to Fickian diffusion for binary mixtures in single-walled carbon nanotubes. *J. Chem. Phys.*, 133(9):094501, 2010.

[17] A. L. Hodgkins and R. D. Keynes. The potassium permeability of a giant nerve fibre. *J. Physiol.*, 128(1):61–88, 1955.

[18] B. Hille. *Ions Channels of Excitable Membrane*. Sinauer Associates INC. Sunderland, Massachusetts, 2001.

[19] U. Siems, C. Kreuter, A. Erbe, N. Schwierz, S. Sengupta, P. Leiderer, and P. Nielaba. Non-monotonic crossover from single-file to regular diffusion in micro-channels. *Sci. Rep.*, 2, December 2012.

[20] E. Locatelli, M. Pierno, F. Baldovin, E. Orlandini, Y. Tan, and S. Pagliara. Single-File Escape of Colloidal Particles from Microfluidic Channels. *Phys. Rev. Lett.*, 117(3):038001, 2016.

[21] S. Y. Yang, J. Yang, E. Kim, G. Jeon, J. Eun, K. Y. Choi, S. K. Hahn, and J. K. Kim. Single-file diffusion of protein drugs through cylindrical nanochannels. *Acs Nano*, 4(7):3817–3822, 2010.

[22] Q. Wei, C. Bechinger, and P. Leiderer. Single-file diffusion of colloids in one-dimensional channels. *Science.*, 287(5453):625–627, January 2000.

[23] C. Lutz, M. Kollmann, and C. Bechinger. Single-File Diffusion of Colloids in One-Dimensional Channels. *Phys. Rev. Lett.*, 93(2):026001, 2004.

[24] F. Salles, S. Bourrelly, H. Jobic, T. Devic, V. Guillerm, P. Llewellyn, C. Serre, G. Ferey, and G. Maurin. Molecular Insight into the Adsorption and Diffusion of Water in the Versatile Hydrophilic/Hydrophobic Flexible MIL-53(Cr) MOF. *J. Phys. Chem. C*, 115(21):10764–10776, 2011.

[25] H. Jobic. Observation of single-file diffusion in a MOF. *Phys. Chem. Chem. Phys*, 18(26):17190–17195, 2016.

[26] P. L. Krapivsky, K. Mallick, and T. Sadhu. Tagged particle in single-file diffusion. *J. Stat. Phys.*, 160(4):1885–925, 2015.

[27] P. Kalinary. Calculation of the mean first passage time tested on simple two-dimensional models. *J. Chem. Phys.*, 126:194708, 2007.

[28] K. K. Mon and J. K. Percus. Self-diffusion of fluids in narrow cylindrical pores. *J. Chem. Phys.*, 117(5):2289–2292, 2002.

[29] C. D. Ball, N. D. MacWilliam, J. K. Percus, and R. K. Bowles. Normal and anomalous diffusion in highly confined hard disk fluid mixtures. *J. Chem. Phys.*, 130(5):054504–054506, 2009.

[30] R. K. Bowles, K. K. Mon, and J. K. Percus. Calculating the hopping times of confined fluids: Two hard disks in a box. *J. Chem. Phys.*, 121(21):10668–10673, 2004.

[31] K. K. Mon and J. K. Percus. Hopping times of two hard disks diffusing in a channel. *J. Chem. Phys.*, 125(24):244704–244705, 2006.

[32] K. K. Mon and J. K. Percus. Hopping time of a hard disk fluid in a narrow channel. *J. Chem. Phys.*, 127(9):094702–094703, 2007.

[33] Z. G. Mao and S. B. Sinnott. Separation of organic molecular mixtures in carbon nanotubes and bundles: Molecular dynamics simulation. *J. Phys. Chem. B*, 105:6916, 2001.

[34] K. H. Lee and S. B. Sinnott. Computational studies of non-equilibrium molecular transport through carbon nanotubes. *J. Phys. Chem. B*, 108:9861, 2004.

[35] J. K. Holt, H. G. Park, Y. M. Wang, M. Stadermann, A. B. Artyukhin, C. P. Grigoropoulos, A. Noy, and O. Bakajin. Fast Mass Transport Through sub-2-nanometer Carbon Nanotubes. *Science.*, 312:1034, 2006.

[36] T. K. Perkins and O. C. Johnston. A Review of Diffusion and Dispersion in Porous Media. *Society of Petroleum Engineers*, pages 70–84, 1936.

[37] H. J. V. Tyrrell and K. R. Harris. *Diffusion in Liquids.* Butterworth-Henemann, New York, 1984.

[38] J. Philibert. One and a half century of diffusion: Fick, einstein, before and beyond. *Diffusion Fundamentals 6*, pages 6.1–6.19, 2005.

[39] R. Brown, F.R.S. Hon. M.R.S.E., and R.I. Acad. V.P.L.S. A brief account of microscopical observation made on the particles contained in the pollen of plants. *Philosophical Magazine Series 2*, pages 161–173, 1827.

[40] D. W. Jepsen. Dynamics of a simple many?body system of hard rods. *J. Math. Phys.*, 6:405, 1965.

[41] J. L. Lebowitz and J. K. Percus. Kinetic equations and density expansions: Exactly solvable one–dimensional system. *J. Phys. Rev*, 155:122, 1967.

[42] S. M. Auerbach, K. A. Carrado, and P. K. Dutta. *Handbook of Zeolite Science and Technology.* Marcel Dekker, Inc., New York. Basel, 2003.

[43] T. E. Harris. Diffusion with "Collision" between Particles. *J. Appl. Probab.*, 2:323–338, 1965.

[44] D. G. Levitt. Dynamics of a Single-File Pore: Non-Fickian Behavior. *Phys. Rev. A.*, 8:3050–3054, 1973.

[45] K. Hahn and J. Kärger. Deviations from the Normal Time Regime of Single–File Diffusion. *J. Phys. Chem. B.*, 102(30):5766–5771, 1998.

[46] B. Lin, M. Meron, S. Rice B. Cui, and H. Diamant. From Random Walk to Single-File Diffusion. *Phys. Rev. Lett.*, 94(21):216001, June 2005.

[47] M. Ø. Jensen, S. Park, E. Tajkhorshid, and K. Schulten. Energetics of glycerol conduction through aquaglyceroporin GlpF. *Proc. Natl. Acad. Sci. USA*, 99(10):6731–6736, May 2002.

[48] J. C. Rasaiah, S. Garde, and G. Hummer. Water in Nonpolar Confinement: From Nanotubes to Proteins and Beyond *. *Annu. Rev. Phys. Chem.*, 59(1):713–740, 2008.

[49] V. Gupta, S. S. Nivarthi, A. V. McCormick, and H. Ted Davis. Evidence for single file diffusion of ethane in the molecular sieve $AlPO_4$–5. *Chem. Phys. Lett.*, 247:596–600, 1995.

[50] J. Kärger. Transport Phenomena in Nanoporous Materials. *Chem. Phys. Chem.*, 16(1):24–51, 2015.

[51] B. Mukherjee, P. K. Maiti, C. Dasgupta, and A. K. Sood. Single-file diffusion of water inside narrow carbon nanorings. *Acs Nano*, 4(2):985–991, 2010.

[52] V. N. Kharkyanen, S. O. Yesylevskyy, and N. M. Berezetskaya. Approximation of super-ions for single-file diffusion of multiple ions through narrow pores. *Phys. Rev. E.*, 82(5):051103, 2010.

[53] V. Kukla, J. Kornatowski, D. Demuth, I. Girnus, H. Pfeifer, L. V. C. Rees, K. K. Unger S. Schunk, and J. Kärger. NMR Studies of Single-File Diffusion in Unidimensional Channel Zeolites. *Science.*, 272(5262):702–704, May 1996.

[54] K. Hahn, J. Kärger, and V. Kukla. Single–File Diffusion Observation. *Phys. Rev. Lett.*, 76(15):2762–2765, 1996.

[55] A. R. Dutta, P. Sekar, M. Dvoyashkin, C. R. Bowers, K. J. Ziegler, and S. Vasenkov. Single-File Diffusion of Gas Mixtures in Nanochannels of the Dipeptide LAlaLVal: High-Field Diffusion NMR Study. *J. Phys. Chem. C*, 120(18):9914–9919, 2016.

[56] P. M. Richards. Theory of One–dimensional Hopping Conductivity and Diffusion. *Phys. Rev. B.*, 16(4):1393, 1977.

[57] S. Alexander and P. Pincus. Diffusion of Labeled Particles on One–dimensional Chains. *Phys. Rev. B.*, 18(4):2011–2012, 1978.

[58] P. Kutner. Chemical Diffusion in the Lattice Gas of Non-interacting Particles. *Phys. Lett. A.*, 81(4):239–240, 1981.

[59] H. van Beijeren, K. W. Kehr, and R. Kutner. Diffusion in Concentrated Lattice Gases. III. Tracer diffusion on a One-dimensional Lattice. *Phys. Rev. B.*, 28(10):5711, 1983.

[60] S. G. Farrell and A. D. Rutenberg. Anomalously Slow Transport in Single-file Diffusion with Slow Binding Kinetics. *Phys. Rev. E.*, 98:022114, 2018.

[61] J. Kärger and D. Ruthven. *Diffusion in Zeolites and Other Microporous Solids.* Wiley, New York, 1992.

[62] D. S. Sholl. Normal, Single–file, and Dual–mode Diffusion of Binary Adsorbate Mixtures in $AlPO_4 - 5$. *J. Chem. Phys.*, 107:4384, 1997.

[63] D. S. Sholl and K. A. Fichthorn. Respond to "Comment on: Normal, Single–file, and Dual–mode Diffusion of Binary Adsorbate Mixtures in $AlPO_4 - 5$". *J. Chem. Phys.*, 109:5693, 1998.

[64] P. Adhangale and D. Keffer. Single–file Motion of Polyatomic Molecules in One–dimensional Nanoporous Materials. *Mol. Phys.*, 100:2727, 2002.

[65] P. Adhangale and D. Keffer. Exploiting single-file motion in one-dimensional nanoporous materials for hydrocarbon separation. *Sep. Sci. Technol.*, 38:977, 2003.

[66] J. Sané, J. T. Padding, and Ard. A. Louis. The crossover from single file to fickian diffusion. *Faraday Discuss.*, 144(0):285–299, 2009.

[67] J. K. Percus. Anomalous Self-Diffusion for One-Dimensional Hard Cores. *Phys. Rev. A*, 9(1):557–559, 1974.

[68] A. Kusumi, K. Ritchie C. Nakada, K. Murase, K. Suzuki, H. Murakoshi, J. Kondo RS. Kasai, and T. Fujiwara. Paradigm shift of the plasma membrane concept from the two-dimensional continuum fluid to the partitioned fluid: high-speed single-molecule tracking of membrane molecules. *Annu. Rev. Biophys. Biomol. Struct.*, 34:351, 2005.

[69] M. H. Jacobs. *Diffusion Processes.* New York, Springer-Verlag, 1967 [©1935].

[70] R. Zwanzig. Diffusion past an entropy barrier. *J. Phys. Chem.*, 96(10):3926–3930, 1992.

[71] P. Kalinay. Projection of two-dimensional diffusion in a narrow channel onto the longitudinal dimension. *J. Chem. Phys.*, 122(20):204701, 2005.

[72] P. Kalinay. Calculation of the mean first passage time tested on simple two-dimensional models. *J. Chem. Phys.*, 126(19):194708–194710, 2007.

[73] M. H. Jacobs. *Diffusion Processes.* Springer-Verlag, New York, 1967.

[74] R. Zwanzig. Diffusion past an entropy barrier. *J. Phys. Chem.*, 96:3926–3930, 1992.

[75] D. Reguera and J. M. Rubí. Kinetic equations for diffusion in the presence of entropic barriers. *Phys. Rev. E*, 64:061106–061113, 2001.

[76] P. Kalinary and J. K. Percus. Corrections to the fick-jacobs equation. *Phys. Rev. E*, 74(4):021103–021117, 2006.

[77] P. Hänggi, P. Talkner, and M. Brrkovec. Reaction–rate theory: Fifty years after kramers. *Rev. Mod. Phys.*, 62(2):251, 1990.

[78] S. Arrhenius. Über die Reaktionsgeschwindigkeit bei der Inversion von Rohrzucker durch Säuren. *Z. Phys. Chem.*, 4(226), 1889.

[79] J. H. Van't Hoff. *in Etudes de Dynamiques Chemiques*. F. Muller and Co., Amsterdam, 1984.

[80] H. Eyring. The Activated Complex in Chemical Reactions. *J. Chem. Phys.*, 3(2):107–115, February 1935.

[81] M. G. Evans and M. Polanyi. Further Considerations on the Thermodynamics of Chemical Equilibria and Reaction Rates. *Trans. Faraday. Soc.*, 31:875, 1935.

[82] P. Pechukas. Transition State Theory. *Ann. Rev. Phys. Chem.*, 32:159–77, 1981.

[83] C. H. Bennett. *Diffusion in Solids: Recent Developments*. Academic Press, New York, 1975.

[84] D. Chandler. Statistical Mechanics of Isomerization Dynamics in Liquids and the Transition State Approximation. *J. Chem. Phys.*, 68(6):2959–2970, 1978.

[85] D. Frenkel and B. Smit. *Understanding Molecular Simulation: From Algorithms to Applications*. Academic Press, New York, 2002.

[86] H. X Zhou and R. Zwanzig. *J. Chem. Phys.*, 94:6147, 1991.

[87] K. K. Mon. Brownian dynamics simulations of two-dimensional model for hopping times. *J. Chem. Phys.*, 129(12):124711, 2008.

[88] K. K. Mon. Brownian dynamics mean first passage time of two hard disks diffusing in a channel. *J. Chem. Phys.*, 130:184701, 2009.

[89] A. Münster. Zur Theorie der generalisierten Gesamtheiten. *Mol. Phys.*, 2(1):1–7, 1959.

[90] R. A. Sack. Pressure-dependent partition functions. *Mol. Phys.*, 2(1):8–22, 1959.

[91] P. Attard. On the density of volume states in the isobaric ensemble. *J. Chem. Phys.*, 103(22):9884, 1995.

[92] D. S. Corti and G. Soto-Campos. Deriving the isothermal–isobaric ensemble: The requirement of a "shell" molecule and applicability to small systems. *J. Chem. Phys.*, 108(19):7959, 1998.

[93] Ger. J. M. Koper and H. Reiss. Length scale for the constant pressure ensemble: application to small systems and relation to einstein fluctuation theory. *J. Phys. Chem.*, 100(1):422–432, January 1996.

[94] D. S. Corti. Monte Carlo simulations in the isothermal—isobaric ensemble: the requirement of a 'shell' molecule and simulations of small systems. *Mol. Phys.*, 100(12):1887–1904, 2002.

[95] P. Schaaf, B. Senger, and H. Reiss. Defining Physical Clusters in Nucleation Theory from the N-Particle Distribution Function. *J. Phys. Chem. B*, 101:8740, 1997.

[96] H. Reiss, W. K. Kegel, and J. K. Katz. Role of the Model Dependent Translational Volume Scale in the Classical Theory of Nucleation. *J. Phys. Chem. A*, 102:8548, 1998.

[97] B. Senger, P. Schaaf, D. S. Corti, R. K. Bowles, J. C. Voegel, and H. Reiss. A Molecular Theory of the Homogeneous Nucleation Rate. II. Application to Argon Vapor. *J. Chem. Phys.*, 110:6438, 1999.

[98] T. L. Hill. *Statistical Mechanics: Principles and Selected Application.* Dover, 1987.

[99] H. Jeffreys. *Theory of Probability.* Clarendon, Oxford, 1950.

[100] D. Chandler. *Introduction to Modern Statistical Mechanics.* Oxford University Press, 6th edit. New York, 1984.

[101] D. A. McQuarrie. *Statistical Mechanics.* Harper and Row, New York, 1976.

[102] D. Soto-Campos, D. S. Corti, and H. Reiss. A Small System Grand Ensemble Method for the Study of Hard-particle Systems. *J. Chem. Phys.*, 108:2563, 1998.

[103] H. Reiss and G. A. Merry. Upper and Lower Bounds on the Chemical Potential of a Hard-Sphere Fluid and Other Inequalities from Scaled Particle Theory. *J. Phys. Chem*, 85:3313, 1981.

[104] D. A. Kofke and A. J. Post. Hard Particles in Narrow Pores - Transfer-Matrix Solution and the Periodic Narrow Box. *J. Chem. Phys.*, 98(6):4853–4861, 1993.

[105] B. Scheifele, I. Saika-Voivod, R. K. Bowles, and P. H. Poole. Heterogeneous Nucleation in the Low-barrier Regime. *Phys. Rev. E.*, 87:042407, 2013.

[106] C. H. Bennett. *In Algorithms for Chemical Computations.* American Chemical Society, Washington, DC, 1977.

[107] E. A. Carter, G. Ciccotti, J. T. Hynes, and R. Kapral. Constrained Reaction Coordinate Dynamics for the Simulation of Rare Events. *Chem. Phys. Lett.*, 156:472, 1989.

[108] P. R. ten Wolde, M. J. Ruiz-Montero, and D. Frenkel. Numerical calculation of the rate of homogeneous gas–liquid nucleation in a lennard-jones system. *J. Chem. Phys.*, 110 (3)(3):1591, 1999.

[109] D. Chandler. *Introduction to Modern Statistical Mechanics.* Oxford University Press, New York,, 1987.

[110] J. C. Keck. Variational Theory of Reaction Rates. *Adv. Chem. Phys.*, 13:85, 1967.

[111] J. T. Hynes. *Theory of Chemical Reaction Dynamics.* CRC, Boca Raton, FL, 1985. Vol. 4.

[112] D. G. Truhlar, B. C. Garrett, and S. J. Klippenstein. *J. Phys. Chem.*, 100:12771, 1996.

[113] S. C. Tucker, edited by P. Hänggi, and P. Talkner. *In New Trends in Kramers Reaction Rate Theory.* Kluwer Academic, Dordrecht, 1995.

[114] R. Hernandez, T. Uzer, and T. Bartsch. Transition State Theory in Liquids beyond Planar Dividing Surfaces. *Ann. Rev. Phys. Chem.*, 370:270, 2010.

[115] E. Pollak and edited by S. D. Schwartz. *In Theoretical Methods in Condensed Phase Chemistry.* Kluwer Academic, Dordrecht, 2000. p. 1.

[116] C. C. Martens. Qualitative Dynamics of Generalized Langevin Equations and the Theory of Chemical Reaction Rates. *J. Chem. Phys.*, 116:2516, 2002.

[117] A. Patti and A. Cuetos. Brownian dynamics and dynamic Monte Carlo simulations of isotropic and liquid crystal phases of anisotropic colloidal particles: A comparative study. *Phys. Rev. E.*, 86(1):011403, 2012.

[118] M. Abramowitz and I. A. Stegun, editors. *Handbook of Mathematical Functions.* Dover, New York, 1965.

[119] M. J. Ruiz-montero, D. Frenkel, and J. J. Brey. Efficient Schemes to Compute Diffiusive Barrier Crossing Rates. *Mol. Phys.*, 90(6):925–941, 1997.

[120] K. Voss. pythOPT: A Problem-solving Environment for Optimization Methods. Master's thesis, University of Saskatchewan, Saskatoon, Canada, 2016.

[121] F. van den Bergh and A. P. Engelbrecht. A new locally convergent particle swarm optimiser. In *IEEE International conference on systems, man and cybernetics*, volume 3, page 6. IEEE, 2002.

[122] M. T. Heath. *Scientific computing*, volume 80 of *Classics in Applied Mathematics*. Society for Industrial and Applied Mathematics (SIAM), Philadelphia, PA, second edition, 2018. An introductory survey.

[123] WT. Kelvin. *J. Oxford Univ Junior Scientific Club.*, 18:1–57, 1894.

[124] IUPAC Recommendations. Basic terminology of stereo-chemistry. *Pure. Appl. Chem.*, 68:2193–2222, 1966.

[125] A. Abate, E. Brenna, C. Fuganti, G. Gatti Francesco, and S. Serra. Odor and (Bio)diversity: Single Enantiomers of Chiral Fragrant Substances. *Chem. Biodivers.*, 1:1888–1898, 2004.

[126] E. Brenna, C. Fuganti, and S. Serra. From Commercial Racemic Fragrances to Odour Active Enantiopure Compounds: the Ten Isomers of Irone. *CR Cbim.*, 6:529–546, 2003.

[127] J. Kärger and D. Ruthven. *Drug Stereochemistry, Analytical Methods and Phamacology.* 2nd ed, Marcel Dekker, New York, 1993.

[128] N. M. Maier, P. Franco, and W. Lindner. Review - Separation of Rnantiomers: Needs, Challenges, Perspectives. *J. Chromatogr.*, 906:3–33, 2001.

[129] X. Cai, W. Liu, and G. Sheng. Enantioselective Degradation and Ecotoxicity of the Chiral Herbicide Diclofop in Three Freshwater Alga Cultures. *J. Agric. Food Chem.*, 56:2139–2146, 2008.

[130] I. Ali, V. K. Gupta, and H. Y. Aboul-Enein. Chiral Resolution of Racemic Environmental Pollutants by Capillary Electrophoresis. *Crit. Rev. Anal. Chem.*, 38:132–146, 2008.

[131] B. S. Sekhon. Chiral Pepticides. *J. Pestic. Sci.*, 34:1–12, 2009.

[132] J. Caldwell. Review - Importance of Stereospecific Bionalytical Monitoring in Drug Development. *J. Chromatogr.*, 719:3–13, 1996.

[133] J. Knabes. *Dtsch. Apoth-Ztg.*, 124:685, 1984.

[134] M. Eichelbaum, B. Testa, and A. Somogyi. *Stereochemical Aspects of Drug Action and Disposition.* Springer, Verlag Berlin Heidelberg, 2003.

[135] R. Gawley and J. Aube. *Principles of Asymmetric Synthesis.* Elsevier, 2012.

[136] A. M. Stalcup. Chiral separations. *Ann. Rev. Anal. Chem.*, 3:341–63, 2010.

[137] L. Pasteur. Louis Pasteur Discovery of Molecular Chirality and Spontaneous Resolution. *Ann. Chem.*, 24:442–459, 1984.

[138] J. Gal. Louis Pasteur, language, and molecular chirality. I. Background and Dissymmetry. *Chirality.*, 23:1–16, 2011.

[139] O. Pastinen, J. Jokela, T. Eerikainen, and T. Schwabe. Cross-linked Glucose Isomerase Crystals as a Liquid Chromatographic Separation Material. *Enzyme Microb. Technol.*, 26:550, 2000.

[140] T. Aoki, M. Ohshima, K. I. Shinihara, T. Kaneko, and E. Oikawa. Enantioselective Permeation of Racemates through a Solid (+)-poly2-[dimethyl)silyl]norbornadiene Membrane. *Polymer.*, 38:235, 1997.

[141] M. Nakamura, S. Kiyohara, K. Saito, K., Sugita, and T. Sugo. Chiral Separation of dl-tryptophan using Porous Membranes containing Multilayered Bovine Serum Albumin Crosslinked with Glutaraldehyde. *J. Chromatogr. A.*, 822:53, 1998.

[142] B. B. Lakshmi and C. R. Martin. Enantioseparation using Apoenzymes Immobilized in a Porous Polymeric Membrane. *Nature.*, 388:758, 1997.

[143] A. Salas-Burgos, P. Iserovich, F. Zungia, J. C. Vera, and J. Fischbarg. Predicting the Three-Dimensional Structure of the Human Facilitative Glucose Transporter Glut1 by a Novel Evolutionary Homology Strategy: Insights on the Molecular Mechanism of Substrate Migration, and Binding Sites for Glucose and Inhibitory Molecules. *Biophys. J.*, 87:2990, 2004.

[144] S. B. Lee, D. T. Mitchell, L. Trofin, T. K. Nevanen, H. S:oderlund, and C. R. Martin. Antibody-based bio-nanotube membranes for enantiomeric drug separations. *Science.*, 127:2197, 2002.

[145] K. Malek and Rutger A. van Santen. Chiral separation in modified silica nanotube membranes: A molecular simulation study. *J. Membr. Sci.*, 311:192–199, 2007.

[146] G. Hummer, J. C. Rasaiah, and J. P. Noworyta. Water Conduction through the Hydrophobic Channel of a Carbon Nanotube. *Nature.*, 414:188–190, 2001.

[147] A. Noy, H. G. Park, F. Fornasiero, J. K. Holt, C. P. Grigoropoulos, and O. Bakajin. Nanofluidics in Carbon Nanotubes. *Nano. Today.*, 2:22–29, 2007.

[148] D. Mattia and Y. Gogotsi. Review: Static and Dynamic Behavior of Liquids inside Carbon Nanotubes. *Microfluid. Nanofluid.*, 5:289–305, 2008.

[149] J. A. Thomas, A. J. H. McGaughey, and O. Kuter-Arnebeck. Pressure-driven water flow through carbon nanotubes: Insights from molecular dynamics simulation. *Int. J. Therm. Sci.*, 49:281–289, 2010.

[150] M. Majumder, N. Chopra, and R. Andrews. Erratum: Nanoscale Hydrodynamics: Enhanced Flow in Carbon Nanotubes. *Nature.*, 438:44, 2005.

[151] J. K. Holt, A. Noy, and T. Huser. Fabrication of a carbon nanotube-embedded silicon nitride membrane for studies of nanometer-scale mass transport. *Nano Lett.*, 4:2245–2250, 2004.

[152] Y. Gao and Y. Bando. Nanotechnology: Carbon nanothermometer containing gallium. *Nature.*, 415:599, 2002.

[153] D. S. Bethune, C. H. Kiang, M. S. de Vries, G. Gorman, R. Savoy, J. Vazquez, and R. Beyers. Cobalt-catalyzed growth of carbon nanotubes with single–atomic–layerwalls. *Nature.*, 363:605–607, 1993.

[154] S. Iijima and T. Ichihashi. Single-shell carbon nanotubes of 1-nm diameter. *Nature.*, 363:603–605, 1993.

[155] S. Iijima. Helical microtubules of graphitic carbon. *Nature.*, 354:56–58, 1991.

[156] J. A. Elliott, J. K. W. Sandler, A. H. Windle, R. J. Young, and M. S. P. Shaffer. Collapse of single-wall carbon nanotubes is diameter dependent. *Phys. Rev. Lett.*, 92:095501, 2004.

[157] J.Wildoer, L. Venema, A. Rinzler, R. Smalley, and C. Dekker. Electronic structure of atomically resolved carbon nanotubes. *Nature.*, 391:59–62, 1998.

[158] Y. Murakami, S. Chiashi, Y. Miyauchi, and S. Maruyama. Direct synthesis of single-walled carbon nanotubes on silicon and quartz-based systems. *Chem. Phys. Lett.*, 377:49, 2004.

[159] M. S. Dresselhaus, G. Dresselhaus, and R. Saito. Physics of Carbon Nanotubes. *Phys. Rev. B.*, 33(3):883–891, 1995.

[160] A. Jorio, R. Saito, J. Hafner, C. Lieber, M. Hunter, T. McClure, G. Dresselhaus, and M. Dresselhaus. *Phys. Rev. Lett.*, 86:085312, 2001.

[161] J. Rowlinson and F. Swinton. *Liquids and Liquid Mixtures.* Butteworth, London, 1982.

[162] R. T. Morrison and R. N. Boyd. *Organic Chemistry.* Allyn and Bacon, Boston, 1987.

[163] J. Costante-Crassous, T. J. Marrone, M. Briggs, J. A. McCammon, and A. Collet. Absolute Configuration of Bromochlorofluoromethane from Molecular Dynamics Simulation of Its Enantioselective Complexation by Cryptophane-C. *J. Am. Chem. Soc.*, 119:3818–3823, 1997.

[164] M. J. Frisch, M. Head-Gordon, G. W. Trucks, J. B. Foresman, H. B. Schlegel, K. Raghavachari, M. A. Robb, J. S. Binkley, C. Gonzalez, D. J. Defrees, D. J. Fox, R. A. Whiteside, R. Seeger, C. F. Melius, J. Baker, R. L. Martin, L. R. Kahn, J. J. P. Stewart, S. Topiol, and J. A. Pople. Gaussian, Inc., Pittsburgh, PA, 1994.

[165] Spartan'14. 1995 Wavefunction, Inc., Irvine. CA. USA, 2013.

[166] Y. Liu, J. D. Moore, T. J. Roussel, and K. E. Gubbins. Dual diffusion mechanism of argon confined in single-walled carbon nanotube bundles. *Phys. Chem.*, 12(25):6632–6640, 2010.

[167] B. Mukherjee, P. K. Maiti, C. Dasgupta, and A. K. Sood. Single-File Diffusion of Water Inside Narrow Carbon Nanorings. *ACS Nano.*, 4(2):985–991, 2010.

[168] G. M. Torrie and J. P. Valleau. Nonphysical Sampling Distributions in Monte Carlo Free-energy Estimation: Umbrella Sampling. *Chem. Phys. Lett.*, 28:578, 1974.

[169] C. H. Bennett. Efficient Estimation of Free Energy Differences from Monte Carlo Data. *J. Comput. Phys.*, 22:245, 1976.

[170] G. Gilat and L. S. Schulman. Chiral Interaction, Magnitude of the Effects and Application to Natural Selection of L-enantiomer. *Chem. Phys. Lett.*, 121:13–16, 1985.

[171] R. K. Bowles, R. McGraw, P. Schaaf, B. Senger, J. C. Voegel, and H. Reiss. A Molecular Based Derivation of the Nucleation Theorem. *J. Chem. Phys.*, 113:4524, 2000.